AD-A092 704 ATMOSPHERIC AND ENVIRONMENTAL RESEARCH INC CAMBRIDGE MA F/G 4/1
MODELING OF CHEMICAL PROCESSES IN THE TROPOSPHERE AND STRATOSPH--ETC(U)
AUG 80 N D SZE, M K KO, R SPECHT, M LIVSHITS F19628-78-C-0215
UNCLASSIFIED AFGL-TR-80-0251 NL

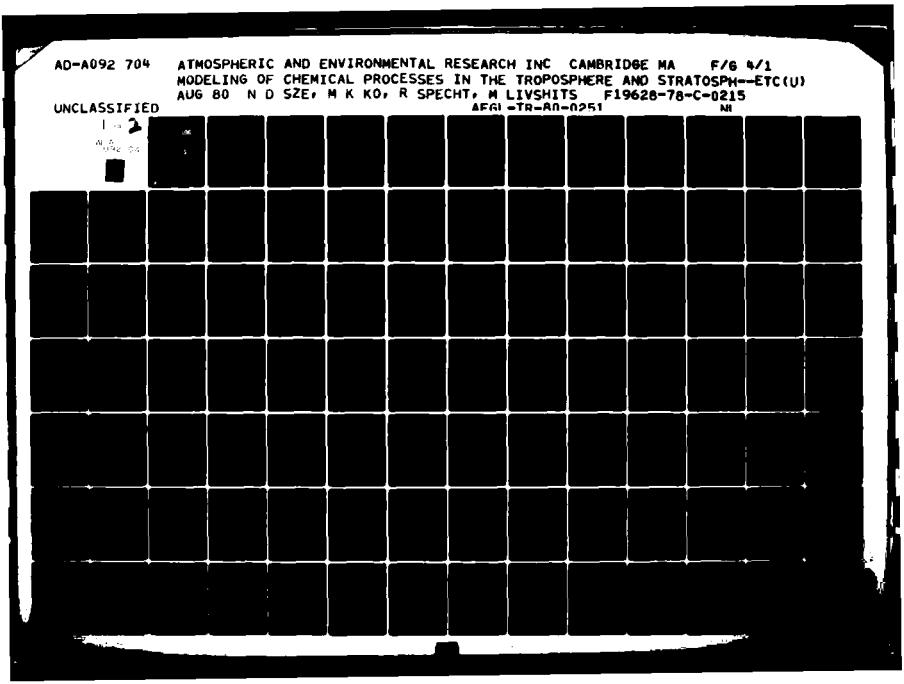

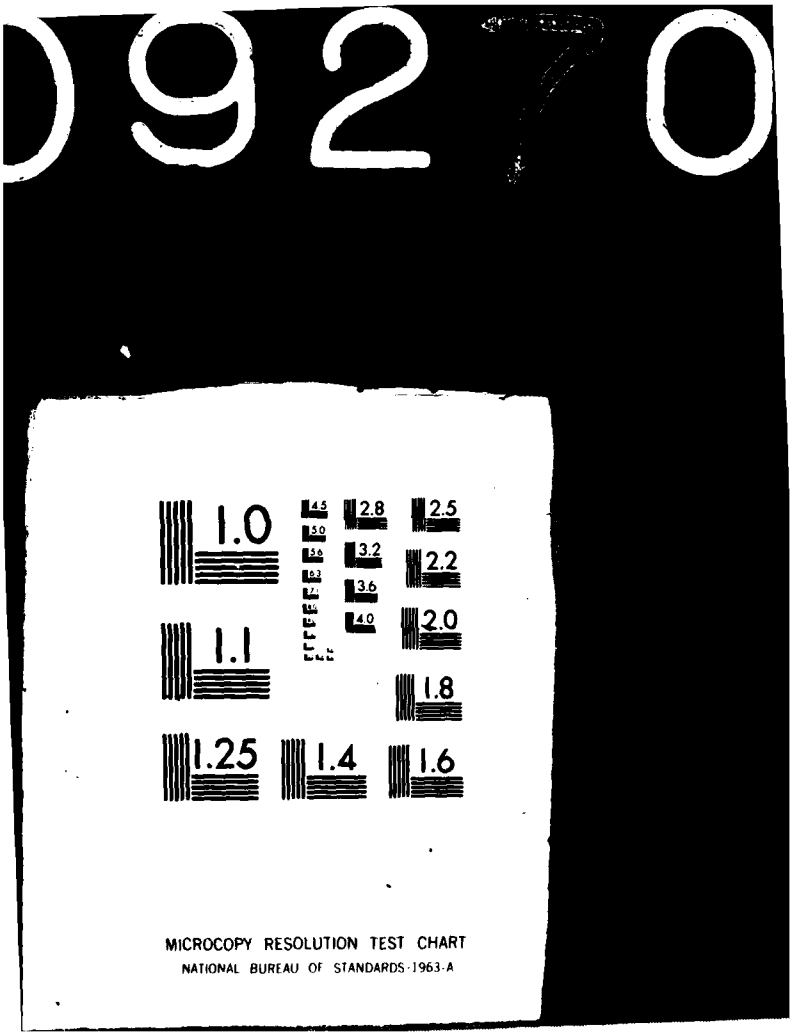
1.0
1.1
1.25
1.4
1.6
2.8
3.2
3.6
4.0
2.5
2.2
2.0
1.8
MICROCOPY RESOLUTION TEST CHART
NATIONAL BUREAU OF STANDARDS-1963-A

Unclassified

SECURITY CLASSIFICATION OF THIS PAGE (When Data Entered)

REPORT DOCUMENTATION PAGE	READ INSTRUCTIONS BEFORE COMPLETING FORM
1. REPORT NUMBER: AFGL-TR-80-0251	2. GOVT ACCESSION NO.: AD-A092 764
3. RECIPIENT'S CATALOG NUMBER:	
4. TITLE (and Subtitle): MODELING OF CHEMICAL PROCESSES IN THE TROPOSPHERE AND STRATOSPHERE	5. TYPE OF REPORT & PERIOD COVERED: Final Report 1 Aug 78 - 31 Oct 80
	6. PERFORMING ORG. REPORT NUMBER:
7. AUTHOR(s): N. D. Sze, R. Specht, M. K. W. Ko, M. Livshits	8. CONTRACT OR GRANT NUMBER(s): F19628-78-C-0215
9. PERFORMING ORGANIZATION NAME AND ADDRESS: Atmospheric and Environmental Research, Inc. 872 Massachusetts Avenue Cambridge, Massachusetts 02139	10. PROGRAM ELEMENT, PROJECT, TASK AREA & WORK UNIT NUMBERS: 62101F 668708AA
11. CONTROLLING OFFICE NAME AND ADDRESS: Air Force Geophysics Laboratory Hanscom AFB, Massachusetts 01731 Monitor/William Swider/LKD	12. REPORT DATE: August 1980
	13. NUMBER OF PAGES: 154
14. MONITORING AGENCY NAME & ADDRESS (if different from Controlling Office)	15. SECURITY CLASS. (of this report): Unclassified
	15a. DECLASSIFICATION DOWNGRADING SCHEDULE

16. DISTRIBUTION STATEMENT (of this Report)

Approved for public release; distribution unlimited.

17. DISTRIBUTION STATEMENT (of the abstract entered in Block 20, if different from Report)

18. SUPPLEMENTARY NOTES

19. KEY WORDS (Continue on reverse side if necessary and identify by block number)

Stratospheric model
Tropospheric model
Atmospheric chemistry

20. ABSTRACT (Continue on reverse side if necessary and identify by block number)

This report presents major accomplishments and significant findings of research conducted during the two years of contract to the Air Force Geophysics Laboratory, ending September 1980. The overall research effort is concerned with numerical modeling of chemical and dynamical processes in the troposphere and stratosphere. It encompasses four major areas of study: coupled chemical kinetics and transport in a one-dimensional diurnal model; tropospheric and stratospheric sulfur budgets; ozone perturbation

DD FORM 1 JAN 73 1473

Unclassified

SECURITY CLASSIFICATION OF THIS PAGE (When Data Entered)

studies; and the development of a two-dimensional model which couples the ozone chemistry with the mean wind field and the eddy transport.

TABLE OF CONTENTS

ACKNOWLEDGEMENT

We would like to thank Dr. J. A. Pyle for his assistance in setting up the dynamic framework for the two-dimensional model in the early stage of the development. We would also like to thank R. Daesen, R. Wells and B. Ryan for assistance in various stages of model development and S. McQuinn for preparation of this report. Part of the model development is supported by a contract from Chemical Manufacturers Association.

1. INTRODUCTION

The objective of the project is to provide a better understanding of the interactions among the chemical, radiative and dynamical processes which govern the behavior of trace gases in the stratosphere and troposphere. The work involved both model development to incorporate the proper mechanisms as well as the interpretation of model results through the comparison with available observations.

The report is organized in seven sections with two appendices. Section 2 provides a general review of numerical modeling of tropospheric and stratospheric processes with emphasis on the more recent theories and experimental data. Section 3 gives a detailed description of the AER one-dimensional photochemical diffusion model which includes the fully time-dependent diurnal code developed under the present contract. Section 4 compares the calculated one-dimensional results with available observations. Section 5 presents a comprehensive study of the tropospheric and stratospheric sulfur budget with emphasis on the chemical interaction of reduced sulfur compounds with OH radicals. Section 6 focuses on the possible ozone perturbation due to man's activities including atmospheric release of fluorocarbons, brominated halocarbons and nitrogen oxides. Finally, in Section 7, the basic approach for two-dimensional zonal-mean models is reviewed. In addition, the development of the AER 2-D model is presented together with the preliminary

model results simulating the present atmosphere.

Appendix A and Appendix B contain descriptions of the AER 1-D and 2-D models respectively. The results from the 2-D modeling efforts are being prepared for submission to technical journals for publication.

2. ATMOSPHERIC MODELING: GENERAL APPROACH

2.1 Background

Atmospheric models are designed to simulate the behavior of atmospheric gases by solving the system of mass continuity equations

$$\frac{\partial n_i}{\partial t} = - \underset{\sim}{\nabla} \cdot \underset{\sim}{\Phi}_i + Q_i \qquad (2.1\text{-}1)$$

for $i = 1, \ldots, N$ where N is the total number of species considered, n_i is the number density of the i^{th} species, $\underset{\sim}{\Phi}_i$ is the flux of the species due to atmospheric motion, Q_i is the net chemical production or loss rate. The system of equations is coupled because the term Q_i for species i will depend on other species concentrations. Equation (2.1-1) can be interpreted as giving the time rate of change of the local species concentration in terms of two components, Q_i the part due to chemical interactions and $\underset{\sim}{\nabla} \cdot \underset{\sim}{\Phi}_i$ the part due to atmospheric motions.

Independent of the dimensionality of the model and the numerical method used, a chemical scheme must be set up to define the term Q_i. The chemical scheme will specify the number of species considered in the computation and also lists the reactions among the various species. In addition, boundary values have to be specified for the differential equations. The setting up of the scheme is guided by atmospheric gas concentration measurements as well as kinetic

measurements in the laboratory. In Section 2.2 the atmospheric chemistry will be reviewed with emphasis on recent developments.

The description of the flux term depends on the dimensionality of the model. In Section 2.3, we will briefly discuss the various possible approaches. The exact approach and the numerical methods currently employed in the AER 1-D and 2-D models will be discussed in Sections 3 and 7 respectively.

2.2 Review of Atmospheric Chemistry

Stratospheric chemistry has been reviewed extensively by several authors (Nicolet, 1975; Johnston and Pokolske, 1978; Logan et al., 1978; Thrush, 1978). An excellent summary of information available up to the mid-1979 is given by NASA (1979). We shall focus here on subsequent development, with particular emphasis on the coupling aspects of various chemical processes which may affect the stratospheric ozone distributions.

The first theoretical model for stratospheric ozone was put forward by Chapman (1930) who invoked four reactions involving pure oxygen chemistry:

$$O_2 + h\nu \rightarrow O + O \qquad (2.2\text{-}1)$$

$$O + O_2 + M \rightarrow O_3 + M \qquad (2.2\text{-}2)$$

$$O_3 + h\nu \rightarrow O_2 + O \qquad (2.2\text{-}3)$$

and

$$O + O_3 \rightarrow 2O_2 \; . \qquad (2.2\text{-}4)$$

Assuming photochemical equilibrium, the concentration of O_3 based on reactions (2.2-1) - (2.2-4) is given by

$$[O_3] = \{\frac{J_1}{J_3} \frac{k_2}{k_4} [O_2]^2 [M]\}^{\frac{1}{2}} , \qquad (2.2\text{-}5)$$

where J_1 and J_3 are the photolysis rates for reactions (2.2-1) and (2.2-3) respectively, and k_2 and k_4 the rate constants for reactions (2.2-2) and (2.2-4) respectively.

Chapman's simple model successfully predicts the approximate altitude ($\sim$25 km) at which the ozone peaks and gives an ozone overburden about a factor of 2 larger than observations. The major deficiencies of Chapmans' model are that:

i) it fails to account for the observed latitudinal and seasonal variations, and

ii) it tends to underestimate the sinks for O_3.

The first deficiency is thought to be caused by the neglect of dynamical transport in Chapman's model, while the second is due to the omissions of important chemical processes which involve hydrogen, nitrogen, chlorine, and perhaps bromine species.

The importance of hydrogen radicals (H, OH, HO_2) in ozone chemistry was recognized by Bates and Nicolet (1950). It is now believed that odd oxygen (O, O_3) may be removed by reactions such as

$$H + O_3 \rightarrow OH + O_2 \qquad (2.2\text{-}6)$$

$$OH + O \rightarrow H + O_2 \qquad (2.2\text{-}7)$$

$$H + O_2 + M \rightarrow HO_2 + M \qquad (2.2\text{-}8)$$

$$HO_2 + O \rightarrow OH + O_2 \qquad (2.2\text{-}9)$$

$$OH + O_3 \rightarrow HO_2 + O_2 \qquad (2.2\text{-}10)$$

$$HO_2 + O_3 \rightarrow OH + 2O_2 \ . \qquad (2.2\text{-}11)$$

Reactions (2.2-10) - (2.2-11) are important only in the lower stratosphere ($z < 28$ km) while reactions (2.2-6) - (2.2-9) are the major sinks for ozone above 40 km.

The source for atmospheric hydrogen radicals (HO_x) is mainly due to the reaction (Cadle, 1964; Hampson, 1964)

$$O(^1D) + H_2O \rightarrow 2OH \qquad (2.2\text{-}12)$$

where $O(^1D)$ is formed by photolysis of O_3 at wavelengths shorter than 3100 Å. The atmospheric sinks for HO_x include the following reactions:

$$OH + HO_2 \rightarrow H_2O + O_2 \qquad (2.2\text{-}13)$$

$$OH + HNO_3 \rightarrow H_2O + NO_3 \qquad (2.2\text{-}14)$$

$$OH + H_2O_2 \rightarrow H_2O + HO_2 \qquad (2.2\text{-}15)$$

$$OH + HO_2NO_2 \rightarrow H_2O + NO_2 + O_2 \ . \qquad (2.2\text{-}16)$$

While reaction (2.2-13) is important throughout the stratosphere, the contributions of reactions (2.2-14) to (2.2-16) as sinks for HO_x are restricted mainly to the lower stratosphere (15-30 km).

Recent laboratory work seems to indicate that rate constants for reactions (2.2-13) to (2.2-15) may be significantly faster than the previous accepted values (cf. NASA, 1979). We summarize in Table 2.2-1 the more recent rate data for reactions (2.2-13) to (2.2-15) along with NASA's (1979) recommendations.

The rate constant k_{16} for reaction (2.2-16) has not been measured, although a tentative upper limit of about 3×10^{-12} cm^3 s^{-1} was set by Trevor et al. (1980). Recent calculations by Sze and Ko (1980c) show that reaction (2.2-16) could be an important sink for HO_x if k_{16} exceeds about 1×10^{-12} cm^3 s^{-1}.

Other major catalytic cycles for removal of atmospheric ozone include the sequences

$$NO + O_3 \rightarrow NO_2 + O_2 \qquad (2.2\text{-}17)$$

$$NO_2 + O \rightarrow NO + O_2 \qquad (2.2\text{-}18)$$

and

$$Cl + O_3 \rightarrow ClO + O_2 \qquad (2.2\text{-}19)$$

$$ClO + O \rightarrow Cl + O_2 \ . \qquad (2.2\text{-}20)$$

The source for stratospheric NO_x (NO, NO_2, HNO_3, NO_3, N_2O_5) is mainly due to the reaction (Nicolet and Vergison, 1971; McElroy and McConnell, 1971; Crutzen, 1971),

$$O(^1D) + N_2O \rightarrow 2NO \qquad (2.2\text{-}21)$$

Table 2.2-1

A Comparison of New Rate Data with NASA's Recommended Values

Reaction	Rate Constant (NASA, 1979)	Rate Constant (New)	$\frac{k(New)}{k(NASA)}\Big\|_{298°K}$	$\frac{k(New)}{k(NASA)}\Big\|_{225°K}$
2. $OH + HNO_3 \rightarrow H_2O + NO_3$	8.3(-14)	$1.5 \times 10^{-14} \exp(\frac{+649}{T})$ (Wine et al., 1980)	1.55	3.15
3. $OH + HO_2 \rightarrow H_2O + O_2$	4.0(-11)	1-2(-10)* (Lii et al., 1980; DeMore, 1979)	2.5-5	2.5-5
4. $OH + H_2O_2 \rightarrow H_2O + HO_2$	$1 \times 10^{-11} \exp(\frac{-750}{T})$	$2.5 \times 10^{-12} \exp(\frac{-126}{T})$ (Keyser, 1980; Kaufman, 1980)	2.0	4.0

* Room temperature value, T-dependent unknown but probably small.

with N_2O emanating from the biosphere. The precursors to stratospheric chlorine are a variety of halocarbons (CH_3Cl, CCl_4, CH_3CCl_3. $CFCl_3$, CF_2Cl_2) as suggested by Rowland and Molina (1975).

The cycles of hydrogen, nitrogen and chlorine species are strongly coupled. For instance, the reaction

$$OH + NO_2 + M \rightarrow HNO_3 + M \qquad (2.2\text{-}22)$$

ties up active NO_2 to form the relatively inert species HNO_3 which does not directly attack ozone. On the other hand, the reaction

$$OH + HCl \rightarrow H_2O + Cl \qquad (2.2\text{-}23)$$

releases active chlorine (Cl) from the inert form HCl. Thus, an increase in OH tends to reduce the NO_x cycle [reactions (2.2-17) + (2.2-18)] but augments the ClX cycle [reactions (2.2-19) + (2.2-20)] as sinks for ozone.

The coupling of NO with HO_2 and ClO through the reactions

$$NO + HO_2 \rightarrow NO_2 + OH \qquad (2.2\text{-}24)$$

and

$$NO + ClO \rightarrow Cl + NO_2 \qquad (2.2\text{-}25)$$

is of considerable importance in the study of O_3 perturbations associated with increases in NO_x and ClX. Note that the following sequence

$$OH + O_3 \rightarrow HO_2 + O_2 \qquad (2.2\text{-}10)$$

$$HO_2 + NO \rightarrow OH + NO_2 \qquad (2.2\text{-}24)$$

$$NO_2 + h\nu \rightarrow NO + O \qquad (2.2\text{-}26)$$

$$O + O_2 + M \rightarrow O_3 + M \qquad (2.2\text{-}3)$$

does not lead to removal of O_3. Similarly, odd oxygen is conserved through the sequence

$$Cl + O_3 \rightarrow ClO + O_2 \qquad (2.2\text{-}19)$$

$$ClO + NO \rightarrow Cl + NO_2 \qquad (2.2\text{-}25)$$

followed by (2.2-26) and (2.2-3). Thus, an increase in NO may either reduce O_3 through reactions (2.2-17) and (2.2-18) or increase ozone through the coupling of NO with HO_2 [reaction (2.2-24)] and ClO [reaction (2.2-25)].

The reactions of ClO with HO_2 and NO_2,

$$ClO + HO_2 \rightarrow HOCl + O_2 \qquad (2.2\text{-}27)$$

and

$$ClO + NO_2 + M \rightarrow ClONO_2 + M \qquad (2.2\text{-}28)$$

introduce two other examples of coupling between ClX, HO_x and NO_x cycles. Note that reaction (2.2-27) followed by the sequence

$$HOCl + h\nu \rightarrow OH + Cl \qquad (2.2\text{-}29)$$

$$Cl + O_3 \rightarrow ClO + O_2 \qquad (2.2\text{-}19)$$

$$OH + O_3 \rightarrow HO_2 + O_2 \qquad (2.2\text{-}10)$$

is equivalent to

$$2O_3 \rightarrow 3O_2 \ .$$

The importance of reaction (2.2-28) involves the removal of two radicals ClO and NO_2 both of which participate in the ozone destruction cycle. Thus, the effect of reaction (2.2-28) is to reduce both the catalytic role of ClX and NO_x in the ozone destruction processes.

In summary, reactions (2.2-22), (2.2-23), (2.2-24), (2.2-25), (2.2-27) and (2.2-28) provide the principal coupling between the HO_x, NO_x and ClX cycles in the stratosphere. Because of the strong coupling between various chemical cycles, it is difficult to study each cycle in isolation. It is clear, however, that a thorough understanding of the coupling mechanisms is needed for the interpretation of field data and for model prediction of the effect of the potential perturbations.

Parallel to the development of the chemical interaction, the importance of dynamic transport also becomes more evident. As observation data accumulates, it becomes clear that the seasonal and latitudinal behavior of many gases cannot be explained by photochemistry alone. In the next section we will review the treatment of dynamic transport in the diffusion equation.

2.3 Treatment of Dynamics

Equation (2.1-1) shows that the divergence of the flux also contributes to the time rate of change of local concentration. In the full 3-dimensional treatment, $\underset{\sim}{\Psi}_i$ is given by the standard form of the Eulerian fluid description,

$$\underset{\sim}{\Phi}_i = n_i \underset{\sim}{v} \qquad (2.3\text{-}1)$$

where $\underset{\sim}{v}$ is the velocity wind field describing the general circulation. It is implicit in (2.3-1) that all trace species follow the same bulk air motion.

Because of its complexity, a full 3-D model calculation places enormous demand on computer core memory and computation time as the velocity wind field is a function of space and time. Somehow, there has to be a trade off between treatment of dynamics and chemistry. In the current 3-dimensional general circulation model, the chemical scheme is not adequate for study of trace gas concentration. An alternate approach is needed if one desires to include complete chemistry.

In a 1-D model, one opts for a more complete treatment of chemistry at the expense of dynamic description. It is difficult to formulate the 1-D model in terms of global averaging from the 3-D equation. Often, it is easier to visualize the 1-D model as describing a one-dimensional atmosphere. The continuity equation for a trace gas takes the form

$$\frac{\partial n_i}{\partial t} + \frac{\partial}{\partial z}(\Phi_i) = Q_i \qquad (2.3\text{-}1)$$

where z is the geometrical altitude, Φ_i is formally Wn_i, with $W = \frac{dz}{dt}$ the vertical velocity. The flux can be thought of as being comprised of two parts, one due to large scale motion and the other due to turbulent diffusive motion. The one-dimensional continuity equation implies that the large scale motion does not contribute to the flux. The flux due to turbulent diffusive motion can be parameterized by the eddy diffusion coefficients and the gradient of the mixing ratio of the trace gas, i.e.,

$$\Phi_i = -K(z)N(z)\frac{\partial f_i}{\partial z} \qquad (2.3\text{-}2)$$

where K(z) is the positive definite eddy diffusion coefficient, N(z) is air number density, $f_i = \frac{n_i}{N}$ is the volume mixing ratio. Note that the flux Φ_i flows in opposite direction to the mixing ratio gradient. In the absence of photochemical interactions, the steady state solution is given by f_i as a constant in altitude. Equation (2.3-1) can be rewritten in the form

$$\frac{\partial n_i}{\partial t} + \frac{\partial}{\partial z}\left(-KN\frac{\partial f_i}{\partial z}\right) = Q_i \quad . \qquad (2.3\text{-}3)$$

In order to solve (2.3-3), one needs a chemical scheme to set up Q_i, and prescribed values for N(z) and K(z). N(z) is usually obtained from tabulated values compiled from obser-

vations (U.S. Standard Atmosphere Supplement, 1966). K(z) is parameterized by a semi-empirical approach. Equation (2.3-3) is solved with parameterized values of K(z) for species for which the chemistry is well understood. K(z) is then adjusted so that the computed altitude profiles compare favorably with observations. Initially, methane has been used in this kind of calibration study (Wofsy and McElroy, 1973; Hunten, 1975) because of its simple chemistry. The resulting K(z) is then used to solve for the altitude profiles of other trace gases. The compuced results compare favorably with observation, thus giving support to the idea that the same eddy diffusion coefficient can be used for all trace gases. The eddy diffusion coefficient used in the present model is taken from Wofsy (1976).

The simulation of transport by vertical mixing in 1-D models has been applied with success to gases like CH_4, N_2O, F-11 and F-12 for which the stratospheric concentrations are maintained by upward diffuson of ground level emissions to balance the stratospheric chemical removals. However, it is found that the 1-D model has trouble accounting for all the observed latitudinal and seasonal behavior of the trace gas. This is particularly true in the case of ozone where the occurrence of a spring time maximum in ozone column (cf. Dütsch, 1971) is completely contrary to one's expectation based on a photochemical argument.

Because of its one-dimensional nature, the 1-D model cannot incorporate horizontal transports. However, the presence of meridional transport is evident even in the study of the

classical structure of the Hadley Cell circulation. Recent measurements of CH_4 and N_2O reported by Ehhalt (1980) indicate that 1-D calculations typically overpredict the stratospheric concentration of the gases around the equator while underpredicting it at high latitude. This is consistent with the idea of the upwelling motion in the equatorial region followed by poleward and downward motion at higher latitudes.

Another aspect of horizontal transport comes from the zonal winds. However, they are of more interest in meteorology rather than photochemistry since the longitudinal behavior of most species are more likely to be dominated by the day-night variations. Though some questions remains as to whether planetary waves could give rise to net meridonal transport (cf. Hartman and Garcia, 1979), at this stage of the development, it seems that the 2-D model is a good compromise for treatment of dynamics and chemistry.

2.4 Concluding Remarks

Within the past five years, because of the ever-increasing computational power of high speed computers, it has become feasible to incorporate a complete chemical scheme into a 2-D model. However, because of the intrinsic time-dependence of the circulation, it is necessary to solve the diffusion equations via a direct time integration. In contrast, the 1-D formulation can be modified to solve for the steady state solution. Because of its flexibility, the 1-D model will remain useful as a tool for identifying problems and

for obtaining first order solutions in sensitivity analysis. In particular, the 1-D model provides the appropriate testing ground for analyzing the ever more complex coupling among the chemical species. On the other hand, as more global observational data accumulates, particularly those derived using satellite observations, it would be increasingly important to use a 2-D model for comparisons. Thus, while it is imperative to develop a more efficient 2-D model, the 1-D model remains indispensible as a diagnostic tool to complement the 2-D model.

3. THE AER ONE-DIMENSIONAL MODEL

3.1 Derivation of Basic Equation

In this section, we will outline the basic assumptions leading to the derivation of the equations used in the AER 1-D photochemical diffusive model models. The structure of the models, with the diurnal option developed under the present contract, will be discussed in Secton 3.2. In addition, the effect of diurnal averaging on the diffusive species calculations will be examined in Section 3.3.

The basic equations in the 1-D model are the system of continuity equations

$$\frac{\partial f_i}{\partial t} = \frac{1}{N}\left\{\frac{\partial}{\partial z}\left(KN\frac{\partial f_i}{\partial z}\right) + (P_i - L_i n_i)\right\} \qquad (3.1\text{-}1)$$

where i is the species index, P_i and $L_i n_i$ are the production and loss rates respectively. The systems of equations are coupled to each other through the production and loss rates. Thus, formally, the systems of equations have to be solved simultaneously.

Using scale analysis, one can define the diffusive lifetime τ_D and chemical lifetime τ_{Q_i} with

$$\frac{\partial f_i}{\partial t} \sim \frac{f_i}{\tau_D} + \frac{f_i}{\tau_{Q_i}} \quad . \qquad (3.1\text{-}2)$$

Note that implicit in (3.1-1) is the assumption that one set of K(z) is applicable to all species. Thus, all species

have the same τ_D while τ_{Q_i} depends on the chemical reactivity of the individual species.

Using the atmospheric scale height

$$H = \frac{kT}{mg} \sim 6 \text{ km}$$

as the typical length scale, one estimates that

$$\tau_D \sim \left(\frac{K}{H^2}\right)^{-1} \sim 1 \text{ month.}$$

For atmospheric species, τ_{Q_i} ranges from seconds to hundreds of years. Thus, it is difficult to find a single numerical method that can handle such a large range of timescales.

To solve this problem, one makes use of the chemical properties of the atmospheric species. The diffusive time scale τ_D provides a convenient standard to separate the atmospheric species into two groups. The first group will be referred to as the photochemical species. This corresponds to species having chemical lifetimes, $\tau_{Q_i} \ll \tau_D$ (about 1 day or less) so that they are always in photochemical equilibrium. As a result, the diffusive term can be ignored for these species. The rest of the species will be referred to as diffusive species. Next we examine the coupling among the various species. Because of their short chemical lifetimes, the photochemical species are strongly coupled to each other while only weakly coupled to the diffusive species. In contrast, the diffusive species are only weakly coupled to each other and the photochemical species. The only exception may be the case of O_3 whose distribution directly affects transmitted solar fluxes and modulates the local photolysis rates. Thus, the chemical properties of the atmospheric species

suggest that the systems of equations should be treated as two separate groups:

for photochemical species

$$\frac{\partial n_i}{\partial t} = [P_i - L_i n_i] \qquad (3.1\text{-}3)$$

and for diffusive species

$$\frac{\partial f_i}{\partial t} = \frac{1}{N}\{\frac{\partial}{\partial t}(KN\frac{\partial f_i}{\partial t}) + (P_i - L_i n_i)\} \qquad (3.1\text{-}4)$$

The partitions of the atmospheric species into the photochemical and diffusive species in the present model are given in Appendix A. The systems of equations are to be solved by an iterative scheme. Within each iteration, equations (3.1-3) are to be solved simultaneously while (3.1-4) are to be solved one at a time. This approach is justified by the characteristic of the chemical couplings discussed before. The feedback between iterations is achieved via the revised production and loss rates arising from newly calculated species densities. The algorithm is schematically outlined in Fig. 3-1.

One major simplification arises in that equations (3.1-3) are uncoupled in their altitude dependence. Thus, they can be solved one altitude at a time. Equations (3.1-4) are second order in the spatial variables and will require boundary values for unique solutions. In modeling, this usually is done by giving the flux at the top of the atmosphere and the value f_i or the flux at the ground level. The exact methods used for solving (3.1-3) and (3.1-4) will be presented

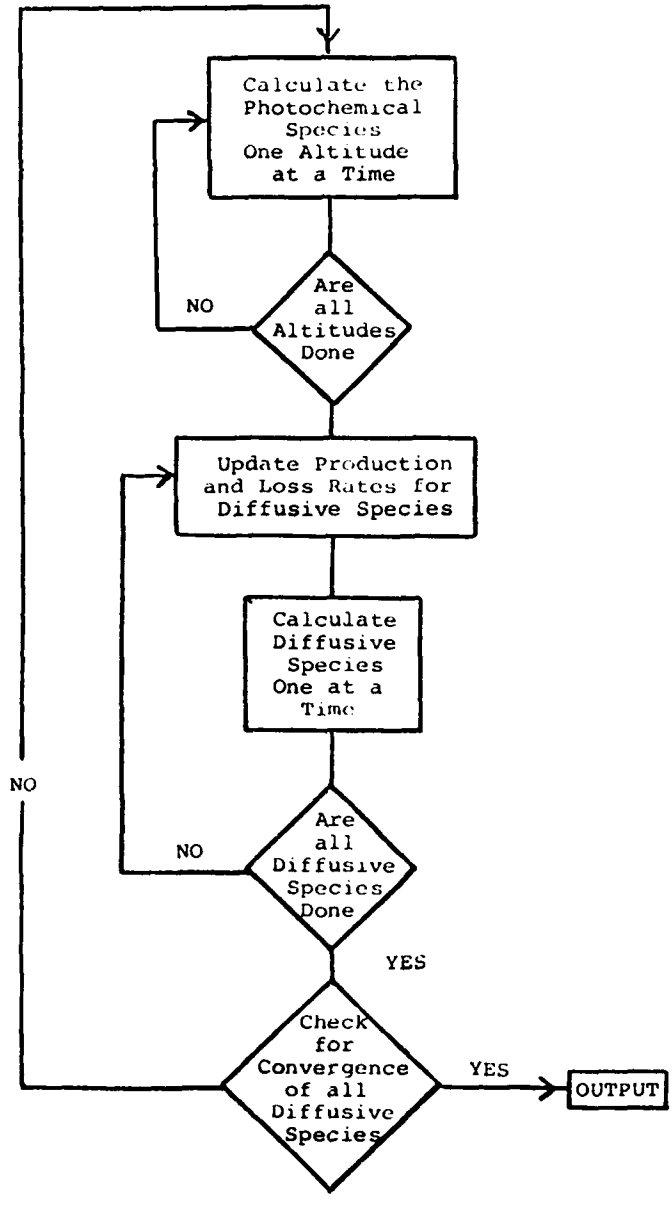

Figure 3-1
Schematic Flow Chart for 1-D Model

in Appendix A. In the next section, the time dependence of the equations will be analyzed.

3.2 The Time Dependence

Solar radiation is the ultimate driving force for atmospheric chemistry. As a result, all the photochemical species inherit the 24 hour periodicity. For the diffusive species, their lifetimes are sufficiently long that they do not respond to the diurnal variation. However, additional time dependence may arise for boundary conditions, e.g., the time-dependent atmospheric injection of F-11 and F-12. In this section, we will concentrate on the treatment of the diurnal time dependence only.

If one is not interested in the diurnal behavior of the species, one can obtain the diurnal-average version of equations (3.1-3) and (3.1-4) by averaging them over a period of one day. One then has

$$0 = \bar{P}_i - \overline{L_i n_i} \qquad (3.2\text{-}1)$$

$$0 = \frac{1}{N}\left\{\frac{\partial}{\partial z}\left(KN\frac{\partial \bar{f}_i}{\partial z}\right)\right\} + \bar{P}_i - \overline{L_i n_i} \qquad (3.2\text{-}2)$$

In the above equations $\overline{\quad}$ denotes diurnal average, i.e., given $h(t,z)$,

$$\bar{h}(z) = \frac{1}{24\ \text{hr}} \int_{\substack{\text{over}\\ 24\\ \text{hours}}} h(t,z)\,dt \ .$$

In deriving (3.2-1) and (3.2-2), it is assumed that K, N are not functions of time and we have ignored other time dependence for the purpose of this discussion. Next, we would like to point out that the terms P_i and $L_i n_i$ consist of sums of terms each of which have either one of the following three forms

$$J_i n_i, \quad k_{ij} n_i n_j, \quad k_{ijk} n_i n_j n_k$$

corresponding to photolysis reaction, two-body and three-body reaction. Thus, one must find some way of evaluating $\overline{J_i n_i}$, $\overline{k_{ij} n_i n_j}$, and $\overline{k_{ijk} n_i n_j n_k}$ before one can solve the systems of equations.

Given g(t,z) and h(t,z), one can define

$$g'(t,z) = g(t,z) - \bar{g}(z)$$

$$h'(t,z) = h(t,z) - \bar{h}(z) .$$

Then, by definition

$$\overline{g'}(z) = \overline{h'}(z) = 0$$

and $$\overline{gh} = \bar{g}\bar{h} + \overline{g'h'} . \qquad (3.2-3)$$

Thus, the mean of a product is not equal to the product of the mean. The correction term $\overline{g'h'}$ cannot be estimated except by performing the full diurnal calculation in obtaining g(t,z) and h(t,z). In the diurnal-average version of the model, we simply assume that the correction terms are small compared to the product. The validity of this assumption has been questioned (NASA, 1977). We will discuss how good this assumption is in the next section.

In the diurnal version of the model, equations (3.1-1) are retained. The systems of equations

$$\frac{\partial n_i(t)}{\partial t} = P_i(t) - L_i(t) n_i(t) \qquad (3.2\text{-}4)$$

is a non-linear system of differential equations in time. Initial conditions must be specified before a unique solution can be obtained. However, since the initial conditions are not exactly known for most calculations, we will instead impose a periodic boundary condition on the system by requiring

$$n_i(t + 24 \text{ hour}) = n_i(t) \qquad (3.2\text{-}5)$$

for all species and at all altitudes. (Note that the z dependence has not been explicitly included in (3.2-4) since the equations are uncoupled in altitude.) The systems of equations are solved by first deriving a finite difference scheme to propagate the solution $n_i(t)$ in time. The equations are then propagated until all species satisfy the periodic boundary conditions. Further details are presented in Appendix A.

The diurnal average version of (3.1-2) is used for the diffusive species even in the diurnal option. The rationale here being that the concentrations of the diffusive species are not going to change appreciably in a day's time. However, in contrast to the diurnal-average option, the term $\bar{P} - \overline{L_i n_i}$ is computed exactly using the time-dependent photochemical species concentrations.

3.3 The Diurnal Model

In this section, we will discuss some of the results from the diurnal model. A detailed description of the model is given in Appendix A.

Clearly, the diurnal model is useful in interpreting the available radical observations. These measurements are made at definite local times with definite sun angles. Since concentrations of radical species can change by orders of magnitude as a function of the time, a diurnal calculation is necessary for a meaningful comparison.

In the present model, a time step of 1 hour is employed during the daylight hours, 2 hours for night time and ½ hour intervals at dawn and dusk. Since an implicit scheme is used, the choice of the time step can be made without worrying about problems of numerical stability. The present choice of time step is adequate for the purpose of obtaining the diurnal behavior of the photochemical species. However, if one is interested in behavior of the species during dusk and dawn (e.g., in case of interpreting limb-scan data), the time resolution during dawn and dusk should be refined.

Our calculation shows that many of the radical species have rather strong diurnal variations. Fig. 3-2 through Fig. 3-4 show the diurnal behavior of O, ClO and NO_2 for selected altitudes. The question arises as to how the diurnal average version of the model approximates the actual behavior of the radical concentrations.

If $n_s(z)$ is the solution to the diurnal average equation (3.2-1), one can compare that to $\overline{n(t,z)}$ where

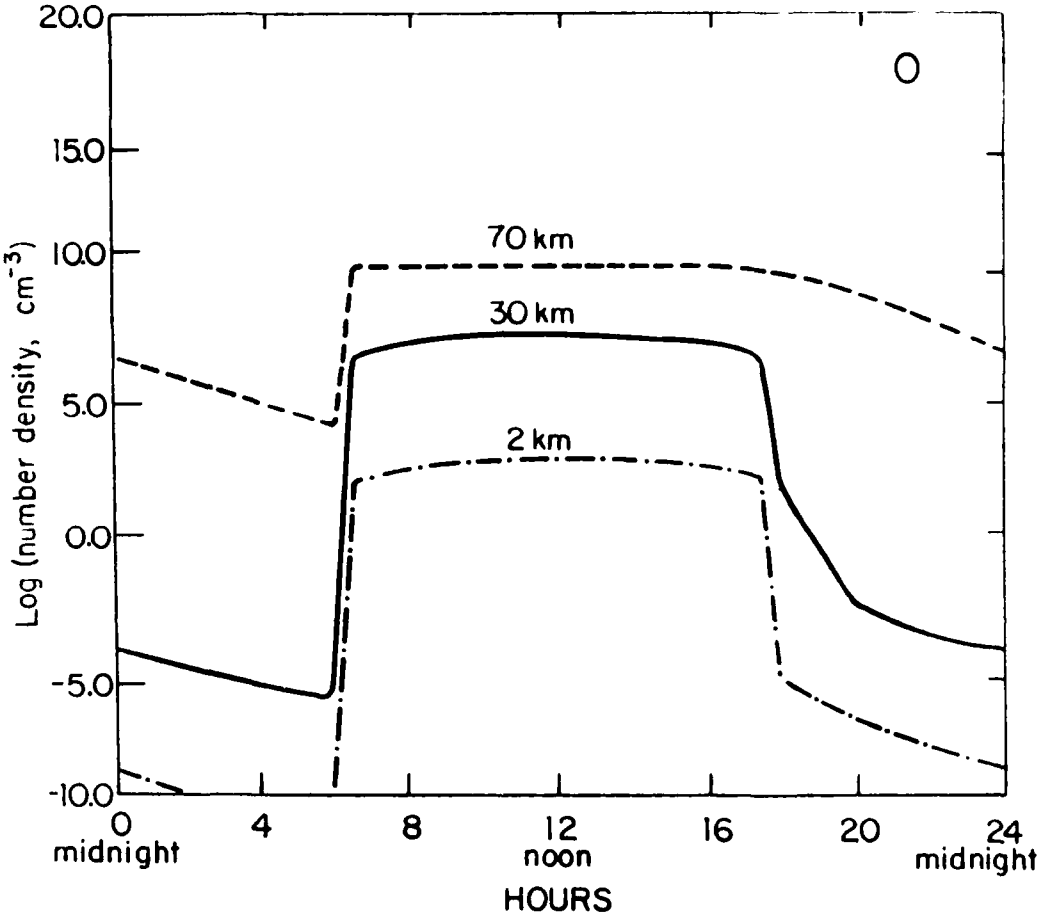

Figure 3-2
n_o (t,z) for Selected Altitudes

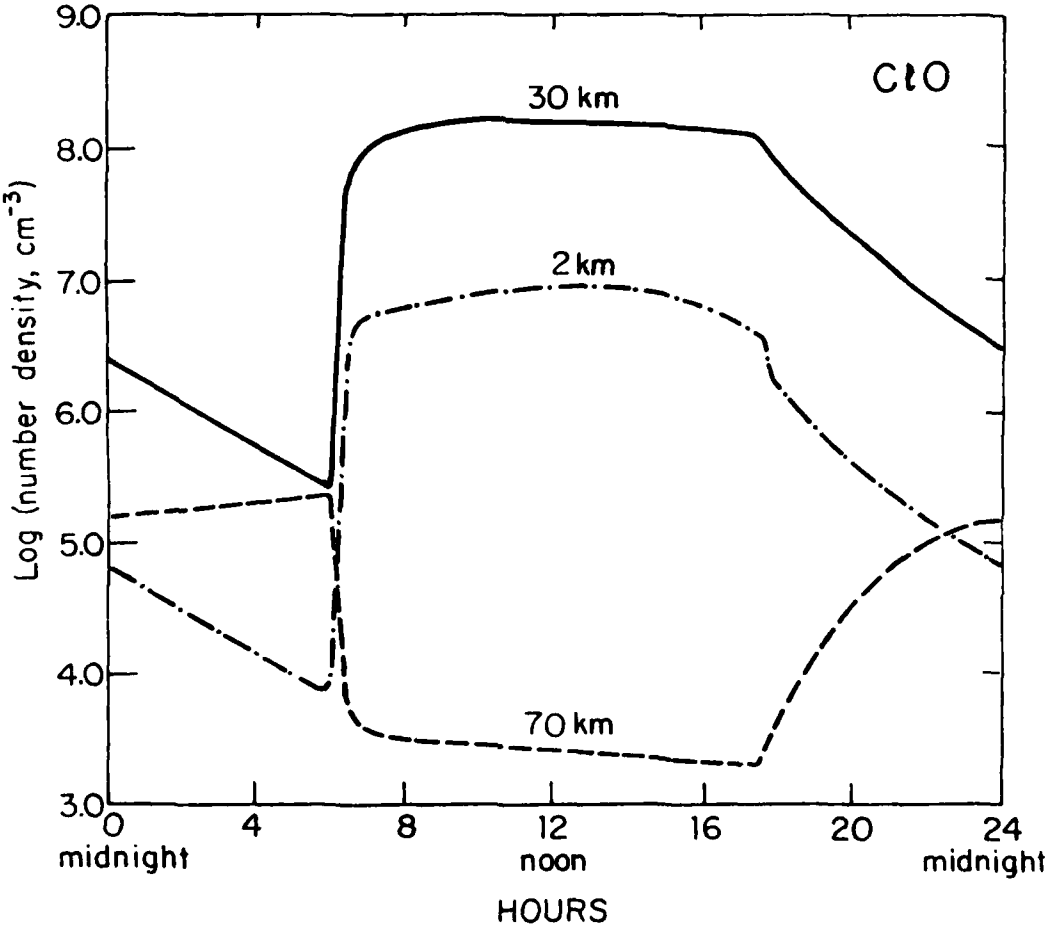

Figure 3-3
$n_{ClO}(t,z)$ for Selected Altitudes

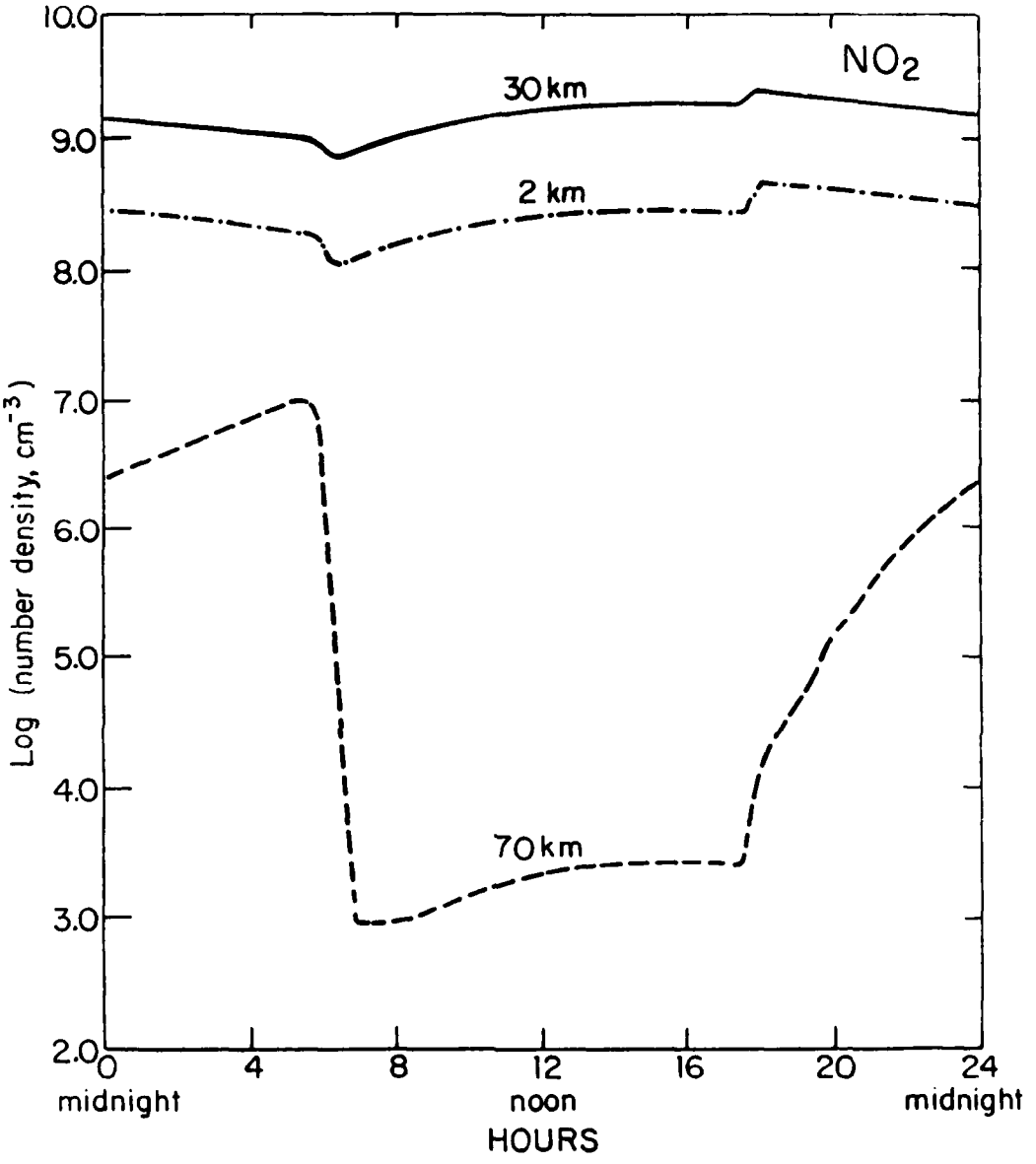

Figure 3-4

$n_{NO_2}(t,z)$ for Selected Altitudes

$$\overline{n(t,z)} = \frac{1}{24\ \text{hour}} \int_{\substack{\text{over}\\ 24\\ \text{hours}}} n(t,z)\, dt$$

with n(t,z) being the solution to (3.2-3). Fig. 3-5 - Fig. 3-7 show the comparison for O, ClO and NO_2 respectively. We note that $n_s(z)$ agrees better with $\overline{n(t,z)}$ for the day time species than the night time species. In particular, $n_s(z)$ grossly underestimates $\overline{n(t,z)}$ for night time species. It is clear why this should be the case as the steady state model represents the case with continuous sunlight and thus would produce results that approxiamte the day time number densities for all species.

In section 3.2, we discussed the question concerning the accuracy of the approximation,

$$\overline{n_i n_j} \simeq \bar{n}_i \bar{n}_j \quad .$$

In the case of O_3, one of the terms in the loss rate is proportional to the production of $n_O(t,z)$ and $n_{ClO}(t,z)$. With proper diurnal averaging, this term should be given by

$$A(z) \equiv \overline{n_O(t,z)\, n_{ClO}(t,z)} \quad .$$

If one ignores the correction term and approximates the mean of the product by the product of the mean, one gets

$$B(z) = \overline{n_O(t,z)}\ \overline{n_{ClO}(t,z)} \quad .$$

Finally, in the diurnal-average version, one simply has

$$C(z) = n_{s_O}(z)\, n_{s_{ClO}}(z) \quad .$$

Fig. 3-8 shows a plot of the three quantities as functions of altitudes. It is evident from the curves that the discrepancy among the various averaging methods could be as

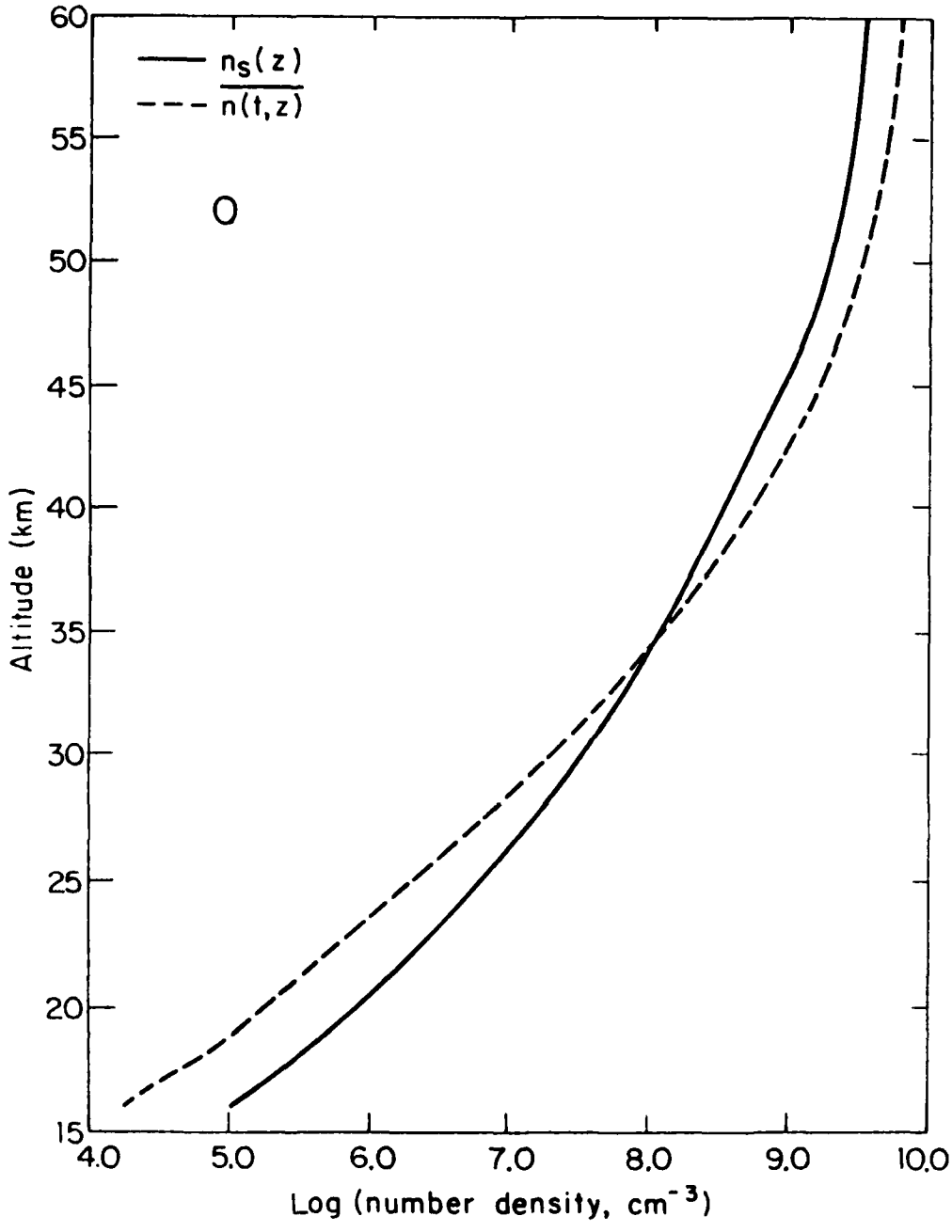

Figure 3-5
Plot of $n_s(z)$ vs $\overline{n(t,z)}$ for O

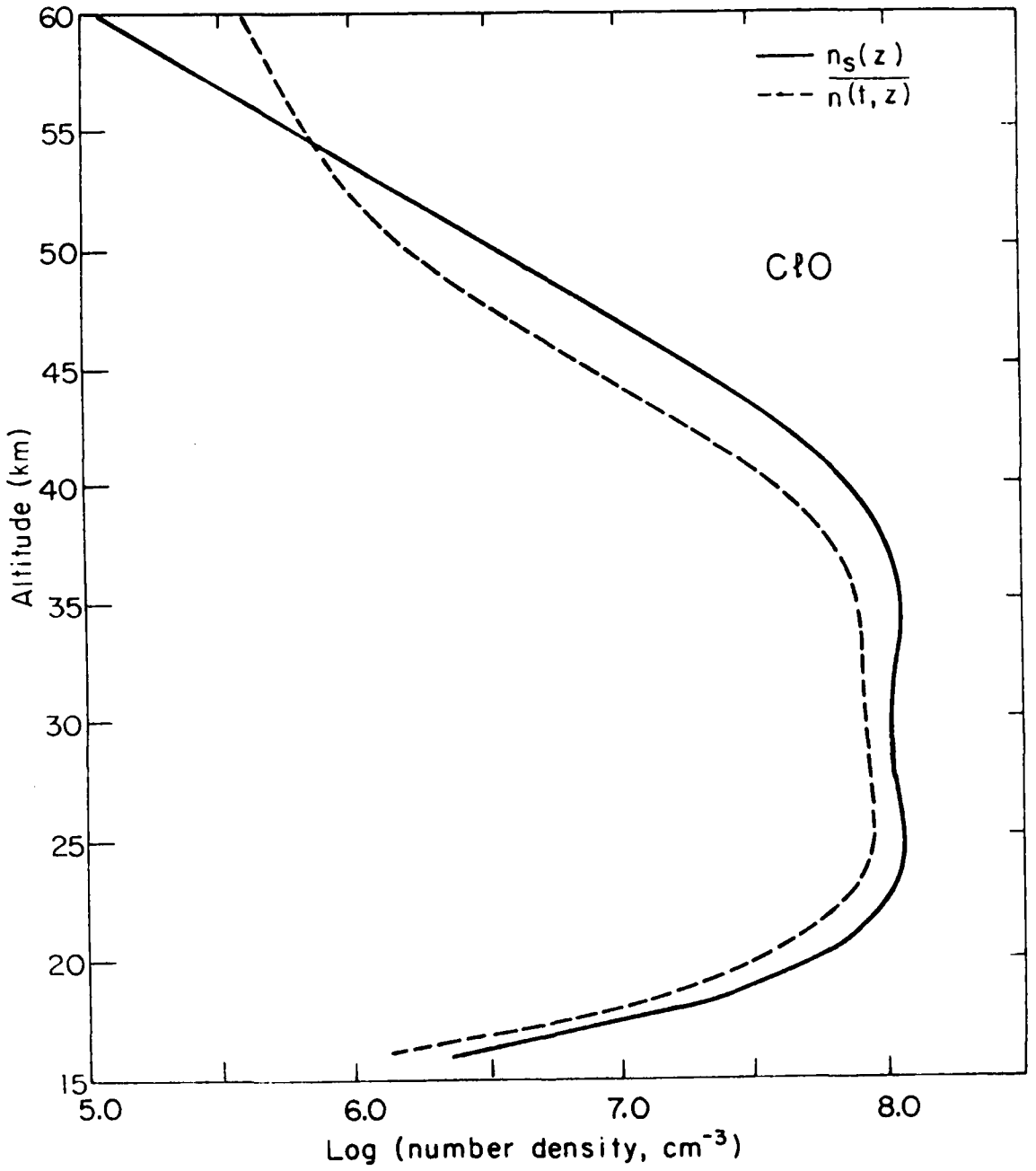

Figure 3-6
Plot of $n_s(z)$ and $\overline{n(t,z)}$ for ClO

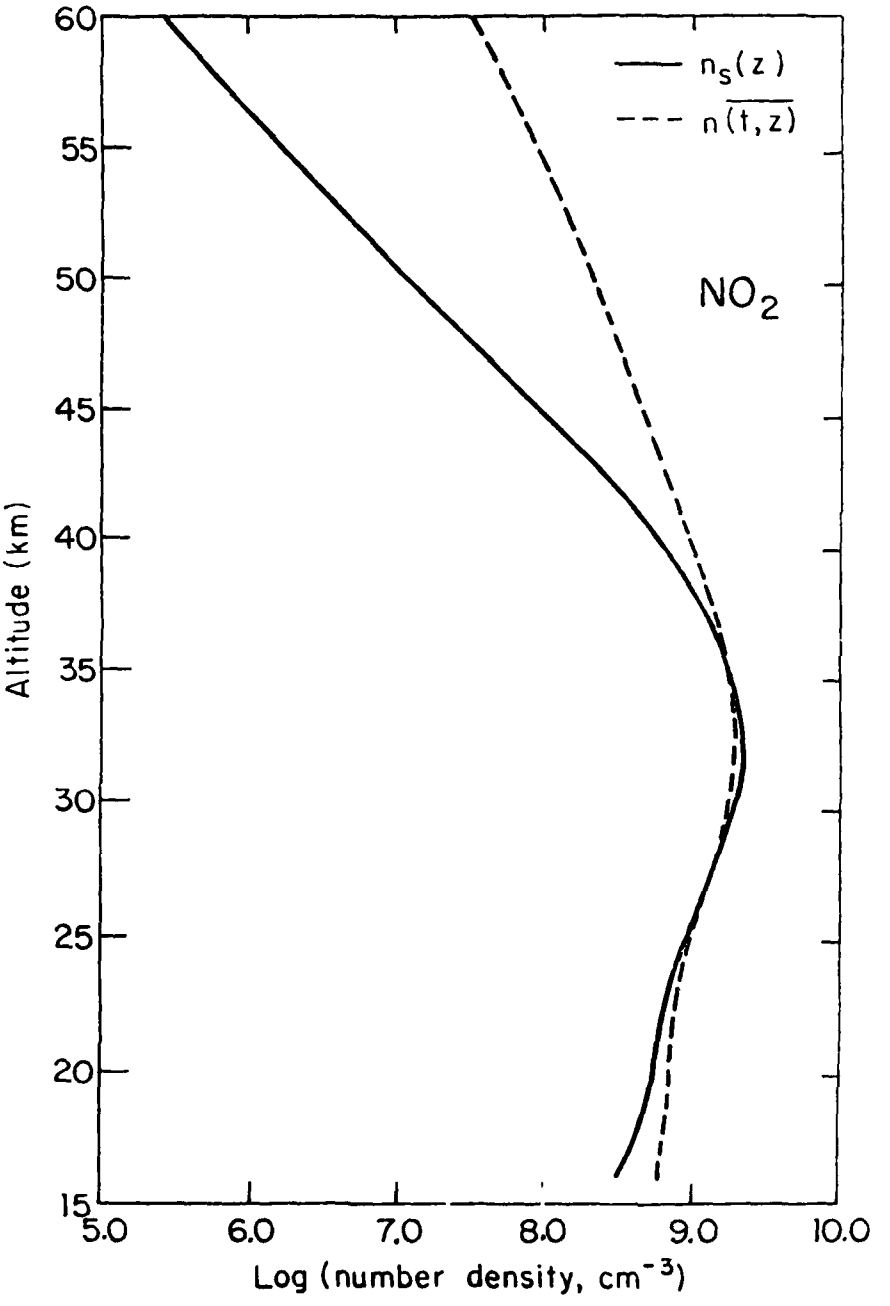

Figure 3-7
Plot of $n_s(z)$ and $\overline{n(t,z)}$ for NO_2

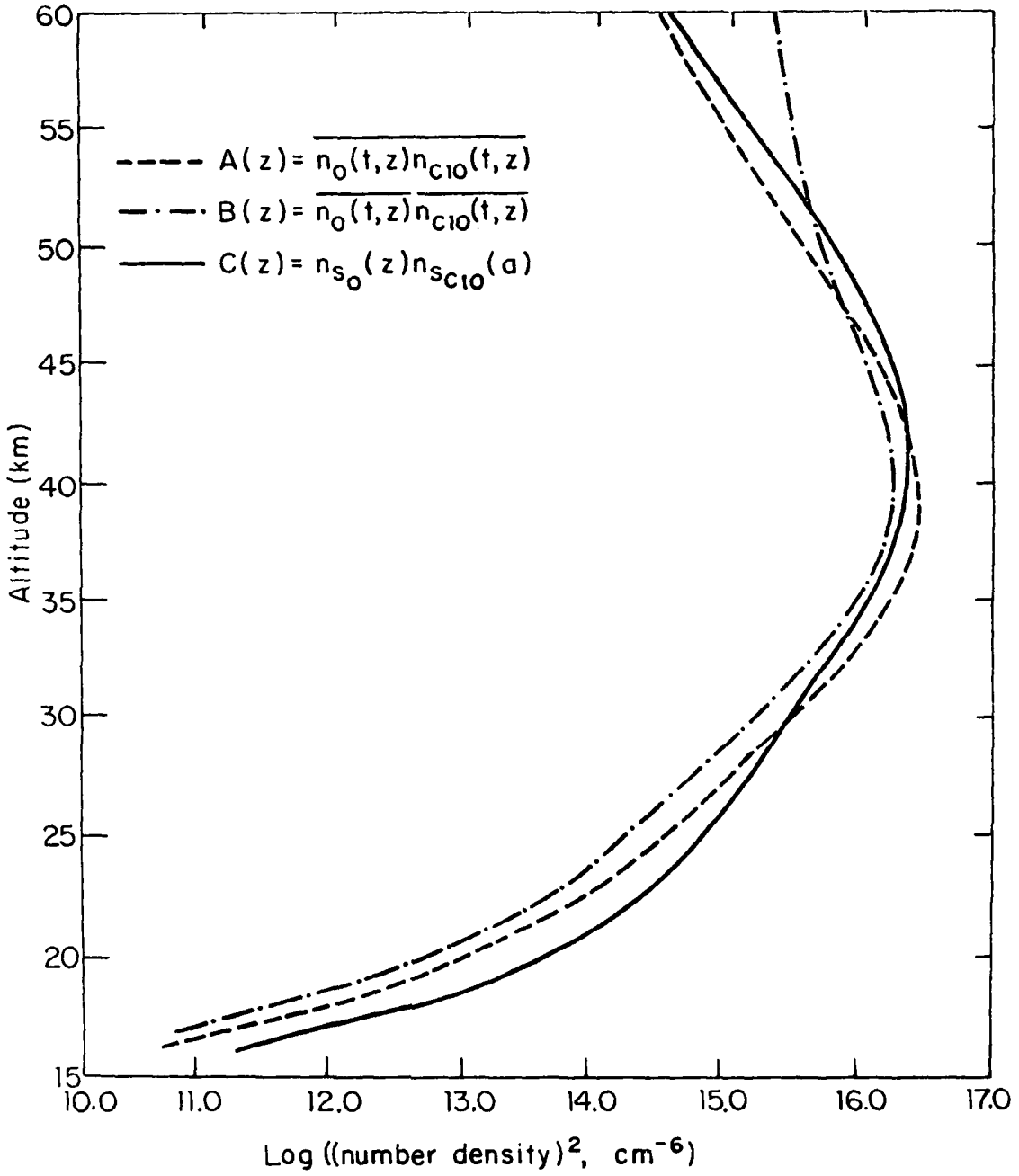

Figure 3-8
Plot of A(z), B(z) and C(z)

high as factor of 3. However, it turns out that the majority of the terms in the production and loss rates for the diffusive species are not comprised of products of photochemical species. Thus, in spite of the large discrepancy in the individual terms, it only contributes to about 10-20% of the net production and loss rates. As a result, for the case of O_3, the differences between the concentrations calculated using the diurnal-average version and the diurnal version are typically about 10-20%.

4. COMPARISON BETWEEN THEORY AND OBSERVATION

The comparison between model calculations with observational data permits an important test for the validity of the theoretical models used in the assessment of any environmental problem including the impact of fluorocarbons on atmospheric ozone. It may also serve as a basis for identifying any important missing elements in our current understanding of the atmospheric chemical and dynamic processes, should there be serious discrepancy between theory and observations.

One of the major difficulties in drawing conclusions from comparing theory with observations lies in the fact that most trace gases exhibit large local variabilities much of which are not well understood. Although current models can simulate diurnal variations of many trace gases, they cannot account for the local variability attributed to dynamics or other atmospheric fluctuations. Nevertheless, within the framework of the 1-D model, a number of observations, notably the ClO/O_3, HNO_3/NO_2 and HF/HCl data, cannot be made entirely consistent with current theory.

The inconsistency could simply be due to the uncertainties in the currently adopted rate constants or the eddy diffusion profile. It may also suggest serious omission of chemistry or dynamics in the models. In either case, this could have important implications for the assessment of the stratospheric pollution problems.

4.1 Odd Oxygen ($O(^3P)$, O_3)

Figure (4.1-1) shows the calculated $O(^3P)$ profiles along with Anderson's data. Although the theoretical $O(^3P)$ profile lies within the envelope defined by the data, it should be noted that the spread in $O(^3P)$ data is relatively wide (~factor ±2) in the region below ~33 km. In the context of present photochemical theory, $O(^3P)$ should be in photochemical equilibrium with O_3. Thus, for a given solar zenith angle, the variations in $O(^3P)$ mainly reflect the variations in O_3 density. Quantification of O_3 variations are therefore important for ascertaining the significance in the observed variability of $O(^3P)$.

Table (4.1-1) shows the calculated $O(^3P)/O_3$ ratio along with Anderson's observations taken on 12/2/77. The calculated ratio is relatively insensitive to the diffusion coefficients and to the photochemistry of NO_x, HO_x and ClX. To an excellent approximation, the $O{:}O_3$ ratio is given by

$$\frac{[O(^3P)]}{[O_3]} = \frac{J_3}{k_1[O_2][M]} \qquad (4.1\text{-}1)$$

where J_3 denotes the photolysis rate of O_3 and k_1 the rate constant for the reaction $O + O_2 + M \rightarrow O_3 + M$. Equation (4.1-1) defines one of the most basic relations in stratospheric chemistry. While there seems to be good agreement between the calculated and observed O/O_3 ratios, a definitive conclusion cannot yet be drawn. It should perhaps be pointed out that the calculated J_3 assumes some kind of planetary albedo,

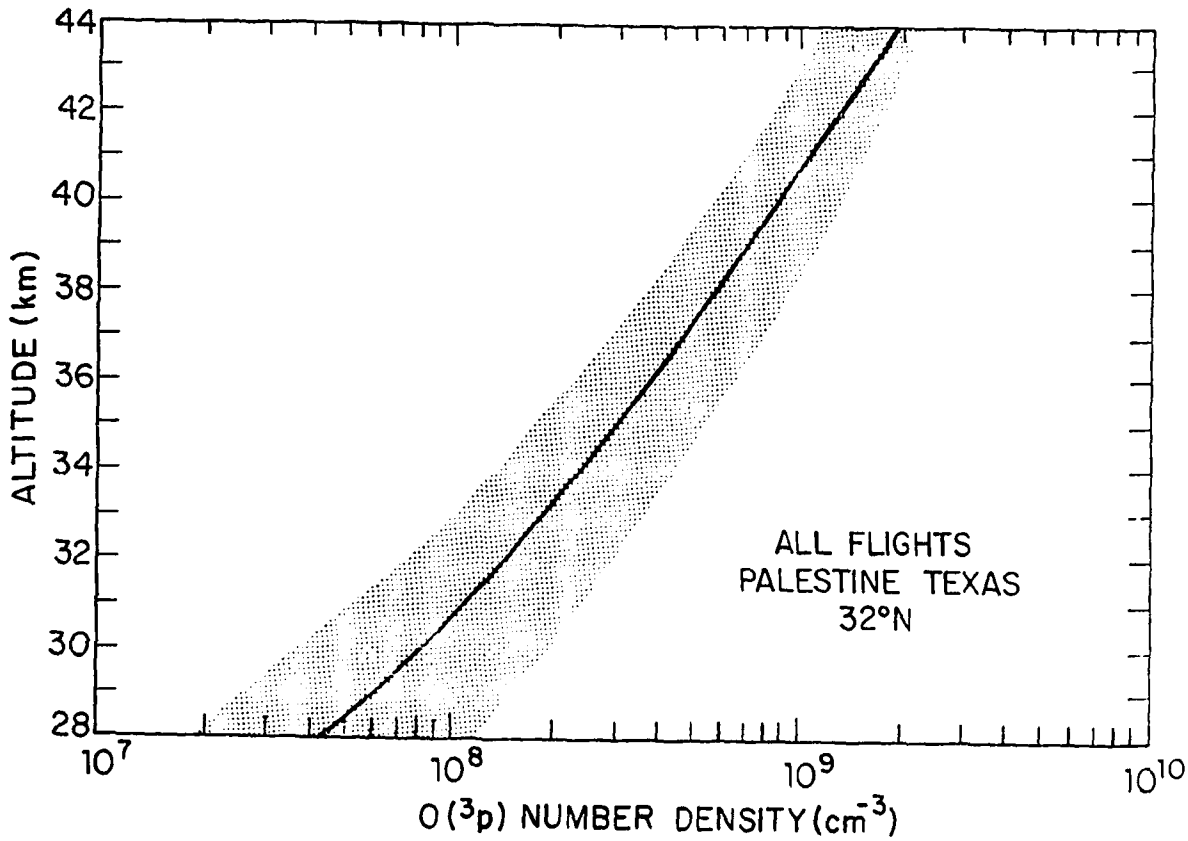

Figure 4.1-1

Calculated profile for O(^{3}P) together with data from Anderson et al.

TABLE 4.1-1

OBSERVED VS. CALCULATED $[O(^3P)]/[O_3]$
12/2/77 $\chi = 50°$

ALTITUDE (km)	OBSERVED $[O(^3P)]/(O_3)$	CALCULATED Logan et al. (1978)	CALCULATED Sze et al. (1978)
42	+4.8 (-3)	3.8 (-3)	4.5 (-3)
41	3.0 (-3)	2.4 (-3)	2.85 (-3)
40	1.6 (-3)	1.6 (-3)	1.8 (-3)
39	1.0 (-3)	1.0 (-3)	1.1 (-3)
38	6.2 (-4)	6.2 (-4)	7.17 (-4)
37	3.7 (-4)	4.1 (-4)	4.5 (-4)
36	2.2 (-4)	2.6 (-4)	2.9 (-4)
35	1.4 (-4)	1.7 (-4)	1.89 (-4)
34	9.6 (-5)	1.1 (-4)	1.05 (-4)
33	7.7 (-5)	7.6 (-5)	8.04 (-5)
32	5.4 (-5)	5.1 (-5)	5.3 (-5)
31	4.3 (-5)	3.4 (-5)	3.5 (-5)
30	3.1 (-5)	2.2 (-5)	2.4 (-5)

+ 4.8 (-3) denotes 4.8×10^{-3}.

while Anderson's experiment did not include a measurement of albedo. Thus the agreement could be fortuitous.

Figure (4.1-2) shows the calculated O_3 profiles along with observations. The O_3 behavior below 26 km is very sensitive to HO_x chemistry. In our earlier calculation, the calculated O_3 concentrations below 26 km as well as the total column density are 20% higher than observation as a result of the revised rate constant (Howard and Evenson, 1977) for the reaction,

$$HO_2 + NO \rightarrow OH + NO_2 \quad . \qquad (4.1\text{-}2)$$

Recent revision in another rate constant for the important reaction of HO_2 with O_3 removes most of the discrepancy between the calculated and the observed ozone abundances below 26 km.

The calculated O_3 concentration above 40 km however, still seems to lie somewhat below most observation data particularly those of Riegler et al. (1977). It is unfortunate that the apparent discrepancy between various sets of O_3 data (Kruger and Minzner, 1976; Wantanabe and Tohmatsu, 1976; Hering and Borden, 1967; Riegler et al., 1977) are not yet resolved. It would seem that simultaneous measurements of $O(^3P)$, O_3 and OH would permit a relatively straight forward test for the odd oxygen balance above 44 km (Sze, 1979), a region where removal of odd oxygen is dominated by the reactions $O + OH \rightarrow H + O_2$; $O + HO_2 \rightarrow OH + O_2$ and $O + O_3 \rightarrow 2O_2$.

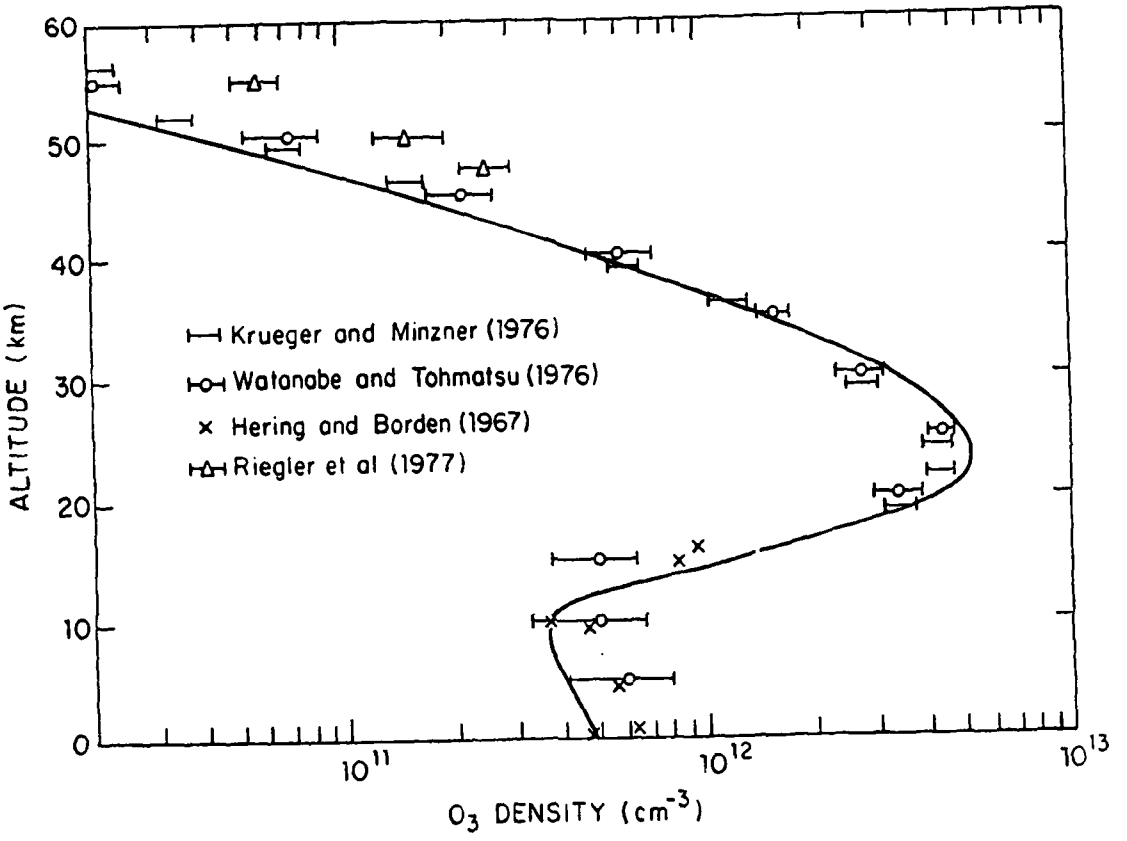

Figure 4.1-2

Calculated O_3 profile along with data.

4.2 Hydrogen Radicals (OH, HO_2)

Figures (4.2-1) and (4.2-2) show the calculated OH and HO_2 profiles at solar zenith angle χ = 40° along with Anderson's data. Agreement between theoretical and observed profiles seems to be reasonably good. Data for OH and HO_2 below 30 km, however, are still lacking. The OH concentration in this region (z < 30 km) may only be inferred indirectly from simultaneous measurements of certain ratios (e.g. HF:HCl; HNO_3:NO_2; ClO:HCl) or from certain atmospheric species (e.g. C_2H_6) whose altitude distributions are extremely sensitive to OH abundance.

4.3 Free Chlorine Species

Figure (4.3-1)shows the calculated ClO profiles along with observations. There are six ClO profiles reported by Anderson et al. (1979) and one by Menzies (1979). An excellent discussion on the ClO data and the implications for stratospheric chemistry is given by Anderson et al. (1980). We shall summarize here some of the interesting features regarding the ClO distribution.

Four of Anderson's ClO profiles measured in fall and winter lie below 1 ppbv, whereas two of the summer profiles exceed 1 ppbv above 30 km. During the July 14, 1977 experiment, simultaneous OH and O_3 concentrations were measured along with ClO. The observed high ClO data (with peak mixing ratio ~8 ppbv) and normal O_3 are not explicable in the present

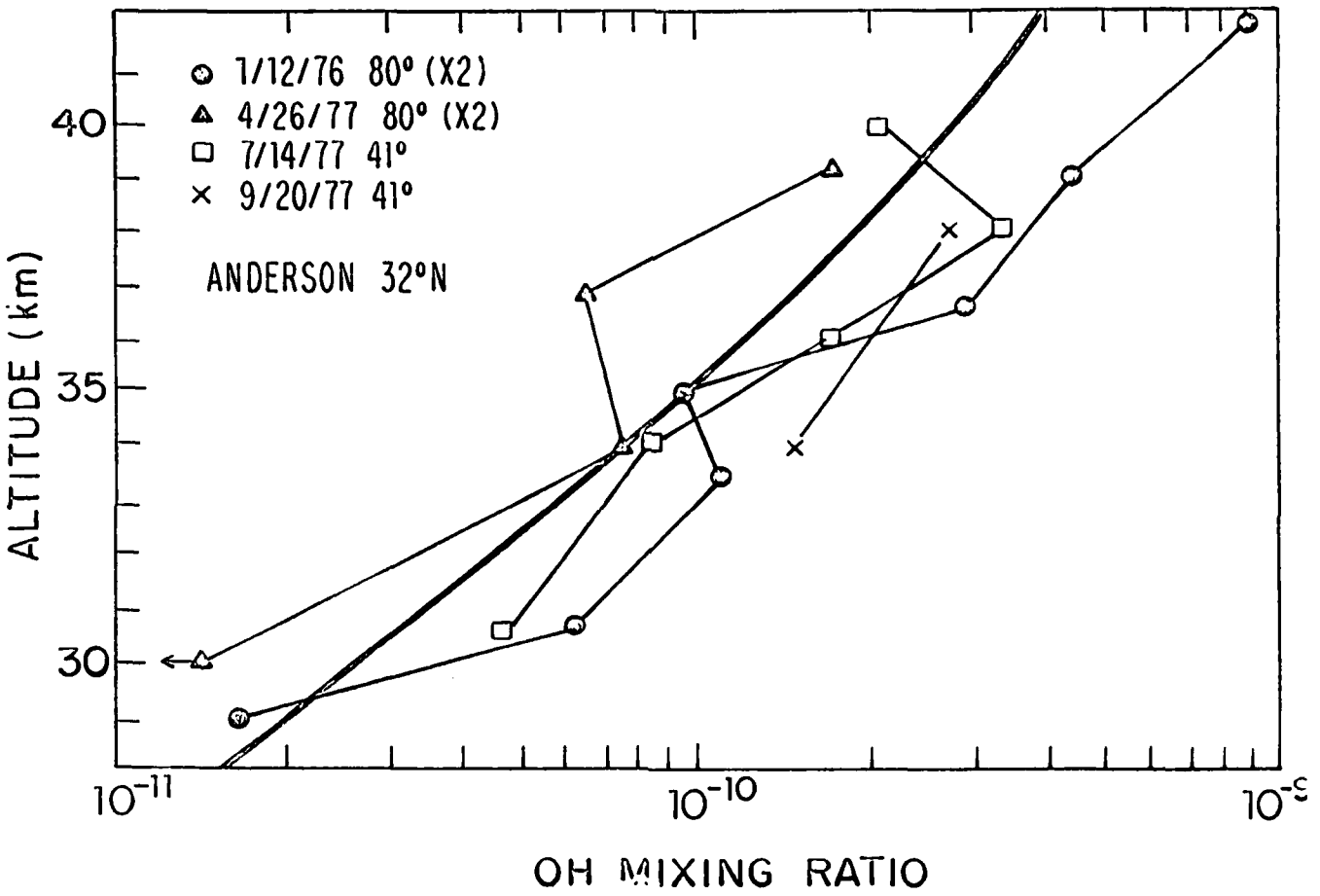

Figure 4.2-1

Calculated altitude profiles for OH mixing ratio corresponding to 41° zenith angle. The data from Anderson (see NASA, 1979) are included for comparison. The observations were made at 32°N. The zenith angles during observations are given in the figure. Note that the observations with zenith angle of 80° have been adjusted by factor of two for comparison purposes.

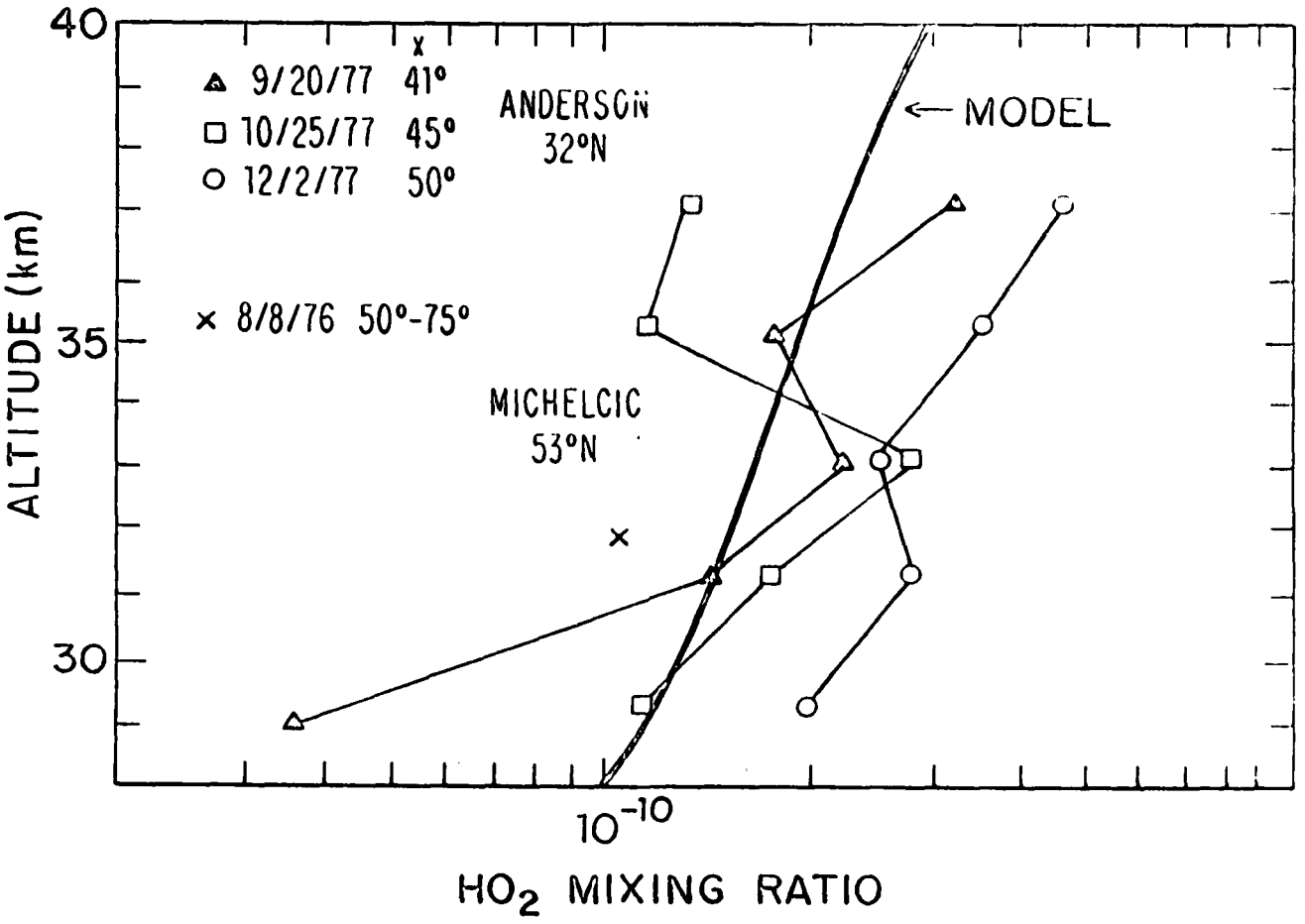

Figure 4.1-2

Calculated altitude profiles for HO_2 mixing ratio corresponding to 41° zenith angle. The data from Anderson (see NASA, 1979) and Mihelcic et al. (1978) are included for comparison. The observations were made at 30°N and 53°N respectively. The zenith angles during observations are given in the figure.

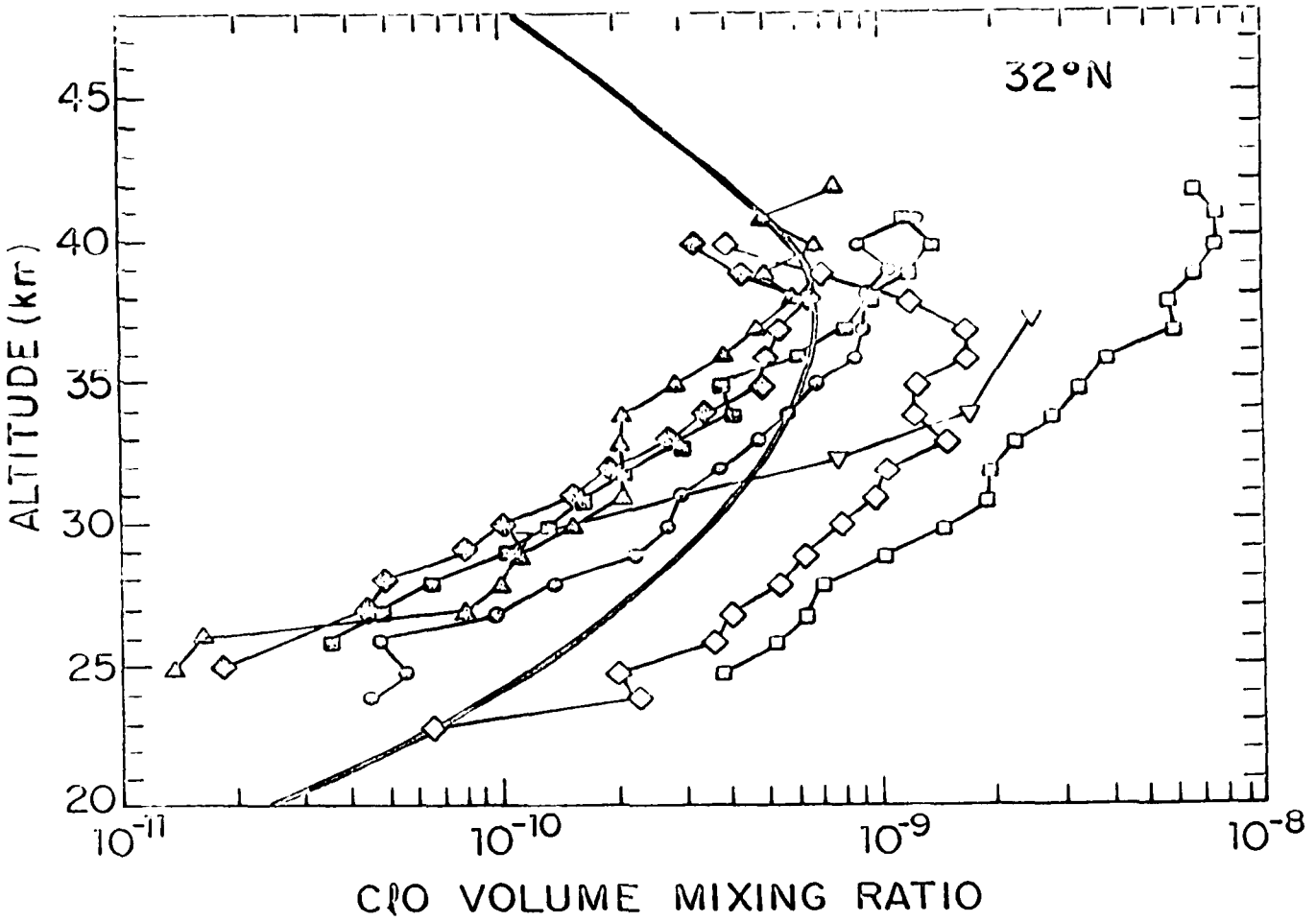

Figure 4.3-1

Calculated altitude profiles of ClO mixing ratio corresponding to 41° zenith angle. The observations from Anderson et al. (1980) and Menzies (1979) are included for comparison. Zenith angles (χ) for the observations are

□	14 July 1977	χ=41°	Anderson et al. (1980)
◇	28 July 1976	χ=43°	
▲	25 Oct 1977	χ=45°	
○	20 Sept 1977	χ=41°	
◆	8 Dec 1976	χ=55°	
■	2 Dec 1977	χ=50°	
▼	20 Sept 1978	χ=95°	Menzies (1979)

theoretical framework. Anderson et al. (1980) argued that the large values of ClO could not be attributed to experimental error. They concluded that the observations implied either (a) that significant quantities of ClO were injected into the study region prior to their measurement, on a time short compared with the chemical response time for odd oxygen (about a day at 40 km), or (b) that the reaction of ClO with O was not rate limiting in the closure of the chlorine catalytic cycle, or (c) that there exist sources for odd oxygen proportional to ClO_x which can compete directly with photolysis of O_2 in the middle and upper stratosphere.

Another serious discrepancy revealed by Anderson et al.'s data concerns the rapid fall off of ClO mixing ratio below 30 km. One straight forward way to reconcile the lower stratospheric ClO data is to suppress the OH concentration below 30 km.

Figure (2.6) shows the calculated $ClONO_2$ profile along with recent data by Murcray et al. (1979). The apparently good agreement between calculated and observed $ClONO_2$ concentrations may be fortuitous in view of the paucity of $ClONO_2$ data and uncertainties in $ClONO_2$ chemistry. For instance, there is no direct evidence that the reaction ClO with NO_2 yields $ClONO_2$ or $ClNO_3$ isomer as the primary product.

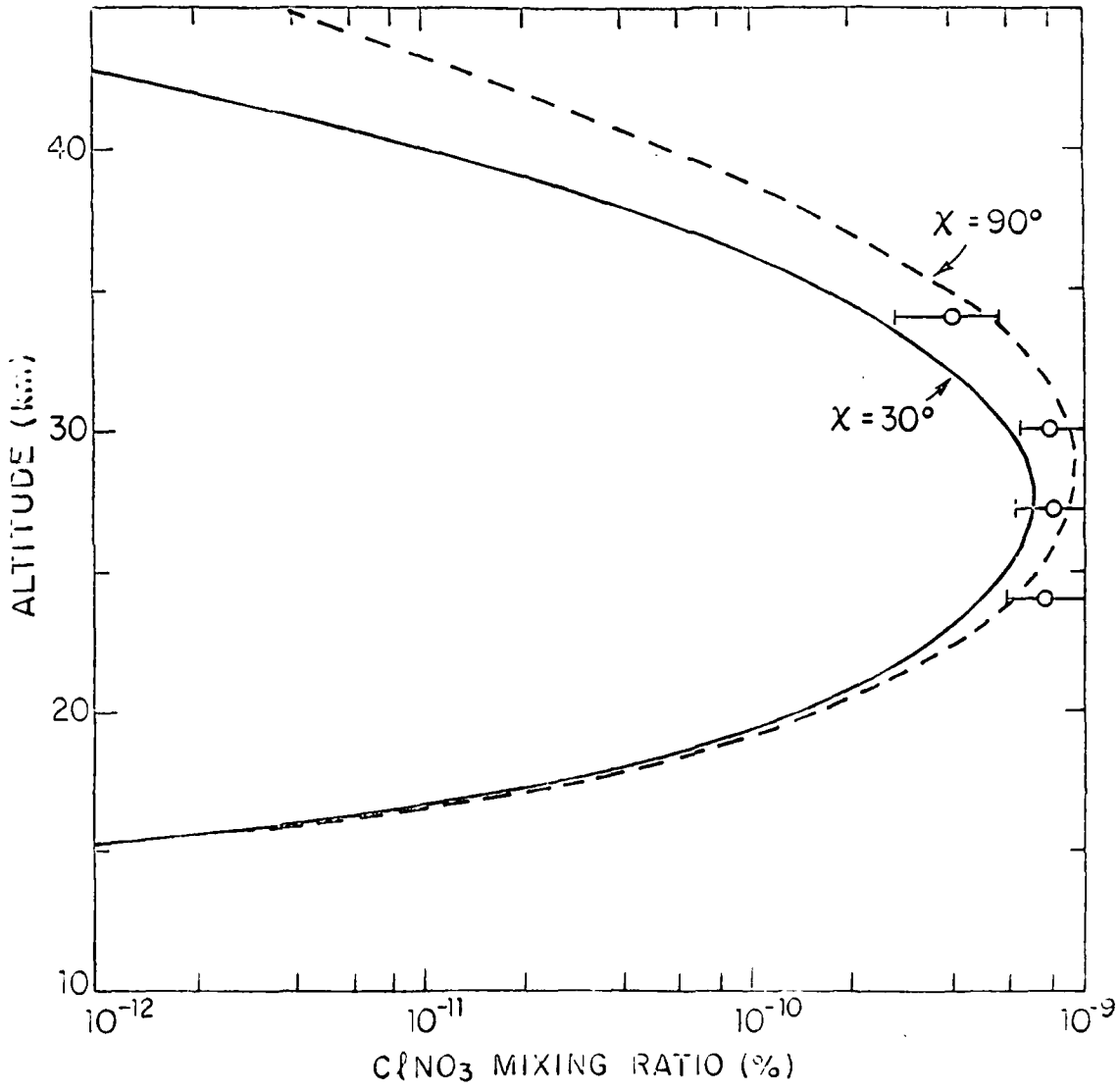

Figure 4.3-2

Calculated altitude profiles of $ClNO_3$ corresponding to 30° and 90° zenith angle. The observations from Murcray et al. (1979) are included for comparison.

4.4 HF:HCl and HNO_3:NO_2 Ratios as Indicators for Stratospheric OH

Figures (4.4-1) and (4.4-2) show the calculated HF:HCl and HNO_3:NO_2 ratios. These two ratios are quite sensitive to stratospheric OH density (NASA, 1977; McConnel and Evans, 1978; Sze, 1978, 1979). Comparison between calculated ratios and observations permits an indirect check on the predicted stratospheric OH abundance below 30 km, where OH data are still lacking.

The calculated HNO_3:NO_2 ratio appears to lie above the observed ratio by about a factor 2-4. The ratio $\frac{[HNO_3]}{[NO_2]}$ in the model is set mainly by a balance of

$$NO_2 + OH + M \xrightarrow{k_1} HNO_3 + M \qquad (4.4\text{-}1)$$

and

$$h\nu + HNO_3 \xrightarrow{k_2} OH + NO_2 \qquad (4.4\text{-}2)$$

$$OH + HNO_3 \xrightarrow{J_3} H_2O + NO_3 \qquad (4.4\text{-}3)$$

with (4.4-2) more important than (4.4-3) It should be defined to adequate precision in the lower stratosphere by

$$\frac{[HNO_3]}{[NO_2]} = \frac{k_1[OH][M]}{J_3 + k_2[OH]} \simeq \frac{k_1[OH][M]}{J_3} . \qquad (4.4\text{-}4)$$

The rate constants k_1 and J_3 are relatively well known. It is difficult therefore to conceive of errors in computation which might cause ratios obtained from (4.4-4) to be high by a factor as large as 4. The discrepancy might be taken to indicate a major error in computed values for OH,

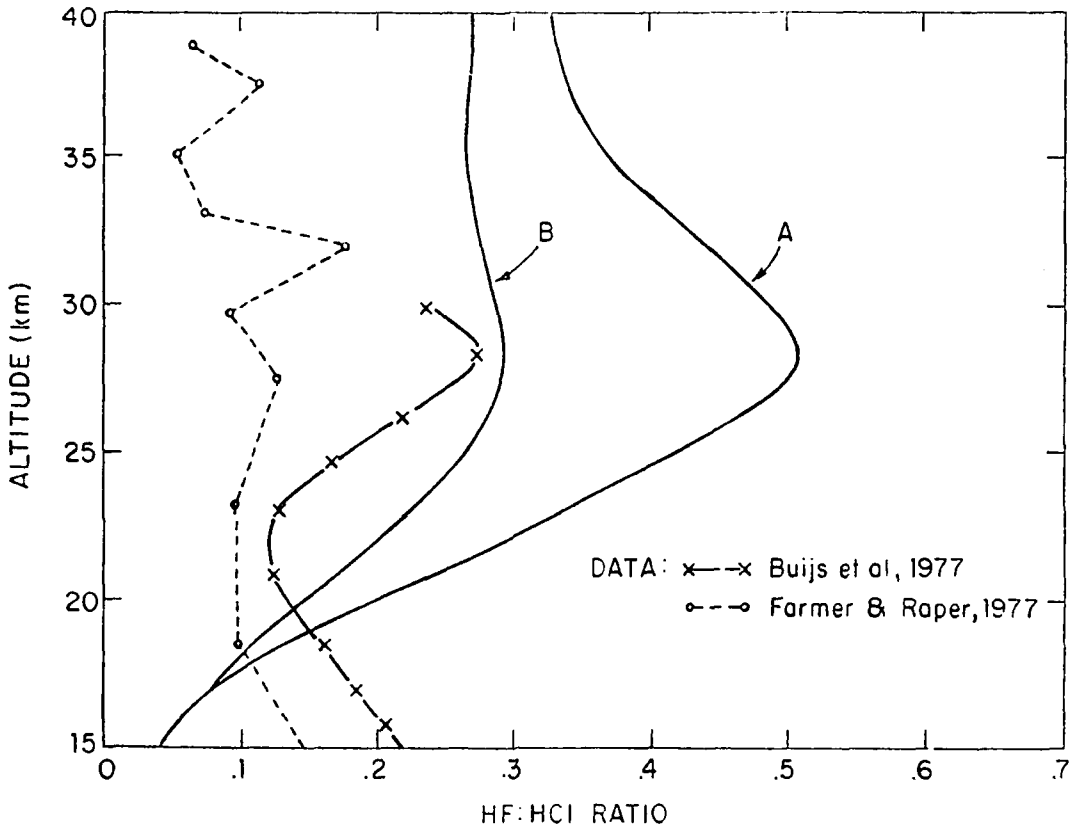

Figure 4.4-1

Calculated HF:HCl ratio corresponding to 30°N equinox condition. H_2O mixing ratios of 4.5 ppmv and 1.0 ppmv are assumed for model A and model B respectively. The observations are

x-x Buijs et al. (1977)
o-o Farmer and Raper (1977)

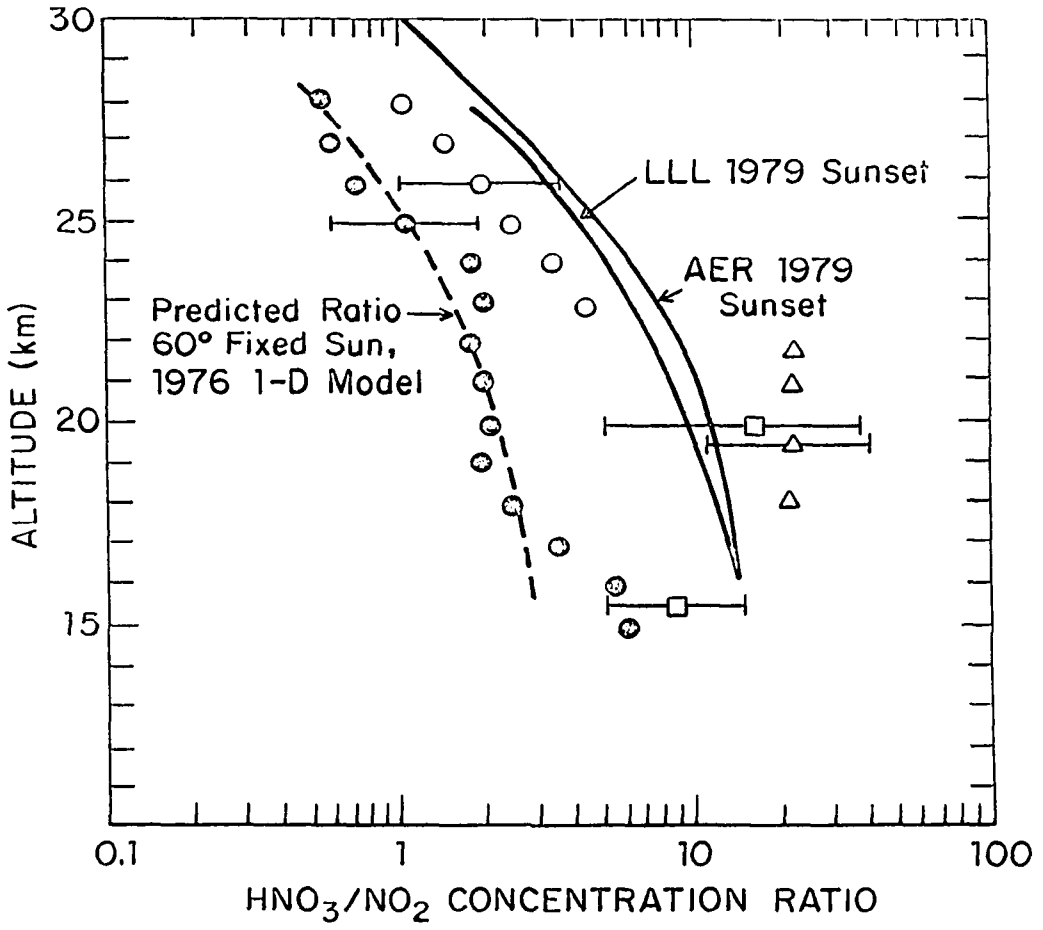

Figure 4.4-2

Ratio of HNO_3/NO_2 as computed from models compared with data. The computed values are for the ratios at sunset for 30°N. The data points are

- Evans et al. (1976) sunset 59°N
- Harris et al. (1976, 1978) noon 44°N
- Fontanella et al. (1975) sunset 45-50°N
- Loewenstein et al. (1978) daytime 20-40°N

in such a sense that model values for OH in the lower stratosphere might be too high. A reduction in OH would be beneficial also for ClO. Reduction in OH would tend to diminish the source of Cl_x from

$$OH + HCl \rightarrow H_2O + Cl \qquad (4.4\text{-}5)$$

and if the change in OH occurred primarily at low altitude, one might expect to find better agreement between model and observed gradients of ClO as well as the ratio of HF:HCl. On the other hand, the model appears to give satisfactory results for OH and HO_2 at higher altitudes as shown in Figures (4.2-1) and (4.2-2).

There are several ways that we might overestimate the OH concentration below 30 km. For example, considerable uncertainty still exists in the rate constant for the reaction

$$OH + HO_2 \xrightarrow{k_6} H_2O + O_2 \qquad (4.4\text{-}6)$$

Laboratory studies by various groups (Hochanadel et al., 1972; Burrows et al., 1978; Chang and Kaufman, 1978; DeMore, 1979) indicate that k_6 may be pressure-dependent. Should k_6 be $\sim 10^{-10}$ cm^3 s^{-1} below 28 km and $\sim 2 \times 10^{-11}$ cm^3 s^{-1} above 34 km, much of the inconsistency between calculated and observed ratios of HF/HCl and HNO_3/NO_2 may be resolved, without contradicting Anderson's OH data above 30 km. It is clear

that the faster rate constants for the reactions of OH with HNO_3 and HO_2NO_2,

$$OH + HNO_3 \xrightarrow{k_7} H_2O + NO_3 \qquad (4.4\text{-}7)$$

$$OH + HO_2NO_2 \xrightarrow{k_8} H_2O + NO_2 + O_2 \qquad (4.4\text{-}8)$$

could also reduce the OH in the lower stratosphere. Recent measurement by Wine et al. (1980) gives the following expression for k_7

$$k_7 = 1.52 \times 10^{-14} \exp\left(\frac{649}{T}\right) \quad . \qquad (4.4\text{-}9)$$

Note that reaction (4.4-7) has a negative activation energy of about 1.3 kcal mol^{-1}. At stratospheric temperatures, the new rate constant k_7 (Wine et al., 1980) is about a factor of 3 faster than the temperature independent value of 8.5×10^{-14} cm^3 s^{-1} recommended earlier by NASA (1979). If Wine et al.'s results are confirmed and H_2O is the major product of reaction (4.4-7), then much of the discrepancy between observed and calculated ratios of HF:HCl and HNO_3:NO_2 may be resolved.

Reaction (4.4-8) may further reduce OH in the low stratosphere if k_8 exceeds 1×10^{-12} cm^3 s^{-1}. Obviously, accurate data for k_6, k_7 and k_8 are needed for modeling the stratospheric OH which plays a central role in the O_3 problem.

5. SULFUR STUDY

5.1 Background

The interests in atmospheric sulfur chemistry originated with the observation of the stratospheric sulfate (Junge) layer (Junge et al., 1961). Studies showed that the sulfate layer contributes to the net albedo of the atmospheric-earth system through absorption and backscattering of solar radiation (Mitchell, 1971; Chylek and Coakley, 1974; Pollack et al., 1976). Consequently, any significant perturbation of the atmospheric sulfur budget may cause changes in the sulfate layer with possible global climatic impact. Thus, it is important to understand the nature of the sulfur sources that maintain the present sulfate layer.

Junge suggested that SO_2 is the gaseous precursor of the sulfate aerosol and that the stratospheric SO_2 concentration is maintained by upward diffusion from the troposphere (1974). In this way, the stratospheric sulfur budget is related to the tropospheric budget. In the meantime, interest in the tropospheric budget is growing because of the emerging problem in visibility reduction, acid rain and respiratory effects associated with enhanced SO_4 concentration due to SO_2 emission from anthropogenic activities.

With the projected increase of coal usage in the future, it becomes increasingly desirable to ascertain the impact of SO_2 emission on the global budget. A natural first step in the study is the establishment of the atmospheric clean air sulfur budget.

5.2 Natural Sulfur Budget

During the past contract year, we initiated a study of the clean air sulfur budget. In this section, some of the major results will be outlined. The reader is referred to the papers cited for more detailed discussion.

The chemistry of the atmospheric sulfur species and available observations are summarized in Sze and Ko (1980b). The measured tropospheric concentration of COS of .5 ppbv makes COS the most abundant sulfur species in the atmosphere. One major conclusion of our study is that reduced sulfur compounds such as H_2S, CS_2, COS, CH_3SCH_3 may play an important role as sources for atmospheric SO_2 and SO_4.

As suggested by Crutzen (1976), photolysis of COS in the stratosphere could provide a source for stratospheric SO_2. Our studies showed that the reaction of CS_2 with O could also provide a source for SO_2 of comparable strength. Furthermore, our model calculations showed that the in situ production of SO_2 from oxidation of COS and CS_2 can explain why SO_2 is well mixed in the lower stratosphere (cf. Sze and Ko, 1979b, 1980a).

Our studies also indicated that CS_2 may be a precursor for atmospheric COS (Sze and Ko, 1979a; Ko and Sze, 1980). Using the chemical scheme discussed in Sze and Ko (1980b), we argued that an atmospheric input of 27 MT(S)/year in the form of reduced sulfur compounds can account for the observed SO_2 and SO_4 tropospheric concentrations at remote areas. This suggests that the anthropogenic input of 65 MT(S)/year could have a significant impact on the global sulfur cycle.

6. EFFECT OF MAN'S ACTIVITIES ON STRATOSPHERIC O_3

Several human activities which could appreciably perturb the stratospheric ozone layer have been identified in recent years. These include the use of high-flying aircraft, halocarbons, and nitrogen fertilizers. Among the various possible threats to the ozone layer, perhaps the release of fluorocarbons appears to be the greatest (NAS, 1980). This section will present the most recent results concerning the O_3 perturbations associated with the release of F-11 and F-12 (Section 6.1), CH_3Br (Section 6.2) and the injection of NO_x by high-flying aircraft (Section 6.3).

6.1 O_3 Depletion due to Fluorocarbons

As discussed in Section 2, chlorine radicals play an important role in stratospheric ozone budget. One potentially large source of stratospheric chlorine is the photolysis of $CFCl_3$ (F-11) and CF_2Cl_2 (F-12),

$$CFCl_3 + h\nu \rightarrow CFCl_2 + Cl \qquad (6.1\text{-}1)$$

and

$$CF_2Cl_2 + h\nu \rightarrow CF_2Cl + Cl \qquad (6.1\text{-}2)$$

as identified by Molina and Rowland (1974).

The two compounds (F-11 and F-12) are believed to be entirely man-made. The production rates of F-11 and F-12 in the period (1950-1979) are summarized in Table 6.1-1.

Table 6.1-1

A Tabulation of the Total Production of F-11 and F-12 on an Annual Basis for the Period 1950-1979 (Source CMA)

Year	F-11 (10^6 pounds)	F-12 (10^6 pounds)
1950	14.6	76.2
1951	20.0	79.9
1952	29.9	82.1
1953	38.1	102.5
1954	46.1	108.3
1955	57.9	127.0
1956	71.6	151.4
1957	74.8	163.5
1958	65.1	161.9
1959	78.4	193.1
1960	109.6	219.2
1961	133.3	239.2
1962	172.2	282.4
1963	205.7	322.8
1964	244.9	375.0
1965	270.8	419.0
1966	310.9	476.6
1967	352.2	535.2
1968	403.7	589.7
1969	479.0	655.4
1970	525.0	707.9
1971	580.2	753.0
1972	676.5	837.5
1973	769.6	933.3
1974	815.1	976.2
1975	692.4	839.9
1976	749.2	905.5
1977	706.5	844.0
1978	680.9	820.3
1979	638.2	787.4

These data were recently compiled by the Chemical Manufacturers Association.

No tropospheric sinks for F-11 and F-12 have yet been identified. Thus, the steady state concentrations of these compounds may reach as high as 1-2 ppb from their present levels of .1-.2 ppb in the next 150 years if the present production rates prevail.

Several groups have calculated the steady state ozone depletions due to the release of F-11 and F-12. The results are summarized in Table 6.1-2. The calculated reductions in ozone range from 15-18 percent based on the rate data recommended by NASA (1979). Note that the current model predicted ozone depletion values are about a factor of two higher than that published in the NAS (1976) report. The revisions in the calculated ozone depletion is mainly caused by the upward revisions in the rate constants for two key reactions,

$$HO_2 + NO \rightarrow OH + NO_2 \qquad (6.1\text{-}3)$$

$$HO_2 + O_3 \rightarrow OH + 2O_2 \ . \qquad (6.1\text{-}4)$$

Both reactions (6.1-3) and (6.1-4) enhance the OH concentrations below 32 km with a consequent increase in the catalytic role of ClX as a sink for O_3.

Figure 6.1-1 shows the steady state local ozone reductions. It should be emphasized that while the relative change in O_3 concentration peaks at about 40 km, the bulk of ozone reduction occurs below 32 km, a region of considerable complexity both in terms of dynamics and chemistry.

Table 6.1-2

Steady-State Pertubations for 1975 Emissions Rates of Fluorocarbons 11 and 12*
(NASA, 1979)

Modeling Group	ΔClX ppbv	$-\Delta O_3$(col) (%)	$-\Delta O_3$(40 km) (%)	$-\Delta O_3$(20 km) (%)	$\frac{-\Delta O_3(col)}{\Delta ClX}$ (%/ppbv)
LLL	5.5	15	38	17	2.7
DuPont	6.2	18.3	46.1	16.5	3.0
LaRC	6.7	16.2	43	14.8	2.4
RDA	5.5	16	42	17	2.9
Harvard	6.6	18	41	19	2.7
Cal Tech	6.9	18	50	19	3.1
NOAA	5.8	18	39	17	3.1
GSFC	7.0	18	39	18	2.6
GSFC-UNC	6.9	15.4	55	9	2.2
AER	5.8	16.7	52	14	2.9

* Fluorocarbon 11 at 9.4×10^6 and Fluorocarbon 12 at 13.0×10^6 molecules cm^{-2} sec^{-1}

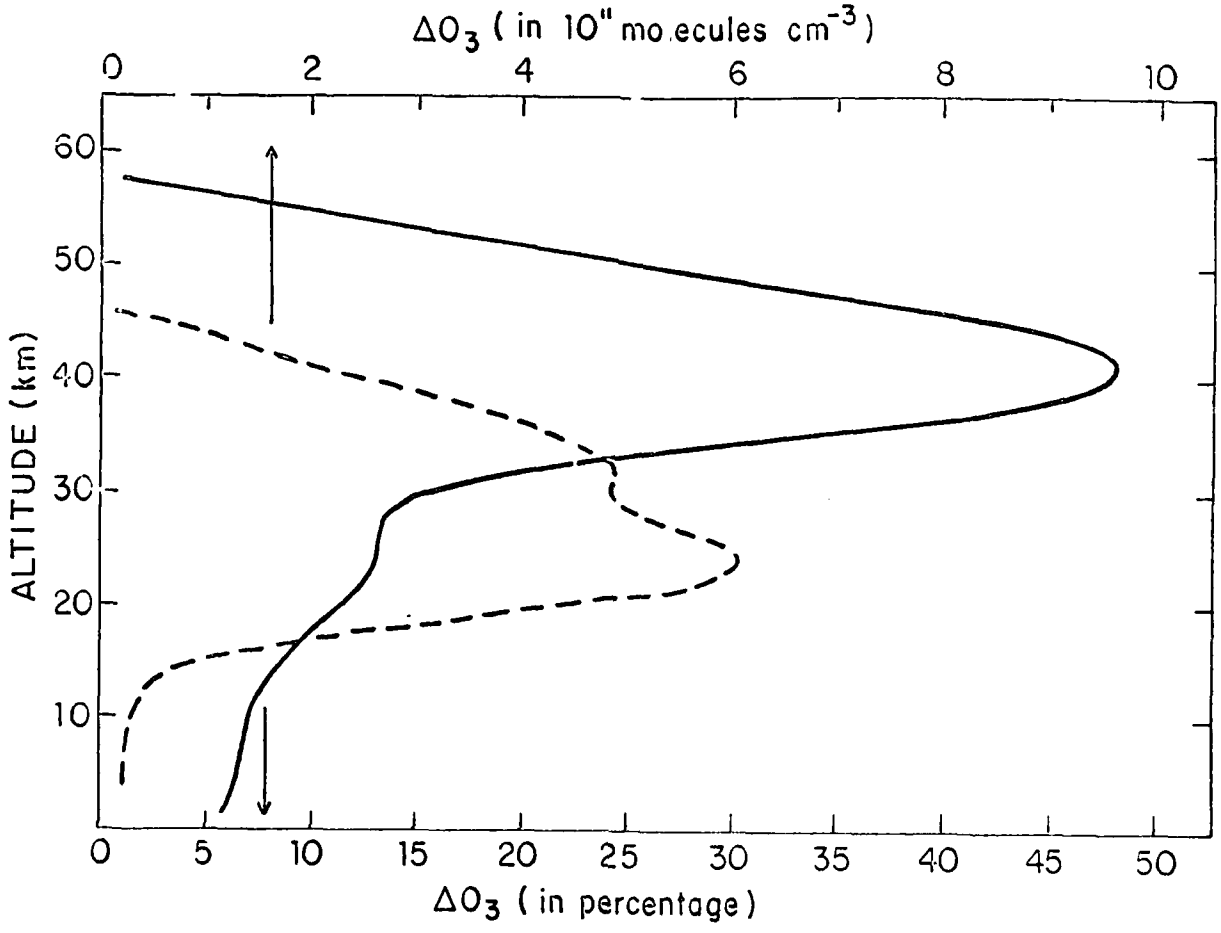

Figure 6.1-1

Calculated steady state local reduction of ozone assuming constant 1977 release rates of F-11, F-12. The dotted curve corresponds to the reduction in number density (upper scale) while the solid curve gives the local percentage reduction (lower scale).

Note that this is also the region where we found significant discrepancy between models and observations (see Section 4). Thus, the calculated changes in ozone, particularly those calculated below 32 km, should be viewed with great caution.

6.2 Perturbation due to Bromine Compounds

Bromine can affect ozone through a number of catalytic cycles:

$$\left.\begin{aligned} Br + O_3 &\rightarrow BrO + O_2 \\ BrO + O &\rightarrow Br + O_2 \end{aligned}\right\} \qquad (6.2\text{-}1)$$

$$\left.\begin{aligned} Br + O_3 &\rightarrow BrO + O_2 \\ BrO + BrO &\rightarrow 2Br + O_2 \end{aligned}\right\} \qquad (6.2\text{-}2)$$

and

$$\left.\begin{aligned} Br + O_3 &\rightarrow BrO + O_2 \\ Cl + O_3 &\rightarrow ClO + O_2 \\ ClO + BrO &\rightarrow Cl + Br + O_2 \end{aligned}\right\} \qquad (6.2\text{-}3)$$

.

The sequence (6.2-1) is equivalent to

$$O + O_3 \rightarrow 2O_2$$

while sequences (6.2-2) and (6.2-3) are equivalent to

$$2O_3 \rightarrow 3O_2 \ .$$

The troposphere contains a variety of brominated organic compounds including CH_3Br, CH_2Br_2, $CHBr_3$, $CHClBr_2$ and $C_2H_2Br_2$

(Singh et al., 1977), with CH_3Br the most abundant. Concentrations of CH_3Br range from 1 to 300 pptv, with values in clean continental air between 5 and 10 pptv. The lifetime of CH_3Br, as set by the reaction with OH, is sufficiently long (of about 3 years) to insure that the gas should be relatively well mixed in the troposphere and act as a bromine-carrier to the stratosphere.

Recently Yung et al. (1980) argued that sequence (6.2-3) may be potentially more important because of the possibility of further increase in ClO concentrations in the stratosphere. They argued that, with 8 ppb of ClX (which corresponds to a steady state stratospheric ClX concentration should emission of F-11 and F-12 continue at present rates), reaction sequence (6.2-3) could deplete an additional 2% column ozone if the background level of BrX in the stratosphere is about 20 ppt. The impact of bromine on ozone, however, would be largest in the lower stratosphere and would involve nonlinear coupling between BrX and ClX cycles. The calculated concentrations of BrO may be subject ot larger errors since the photolysis rate of BrO is not known within a factor of 4. The perturbation results concerning the brominated compounds should be considered therefore subject to the usual caveats as noted in Section 6.1.

6.3 NO_x Injection Studies

Earlier model calculations (Crutzen, 1970; Johnston, 1971; McElroy et al., 1974; CIAP, 1974) indicate that a potential fleet of operations of supersonic aircraft as contemplated by the United States in 1970 (500 aircraft flying approximately 7 hours per day at 17-18 km) could lead to major reduction in the stratospheric column O_3 abundance and thus cause an increase in the flux of ultraviolet radiation reaching the earth's surface. This could result in a variety of environmental consequences, including a possible increase in the incidence of skin cancer (McDonald, 1971).

Removal of O_3 by aircraft injectant NO_x radicals is primarily due to the pair of reactions

$$NO + O_3 \rightarrow NO_2 + O_2 \qquad (6.3\text{-}1)$$

followed by,

$$NO_2 + O \rightarrow NO + O_2 \quad . \qquad (6.3\text{-}2)$$

The natural source for NO_x in the stratosphere is thought to emanate from the reaction of $O(^1D)$ with N_2O (Nicolet and Vergison, 1971; Crutzen, 1971; McElroy and McConnell, 1971),

$$N_2O + O(^1D) \rightarrow 2NO \quad . \qquad (6.3\text{-}3)$$

Much of the revision in model predictions since 1976 may be ascribed to a change in the rate constant for the reaction of NO with HO_2,

$$NO + HO_2 \rightarrow NO_2 + OH \quad . \qquad (6.3\text{-}4)$$

Recent measurements (Howard and Evenson, 1977) indicate that the rate constant for reaction (6.3-4) is faster than previously thought, by about a factor of 30. An increase in the rate constant for reaction (6.3-4) tends to shift the equilibrium in HO_x from HO_2 toward OH. Below 30 km, removal of ozone by HO_x radicals proceeds mainly by,

$$OH + O_3 \rightarrow HO_2 + O_2 \qquad (6.3\text{-}5a)$$

$$HO_2 + O_3 \rightarrow OH + 2O_2 \quad . \qquad (6.3\text{-}5b)$$

We may note that reactions (6.3-5a) and (6.3-4) followed by photolysis of NO_2,

$$NO_2 + h\nu \rightarrow NO + O \qquad (6.3\text{-}6)$$

do not affect odd oxygen removal. Thus addition of NO would reduce the catalytic role of HO_x as described by (6.3-5a,b). Furthermore, an increase in OH causes an increase in the rate for the reaction

$$OH + NO_2 + M \rightarrow HNO_3 + M \quad , \qquad (6.3\text{-}7)$$

with subsequent decrease in the concentration of the free nitrogen radicals ($NO + NO_2$) and reduction in the efficiency of the nitrogen cycle as a sink for odd oxygen.

In this section, we present the result of a model calculation simulating the effect of NO_x injection in the stratosphere due to aircraft operation. The calculations are done using the diurnal average version of the AER 1-D photochemical model with the rate data as taken from NASA (1979). As discussed in Section 3 and Appendix A, the model atmosphere is taken from U.S. Standard Atmosphere Supplement (1966) and the eddy diffusion coefficients from Wofsy (1976).

In the study, we assume that all NO_x are injected in the form of NO. This is a valid approximation as the CIAP studies (CIAP, 1975) have shown that 90-95% of the NO_x is emitted in the form of NO. It is estimated that 1,000 aircrafts flying 7 hours per day will deposit 1.7 MT (NO_x) yr^{-1} in the stratosphere. Assuming the emitted NO_x to be uniformly distributed over a 1 km thick layer, we estimate the equivalent injection rate of NO to be 1.4×10^3 molecules (NO) cm^{-3} s^{-1}. Two separate studies were performed assuming injection at 15 km and 20 km respectively.

Figures 6.3-1 and 6.3-2 show the resulting changes in O_3 and NO_x profiles as functions of altitude for the two studies. Our results also show a net increase in O_3 column density of 1.7% and 4.0% for the 15 km and 20 km injections respectively.

The following points have to be taken into account in interpreting the 1-D model results. There is little doubt

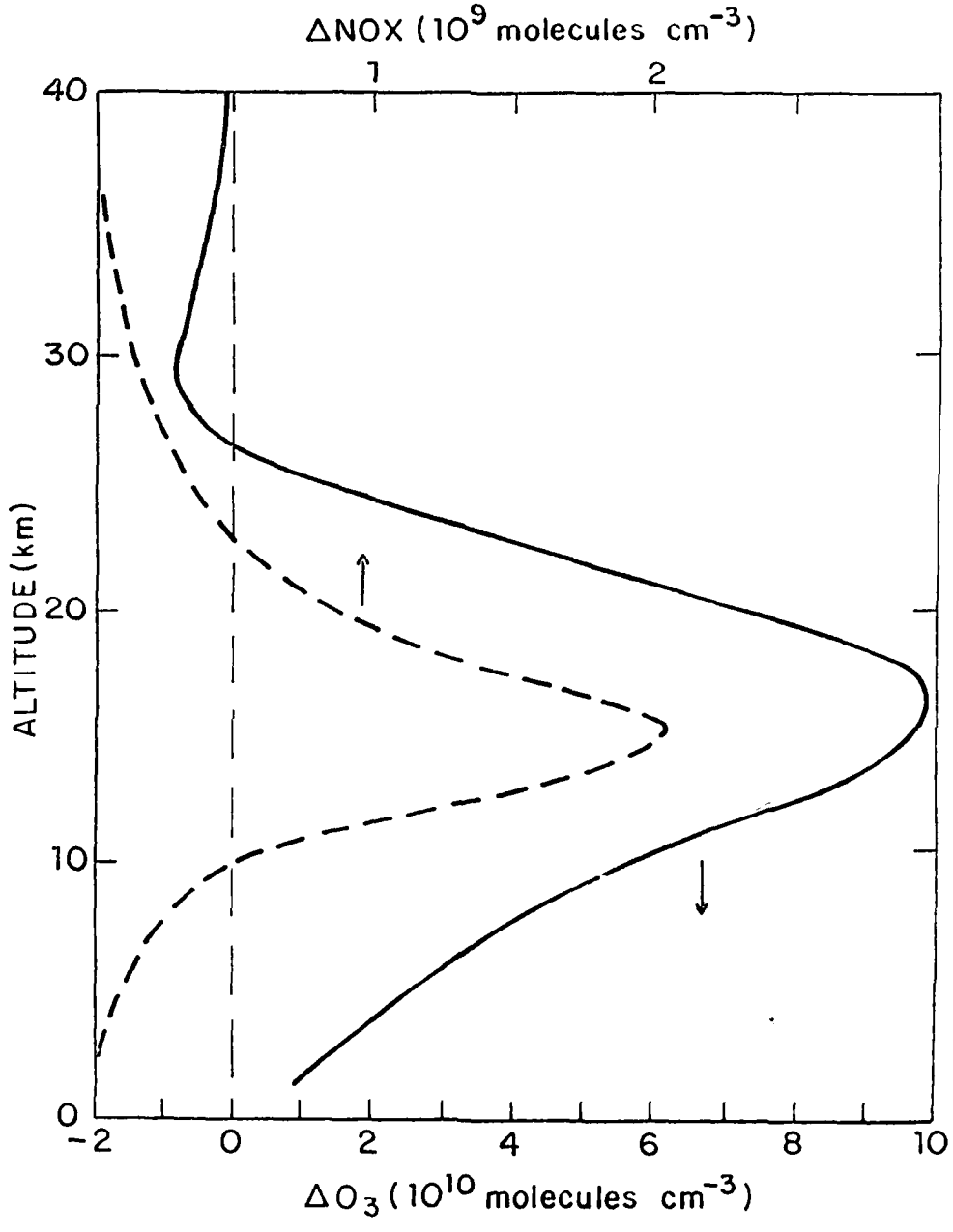

Figure 6.3-1

Calculated changes in O_3 and NO_x profiles for model A due to an injection of 1.4×10^{83} molecules (NO) cm^{-2} s^{-1} at 15-16 km.

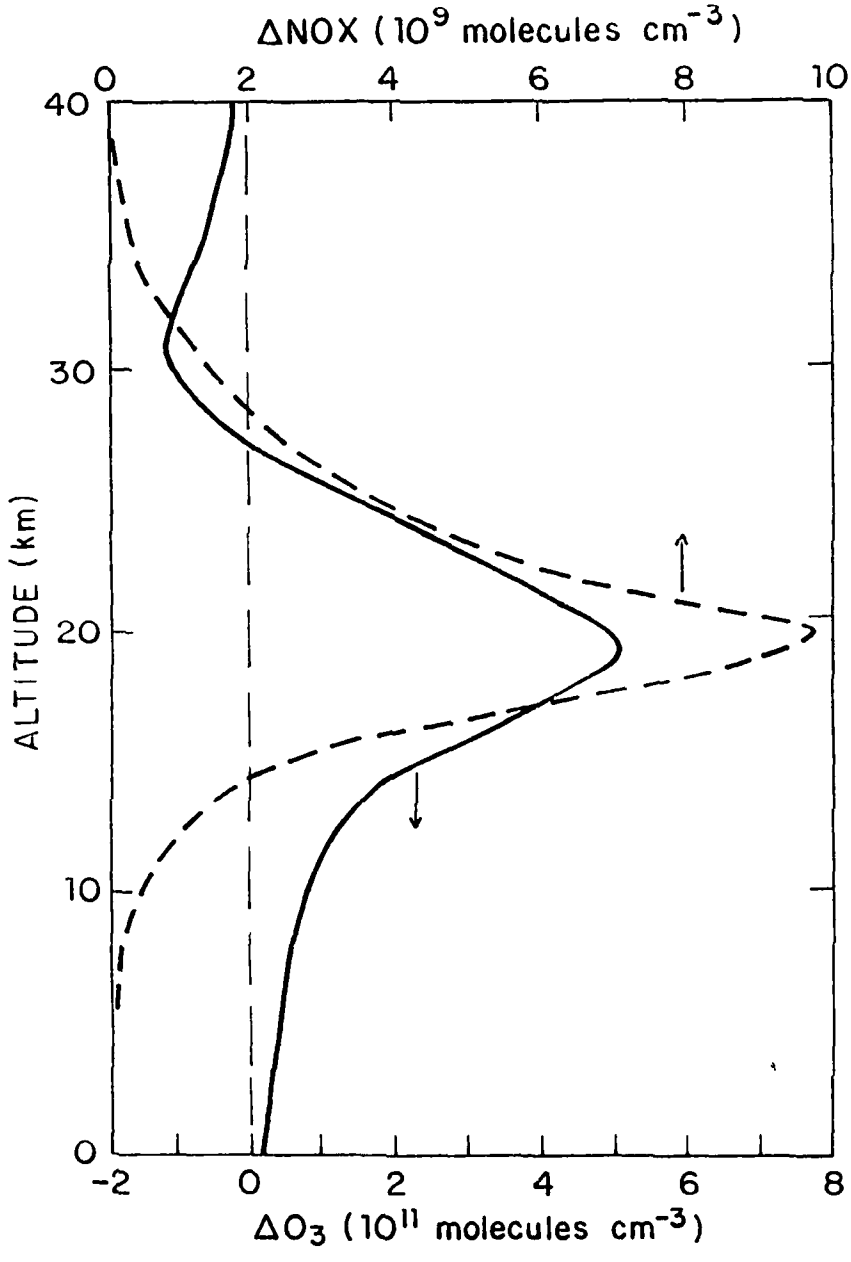

Figure 6.3-2
Same as Figure 2-5a but with injection at 20-21 km.

that OH plays a pivotal role in stratospheric chemistry and that exact responses of the O_3 distribution to the NO_x injection. While the kinetic data base for HO_x reactions has been significantly improved over the past years, remaining uncertainties in HO_x chemistry still, perhaps, represent the largest source of error for model predictions. In fact, a comparison between model calculations and observations reveals several significant discrepancies which might be attributed to errors in the calculated OH concentrations in the altitude region 15-35 km. It was argued elsewhere (Sze, 1978, 1979) that significantly lower stratospheric OH concentrations than those calculated by current models are needed to account for the observed gradients of ClO (Anderson et al., 1979) and for the observed ratios of HNO_3/NO_2 (NASA, 1977, 1979; McConnell and Evans, 1978) and HF/HCl (Sze, 1978).

Another area of major uncertainty concerns atmospheric transport of trace species. Current one-dimensional models parameterize vertical transport by the so-called eddy diffusion coefficients which were mainly derived from observation of N_2O and CH_4. These models therefore ignore horizontal transport, while the natural distribution of ozone exhibits significant latitudinal and seasonal variations.

It is probably desirable to perform similar studies using a two-dimensional model once some of the uncertainties in the HOX chemistry can be removed.

7. THE AER TWO-DIMENSIONAL MODEL

7.1 Current Status

The development of the AER 2-D model started in the summer of 1979. The approach to dynamic treatment follows that of the Oxford Model (Harwood and Pyle, 1975, 1977). The model is designed ultimately to calculate all dynamic variables together with atmospheric species concentrations incorporating feedback mechanisms between chemistry, radiation and dynamics.

In the early stage of the development, we have set up the program to solve the zonal-mean diffusion equation with pre-calculated dynamic variables that are specified externally as functions of time and space. The values are taken from earlier work of Harwood and Pyle (1977). This model was used to perform inert tracer studies to assure the proper treatment of the equation.

Our next step was to interface a photochemical scheme with the model. We decided to build up the chemistry in stages. The first chemical scheme corresponds to the classical Chapman scheme. We next added hydrogen chemistry and finally implemented the full O_x-HO_x-NO_x-Cl_x chemistry to simulate the present atmosphere. It is hoped that by examining the behavior of O_3 in each case, one can get a better idea of the role of chemistry and dynamics in determining trace gas distribution.

In the next section, we will discuss the derivation of the basic equations used in our zonal model. Emphasis will

be put on the physical assumptions that are adopted in order to obtain a set of manageable equations from the full three-dimensional primitive equations. A brief description of the model can be found in Appendix B. The results of the numerical calculations will be discussed in Section 7.3.

7.2 Basic Equations for Zonal-Mean Model

The basic equations used in zonal models can be considered as obtained from the full three-dimensional equations by zonal averaging. In what follows, we will begin with a discussion of the assumptions usually adopted to obtain the set of primitive equations in 3-dimensions. Then the method of zonal-mean averaging is outlined to show how the set of equations is reduced to 2-dimensions.

The local concentration of a trace gas is governed by the three-dimensional continuity equation

$$\left(\frac{\partial}{\partial t} + \underset{\sim}{v} \cdot \nabla\right) f = Q/\rho \qquad (7.2\text{-}1)$$

where $f(t,\underset{\sim}{x})$ is the mixing ratio, $v(t,x)$ the velocity wind fields describing the general circulation, $\rho(t,x)$ the air number density and $Q(t,\underset{\sim}{x})$ is the local net production or loss (by chemical and/or physical transformation) of the trace gas. Equation (7.2-1) gives the time rate of change of f in the Eulerian description of fluid motion. The quantities f, $\underset{\sim}{v}$, ρ and Q are to be considered as Eulerian field quantities as functions of time and spatial location with coordinates $\underset{\sim}{x}$.

In order to solve equation (7.2-1) for the species concentration, one must be able to provide values of v and temperature T (T is necessary for calculation of reaction rates) as functions of space and time either by parameterization or by solving the system of dynamic equations. The atmospheric circulation is governed by the coupled system of dynamic and thermodynamic equations (cf. Lorentz, 1967):

momentum equation

$$\frac{d\underset{\sim}{v}}{dt} = -2\underset{\sim}{\Omega} \times \underset{\sim}{v} - \frac{1}{\rho M} \nabla p - \nabla\Psi \qquad (7.2\text{-}2)$$

thermodynamic equation

$$\frac{d\theta}{dt} = J \qquad (7.2\text{-}3)$$

continuity equation

$$\frac{d\rho}{dt} = -\rho\nabla\cdot\underset{\sim}{v} \qquad (7.2\text{-}4)$$

equation of state: ideal gas law

$$p = \rho R T \qquad (7.2\text{-}5)$$

where $\frac{d}{dt} \equiv \frac{\partial}{\partial t} + \underset{\sim}{v}\cdot\nabla$ is the total time derivative.

The above are to be considered as equations for the Eulerian field variables $\underset{\sim}{v}$, ρ, p and θ. The newly introduced symbols have the following meaning:

$\underset{\sim}{\Omega}$ = angular velocity of earth

M = average mass of an air molecule

p = pressure

Φ = the geopotential gz where g is acceleration due to gravity, z is geometrical altitude

θ = the potential temperature related to temperature T by $\theta = T(\frac{p_o}{p})^K$ with $K = R/C_p$; R the gas constant and C_p the specific heat at constant pressure

J = the diabatic influence with $C_p J\frac{T}{\theta}$ the heating rate per unit mass

R = the gas constant

T = temperature.

Note that we have left out frictional forces in the momentum equations (7.2-2) under the assumption that they are unimportant for large scale motion.

The system of equations (7.2-2) to (7.2-5) is coupled to the specie equation through the J term which depends on distribution of gases such as O_3, CO_2, N_2O and CH_4 in the atmosphere. Thus, in principle, equation (7.2-1) through (7.2-5) must be solved simultaneously as a system.

In practice, the system of equations presents a formidable numerical problem and put enormous demand on both computer core memory and computation time. This is particularly true if one is interested in a realistic chemical scheme in order to simulate the distribution of the various species in the atmosphere. Besides, the set of exact equations also simulates phenomena of little interest for large scale motions. The following physical assumptions are usually adopted:

A) Replacement of the vertical momentum equation by the hydrostatic equilibrium condition, i.e., the pressure gradient force is balanced by geopotential term)

$$\frac{\partial p}{\partial z} = -M \rho g \ . \qquad (7.2\text{-}6)$$

It is observed that motions due to deviation away from hydrostatic equilibrium are restricted to oscillations about the equilibrium state with time scales of order hour. The adoption of (7.2-6) effectively filters out vertically travelling sound waves.

B) Discard terms containing the vertical velocities in the remaining two components of the momentum equation. This approximation appears to be justified because of the fact that the vertical component of the velocity is about two orders of magnitude smaller than the horizontal components.

C) Replace r in the resulting equation by a where r is the distance from the earth's center; a is the radius of the earth.

The above assumptions lead to a system of equations usually referred to as the primitive equations. Next, it would be desirable to write the momentum equation in scaler form. For this purpose, it is convenient to introduce a

coordinate system where the pressure p is used as the vertical coordinates in conjunction with λ the longitude and ϕ the latitude. In this coordinate system, the components of the velocity vectors are

$$u = a\cos\phi\frac{d\lambda}{dt}$$
$$v = a\frac{d\phi}{dt}$$
$$w = \frac{dp}{dt} \quad .$$

The continuity equation takes the form

$$\frac{1}{a\cos\phi}\frac{\partial u}{\partial\lambda} + \frac{1}{a\cos\phi}\frac{\partial}{\partial\phi}(v\cos\phi) + \frac{\partial w}{\partial p} = 0 \quad . \tag{7.2-7}$$

This is sometimes written in the form

$$\nabla\cdot\underset{\sim}{v} = 0 \quad . \tag{7.2-8}$$

However, (7.2-8) holds only in pressure coordinates. Since (7.2-7) is derived using only the hydrostatic equation, it is more general than the incompressible fluid assumption. Finally, from (7.2-7), one can derive (cf. Lorentz, 1967)

$$\frac{ds}{dt} = \frac{\partial s}{\partial t} + \frac{1}{a\cos\phi}\frac{\partial}{\partial\lambda}(us) + \frac{1}{a\cos\phi}\frac{\partial}{\partial\phi}(v\cos\phi\, s) + \frac{\partial}{\partial p}(ws) \tag{7.2-9}$$

for any scaler s.

In this coordinate system, the primitive equations are (cf. Lorentz, 1967; Holton, 1975)

$$\frac{\partial f}{\partial t} + \frac{1}{a\cos\phi}\frac{\partial}{\partial\lambda}(fu) + \frac{1}{a\cos\phi}\frac{\partial}{\partial\phi}(f v\cos\phi) + \frac{\partial}{\partial p}(fw) = \frac{Q}{\rho} \tag{7.2-10}$$

$$\frac{\partial u}{\partial t} + \frac{1}{a\cos\phi}\frac{\partial}{\partial\lambda}(u^2) + \frac{1}{a\cos\phi}\frac{\partial}{\partial\phi}(u v\cos\phi) + \frac{\partial}{\partial p}(uw) - \frac{u v\tan\phi}{a} - 2\Omega v\sin\phi - \frac{g}{a\cos\phi}\frac{\partial z}{\partial\lambda} = 0 \; . \tag{7.2-11}$$

$$\frac{\partial v}{\partial t} + \frac{1}{a\cos\phi}\frac{\partial}{\partial\lambda}(vu) + \frac{1}{a\cos\phi}\frac{\partial}{\partial\phi}(v^2\cos\phi) + \frac{\partial}{\partial p}(vw) + \frac{u^2\tan\phi}{a} + 2\Omega u\sin\phi - \frac{g}{a}\frac{\partial z}{\partial\phi} = 0 \tag{7.2-12}$$

$$\frac{\partial\theta}{\partial t} + \frac{1}{a\cos\phi}\frac{\partial}{\partial\lambda}(\theta u) + \frac{1}{a\cos\phi}\frac{\partial}{\partial\phi}(\theta v\cos\phi) + \frac{\partial}{\partial p}(\theta w) = J \tag{7.2-13}$$

$$\frac{1}{a\cos\phi}\frac{\partial u}{\partial\lambda} + \frac{1}{a\cos\phi}\frac{\partial}{\partial\phi}(v\cos\phi) + \frac{\partial w}{\partial p} = 0 \tag{7.2-14}$$

$$p = \rho R T \tag{7.2-15}$$

$$g\frac{\partial z}{\partial p} = -\frac{1}{\rho M} \; . \tag{7.2-16}$$

In the above equations, the terms $\frac{u v\tan\phi}{a}$ and $\frac{u^2\tan\phi}{a}$ are curvature terms arising from the non-Euclidian nature of the coordinate frames. The geopotential term $\frac{1}{a}\frac{\partial\Phi}{\partial\phi}$ and $\frac{1}{a\cos\phi}\frac{\partial\Phi}{\partial\lambda}$ has been written out explicitly with $\Phi = gz$.

In this arrangement, equations (7.2-10) through (7.2-13) are prognostic equations for f, u, v and θ respectively, while (7.2-14) and (7.2-15) can be considered as diagnostic equations for w and p. Since p is being used as an independent variable, equation (7.2-16) serves the purpose of transforming between geometrical altitude and the pressure coordinate.

In the zonal mean model, the set of equations is reduced to two dimensions by the Eulerian mean averaging. The Eulerian mean operator averages over one of the coordinates while holding all other coordinates fixed. In the case of the atmospheric models, the integration over the longitude is done along constant latitude circles, altitudes and time. Thus, given $g(t,\phi,p,\lambda)$, (where t is time, ϕ the latitude, p the pressure height coordinates and λ the longitude), one obtains

$$\bar{g}(t,\phi,p) = \frac{\int g(t,\phi,p,\lambda)\,d\lambda}{\int d\lambda} \quad . \tag{7.2-17}$$

It is convenient to define g', the deviation from the mean, by

$$g'(t,\phi,p,\lambda) = \bar{g}(t,\phi,p) - g(t,\phi,p,\lambda) \quad . \tag{7.2-18}$$

It follows from (7.2-17) that

$$\overline{g'(t,\phi,p,\lambda)} = 0 \tag{7.2-19}$$

and

$$\overline{gh} = \bar{g}\bar{h} + \overline{g'h'} \quad . \tag{7.2-19}$$

When the Eulerian mean operation is applied to (7.2-10) to (7.2-16) using the fact that $\overline{}$ commutes with the coordinate differential operators, we have

$$\frac{\partial \bar{f}}{\partial t} + \frac{1}{a\cos\phi}\frac{\partial}{\partial \phi}(\bar{f}\,\bar{v}\cos\phi) + \frac{\partial}{\partial p}(\bar{f}\,\bar{w}) = \overline{\left(\frac{Q}{\rho}\right)} - F_f \tag{7.2-20}$$

$$\frac{\partial \bar{u}}{\partial t} + \frac{1}{a\cos^2\phi}\frac{\partial}{\partial \phi}(\bar{u}\,\bar{v}\cos^2\phi) + \frac{\partial}{\partial p}(\bar{u}\,\bar{w}) - 2\Omega\,\bar{v}\cos\phi = -F_u \tag{7.2-21}$$

$$\frac{\partial \bar{v}}{\partial t} + \frac{1}{a\cos\phi}\frac{\partial}{\partial \phi}(\bar{v}^2\cos\phi) + \frac{\partial}{\partial p}(\bar{v}\,\bar{w}) + \frac{\bar{u}^2\tan\phi}{a} + 2\,\bar{u}\,\Omega\sin\phi - \frac{g}{a}\frac{\partial \bar{z}}{\partial \phi} = -F_v \tag{7.2-22}$$

$$\frac{\partial \bar{\theta}}{\partial t} + \frac{1}{a\cos\phi}\frac{\partial}{\partial \phi}(\bar{\theta}\,\bar{v}\cos\phi) + \frac{\partial}{\partial p}(\bar{\theta}\,\bar{w}) = \bar{J} - F_\theta \tag{7.2-23}$$

$$\frac{1}{a\cos\phi}\frac{\partial}{\partial \phi}(\bar{v}\cos\phi) + \frac{\partial \bar{w}}{\partial p} = 0 \tag{7.2-24}$$

$$\frac{p}{\bar{\rho}} = R\,\bar{T} \tag{7.2-25}$$

$$g\frac{\partial \bar{z}}{\partial p} = -\frac{1}{M\bar{\rho}} = -\frac{R\,\bar{T}}{M\,p} \tag{7.2-26}$$

where $F_f = \frac{1}{a\cos\phi}\frac{\partial}{\partial\phi}(\overline{f'v'}\cos\phi) + \frac{\partial}{\partial p}(\overline{f'w'})$

$F_u = \frac{1}{a\cos^2\phi}\frac{\partial}{\partial\phi}(\overline{v'u'}\cos^2\phi) + \frac{\partial}{\partial p}(\overline{u'w'})$

$F_v = \frac{1}{a\cos\phi}\frac{\partial}{\partial\phi}(\overline{v'^2}\cos\phi) + \frac{\partial}{\partial p}(\overline{v'w'}) + \frac{\overline{u'^2}\tan\phi}{a}$

$F_\theta = \frac{1}{a\cos\phi}\frac{\partial}{\partial\phi}(\overline{\theta'v'}\cos\phi) + \frac{\partial}{\partial p}(\overline{\theta'w'})$

are the eddy flux divergence terms. Note that in (7.2-21) we have incorporated the curvature term $(\frac{u\,v\tan\phi}{a})$ into the $\frac{\partial}{\partial\phi}$ term. It should be emphasized that the eddy flux terms are not constrained by the system of equations and must be specified or parameterized in terms of other variables.

In zonal-mean models, a further physical assumption is usually adopted. From scale analysis, it can be shown (cf. Holten, 1975) that equation (7.2-22) reduces to

$$2\Omega\sin\theta\,\bar{u} = \frac{g}{a}\frac{\partial\bar{z}}{\partial\phi} \qquad (7.2\text{-}27)$$

the lowest order of a Rossby number expansion. This is the geostrophic assumption which provides a good approximation for midlatitude dynamics though some authors (Harwood and Pyle, 1975) argued that the approximation is reasonable up to about 5°. The geostrophic assumption filters out occurrance of gravity waves and other equatorial waves that cause the quasi-biennial oscillations in the stratosphere. (7.2-27) is awkward to use as $\bar{z}$ is not one of the dependent variables. One can differentiate the equation with respect to p and use the hydrostatic equation to obtain the thermal wind relation

$$p\frac{\partial \bar{u}}{\partial p} = -\frac{\left(\frac{R}{M}\right)\left(\frac{p}{p_o}\right)^K}{2\Omega \sin\phi}\ \frac{1}{a}\ \frac{\partial \bar{\theta}}{\partial \phi} \qquad (7.2\text{-}28)$$

to replace (7.2-22). This eliminates F_v as an extra variable. However, one still needs ways of determining F_f, F_u and F_θ to close the system of equations.

All existing zonal-mean models use the method of parameterization via eddy diffusion tensor originally proposed by Reed and German (1965). Using mixing length type arguments, Reed and German argued that for a quantity x which is conserved along its flow, the eddy fluxes are related to the gradient zonal mean quantity $\bar{x}$ via

$$\begin{pmatrix} \overline{v'x'} \\ \overline{w'x'} \end{pmatrix} = -\begin{pmatrix} K_{\phi\phi} & K_{\phi p} \\ K_{p\phi} & K_{pp} \end{pmatrix} \begin{pmatrix} \frac{1}{a\cos\phi}\frac{\partial \bar{x}}{\partial \phi} \\ \frac{\partial \bar{x}}{\partial p} \end{pmatrix} \qquad (7.2\text{-}29)$$

where K is a symmetric tensor. Following the procedure similar to the one suggested by Reed and German, Luther (1973) analyzed the heat transfer, temperature and wind variance data of Oort and Rasmussen (1971) and derived a set of K tensors as a function of time and space. It should be noted that the data only covered part of the northern hemisphere. Extrapolations were used to deduce the K's at places where there is no data based on results of Newell et al. (1966) and Wofsy and McElroy (1973). Furthermore, the K's for the southern hemisphere are obtained by reflecting the northern hemispheric values in the appropriate seasons. The set of

K's from Luther (1973) is by far the most complete with a set of values for each month covering the meridional plane from the surface to 60 km. In almost all of the zonal models, this set of K's provides the basis for eddy transport. We would like to emphasize here the limitation of this approach:

(i) the original argument of Reed and German (1965) was presented to treat turbulence diffusive type motions. Thus, the approach may not be appropriate if there is organized wave-type motion in the zonal direction. This has been demonstrated in studies of 3-D circulation by Mahlman (1975), Matsuno (1975), Matsuno and Nakamura (1979) and Plumb (1979) in the case of planetary wave motions. To date, no satisfactory justification for applying the eddy diffusion theory to stratospheric motion has been presented.

(ii) The argument only applies to conservative flow. Thus, strictly speaking, it can only be applied to inert tracers or to potential temperatures in adiabatic flow. However, in zonal-mean models, it is applied to chemical species with finite chemical lifetimes and to the potential temperature where the condition of adiabatic flow is not strictly satisfied.

The treatment of F_u presents special problems and will be discussed later.

Next, we will examine how to handle the equations for determining $\bar{u}$, $\bar{v}$ and $\bar{w}$.

Equations (7.2-21) and (7.2-23) can be written as

$$\frac{\partial \bar{u}}{\partial t} = \mathcal{A} \tag{7.2-30}$$

$$\frac{\partial \bar{\theta}}{\partial t} = \mathcal{B} \tag{7.2-31}$$

where $\mathcal{A}$ and $\mathcal{B}$ do not contain any time derivatives. If one differentiates (7.2-30) by p and (7.2-31) by ϕ and takes the appropriate linear combination of the resulting equation, by virtue of the thermal wind relations (7.2-28) one obtains

$$p \frac{\partial \mathcal{A}}{\partial p} + \frac{\left(\frac{R}{M}\right)\left(\frac{p}{p_o}\right)^K}{2\,\Omega \sin\phi} \frac{1}{a} \frac{\partial \mathcal{B}}{\partial \phi} = 0 \quad . \tag{7.2-32}$$

Note that there is no time derivative in equation (7.2-32). Equation (7.2-24) implies the existence of a function ψ where

$$\begin{aligned} \bar{v} &= -\frac{1}{\cos\phi} \frac{\partial \psi}{\partial p} \\ \bar{w} &= \frac{1}{a \cos\phi} \frac{\partial \psi}{\partial \phi} \end{aligned} \tag{7.2-33}$$

Using (7.2-33) to illiminate $\bar{v}$ and $\bar{w}$ in (7.2-32), we obtain a second order partial linear differential equation for ψ where the coefficients are functions of $\bar{u}$, $\bar{\theta}$, $\bar{J}$, F_u, F_θ and

their spatial derivatives. The system of equations can now be solved as follows. Given $\bar{f}$, $\bar{\theta}$, $\bar{u}$, $\bar{v}$ and $\bar{w}$ at one instance in time, one can compute $\overline{Q/\rho}$, $\bar{J}$, F_f, F_θ and F_u and solve the prognostic equations (7.2-20), (7.2-21) and (7.2-23) for $\bar{f}$, $\bar{u}$ and $\bar{\theta}$ at a later time. With these new values, one solves (7.2-32) for ψ with appropriate boundary conditins and generate new $\bar{v}$ and $\bar{w}$ via equation (7.2-33).

We will next discuss how to obtain $\overline{Q/\rho}$ once a photochemical scheme has been set up. The term Q/ρ consists of sums of terms each of which take one of the following forms

$$\mathcal{J}_i f_i;\ \rho\, k_{ij}(T)\, f_i f_j;\ \rho^2 k_{ijk}(T) f_i f_j f_k$$

for photolytic processes and two-body and three-body reactions respectively. Note that the temperature dependence of the reaction rates k_{ij} and k_{ijk} are explicitly displayed. The longitudinal behavior of $\mathcal{J}_i$ and f_i arise from the diurnal effect since each longitude is at a different local time at any instant in time. A similar problem arises in the 1-D model and is usually taken care of by putting diurnal averaged photolysis rates in the chemical scheme so that the resulting species concentrations represent diurnally averaged values. In addition, the longitudinal distribution of the gas may be affected by wave motion in the zonal direction. No attempts are made to treat such effects. In the zonal averaging process, the term $\overline{\overline{Q/\rho}}$ is obtained by taking the sum of the corresponding products of the zonal-meaned quantities. Eddy flux terms are ignored. The treatment of $\bar{J}$ is

similar in that the term is obtained by using zonally-meaned values in the expression while ignoring eddy flux terms.

The treatment of F_u is more difficult because the u momentum is definitely not conserved in the flow. Attempts to parameterize F_u in terms of potential vorticity and potential temperature have had little success (Green, 1970; Wiin-Neilsen and Sela, 1971). Vupputuri (1979) employed an ad hoc parameterization while Harwood and Pyle (1975) deduced the momentum fluxes from Nimbus V SCR data. Until a more satisfactory theoretical approach is available, the satellite data approach seems to be preferrable at this stage.

7.3 AER 2-D Model: Intermediate Results

During the second stage of the development, we have concentrated our efforts on interfacing the chemical scheme with the rest of the model. At the present stage, the model only solves (7.2-20) for the diffusive species. The values necessary for $\bar{v}$, $\bar{w}$, K's are read in from input files. A description of the model can be found in Appendix B.

Three series of chemical studies were made using the oxygen chemistry, the oxygen + HO_x chemistry and the full O_x-HO_x-NO_x-Cl_x chemistry. In each of the studies, we have concentrated on the latitudinal and seasonal behavior of the calculated ozone column densities. This approach is taken because O_3 is a dominant factor in determining the behavior of other trace gases. In addition, observations of the ozone network over the past 10 years have provided a data base with

complete global coverage appropriate for model validation analysis. Fig. 7.1 shows the observed ozone column density as a function of latitude and season. The calculated results will be compared with Fig. 7.1 to judge how well they agree with observations.

In the oxygen chemistry, the classical Chapman scheme is adopted

$$\begin{aligned} O_2 + h\nu &\rightarrow O + O & J_2 \\ O_3 + h\nu &\rightarrow O_2 + O & J_3 \\ O_2 + O + M &\rightarrow O_3 + M & k_2 \\ O + O_3 &\rightarrow 2O_2 & k_3 \end{aligned} \qquad (7.3\text{-}1)$$

where the J's are photolysis rates, k's are reaction rate constants.

The production term takes the form

$$Q_i = 2J_2[O_2] - \frac{k_3 J_3}{k_2[O_2][M]}\,[O_3]^2 \quad . \qquad (7.3\text{-}2)$$

Taking $[O_2] = [M]/4.75$, equation (7.2-20) is solved with the above production terms. The calculated O_3 column densities as a function of latitude and time are given in Figure 7.2. Note that the overall features of the spatial and temporal behavior of the observed O_3 distribution are reproduced. These include:

- The spring time column ozone maximum in the northern hemisphere at 70° N and extending all the way to the pole.

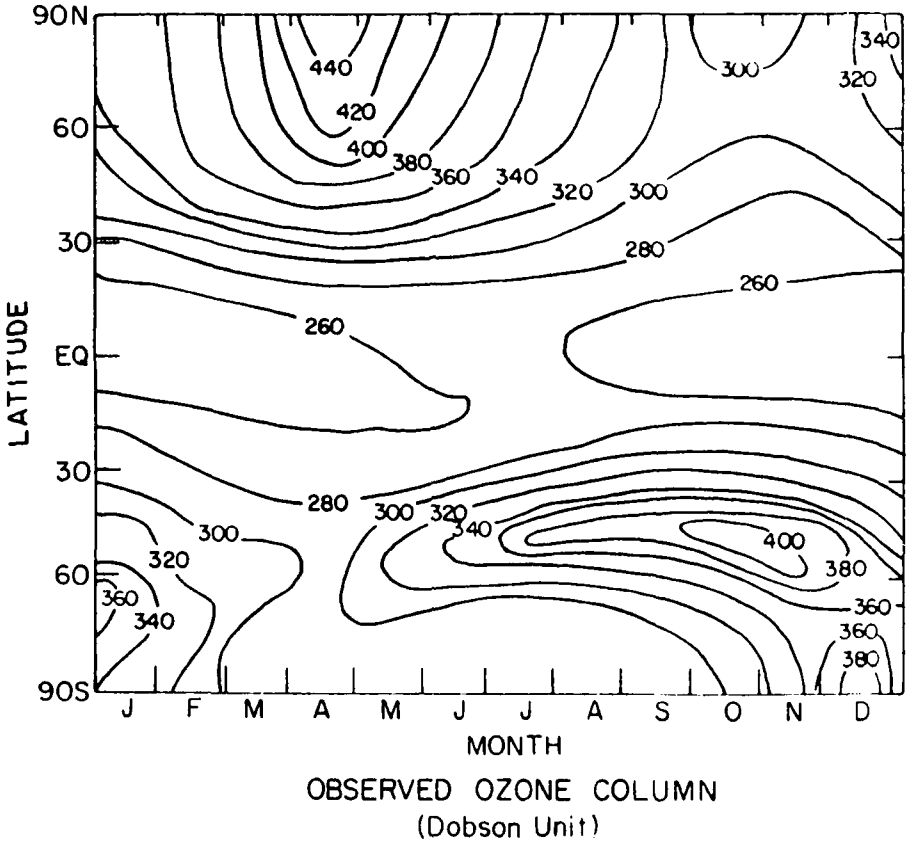
90N
60
30
EQ
30
60
90S
LATITUDE
440
420
400
380
360
340
320
300
280
260
J F M A M J J A S O N D
MONTH
OBSERVED OZONE COLUMN
(Dobson Unit)

Figure 7.1

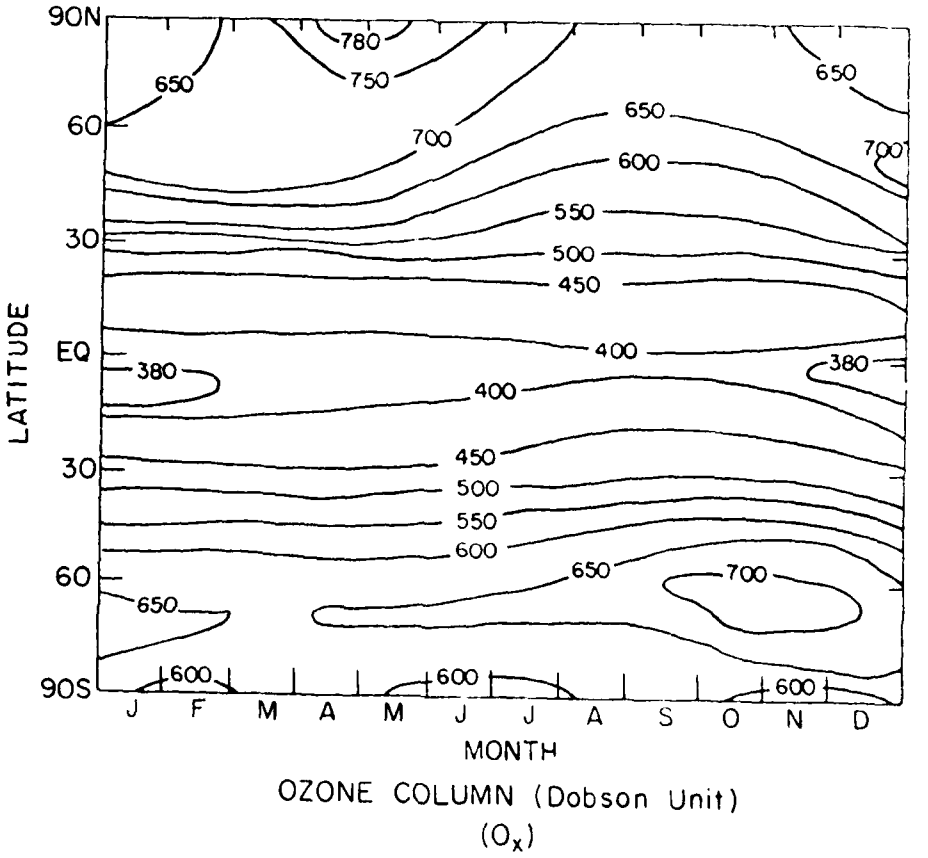

Figure 7.2

Calculated ozone column density as a function of latitude and season using oxygen chemistry only.

- The spring time column ozone maximum in the southern hemisphere at about 60° S.
- The relatively small seasonal variation of the ozone column in the equatorial region.
- The relative magnitudes of the two maxima at high latitudes compared with the values at the equatorial region.

However, the magnitude of the column densities is about a factor of 2 larger than the observed values, suggesting that certain loss terms had been ignored.

In the next series of studies, the $O_x + HO_x$ chemistry is employed. The reactions included are

$$
\begin{aligned}
H_2O + O(^1D) &\rightarrow 2OH & k_a \\
H_2 + O(^1D) &\rightarrow H + OH & k_b \\
OH + HO_2 &\rightarrow H_2O + O_2 & k_c \\
OH + H_2O_2 &\rightarrow H_2O + HO_2 & k_d \\
OH + CO &\rightarrow CO_2 + H & k_e \\
OH + O_3 &\rightarrow HO_2 + O_2 & k_f \\
OH + O &\rightarrow H + O_2 & k_g \\
HO_2 + HO_2 &\rightarrow H_2O_2 + O_2 & k_h \\
HO_2 + O_3 &\rightarrow OH + 2O_2 & k_i \\
HO_2 + O &\rightarrow OH + O_2 & k_j \\
H_2O_2 + h\nu &\rightarrow 2OH & J_a
\end{aligned}
\qquad (7.3\text{-}3)
$$

The chemical production term for O_3 takes the form

$$Q_i = 2J_2[O_2] - 2k_3[O][O_3] - k_f[OH][O_3] - k_i[HO_2][O_3] - 2k_j[O][HO_2] \quad . \tag{7.3-4}$$

The calculated ozone column densities are shown in Fig. 7.3. The magnitude of the column densities is reduced by a factor of 1.8 compared to the oxygen case. It is interesting to note, however, the latitudinal and seasonal behavior remains remarkably similar to the oxygen case. This seems to suggest that although local photochemistry may be responsible for the magnitudes of the calculated ozone column, dynamical transport plays an important role in determining the corresponding seasonal and latitudinal behavior.

In simulating the present atmosphere, the time dependent diffusion equations are solved for the following species:

- Cl_x and its precursor molecules via CH_3Cl, CH_3CCl_3, CCl_4, F-11, F-12
- NO_x and its precursor molecule N_2O
- O_3.

In addition, the following species are calculated assuming photochemical equilibrium:

- $O(^1D)$, $O(^3P)$
- H, OH, HO_2, H_2O_2
- Cl, ClO, HCl, HOCl, $ClNO_3$
- NO, NO_2, HNO_3.

Fixed mixing ratio boundary conditions are used on all the diffusion species except F-11 and F-12 for which time-dependent flux boundary conditions are used. The release of

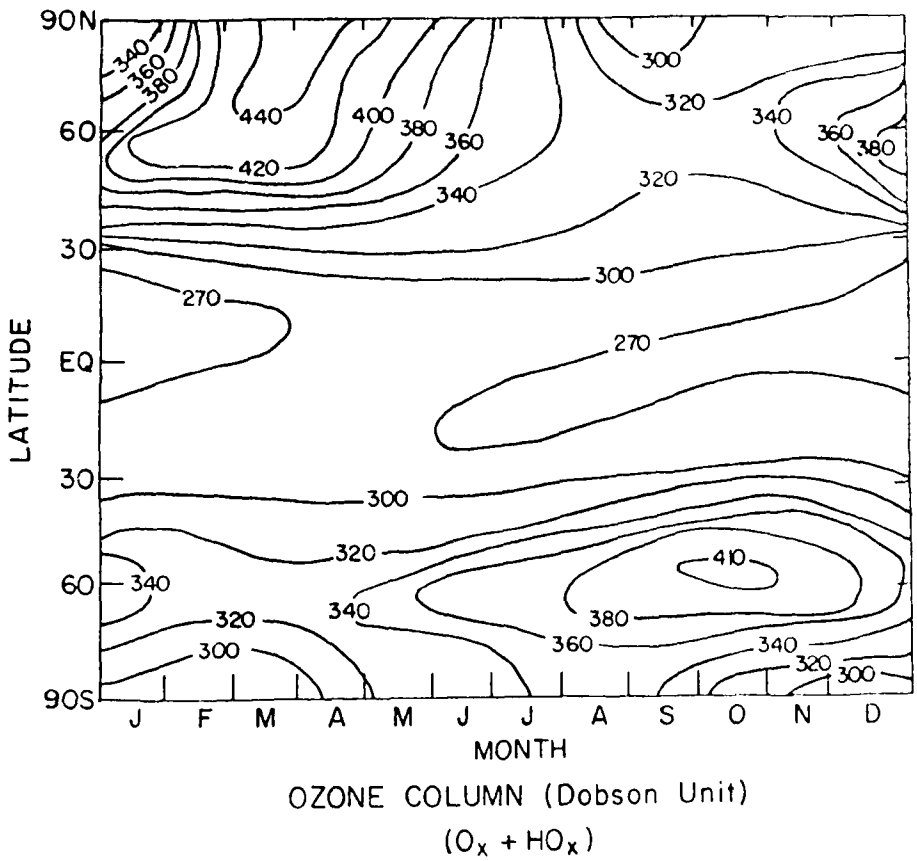

Figure 7.3

Calculated ozone column densities as a function of latitude and season using (oxygen + HO_x) chemistry.

F-11 and F-12 is restricted to between 25° N to 60° N. The release rate follows the data compiled by the CMA Fluorocarbon Panel (1980). In the present model calculation, CH_4, CO and H_2O are specified as a function of latitude, altitude and time.

The distributions of NO_x and Cl_x play an important role in controlling the local radical concentrations which in turn determine the local ozone production and loss rates. Figure 7.4 shows a typical calculated distribution of Cl_x from our simulation. It is worthy of note that in the case of Cl_x and NO_x, the concentrations at the equator are lower than the corresponding concentrations at high latitudes in the lower stratosphere. This is indicative of the upwelling air motion at the equator and subsequent transport of material towards higher latitude. In our calculation, the upper stratosphere concentrations of Cl_x and NO_x are 2 ppbv and 17 ppbv respectively.

Figure 7.5 shows the latitudinal and seasonal variation of calculated ozone column. The magnitude of the ozone column compares favorably with observation around the equatorial region. However, the magnitude of the spring time maxima in both hemispheres is about 30% too low compared to observation.

Figure 7.6 shows the number density distribution of ozone corresponding to the month of April. The maximum number density occurs at 25 km. The slightly higher concentration near the North Pole is indicative of the spring time maximum. Again, compared to observation (cf. Dütsch, 1978), the calculated number density around the North Pole is on the

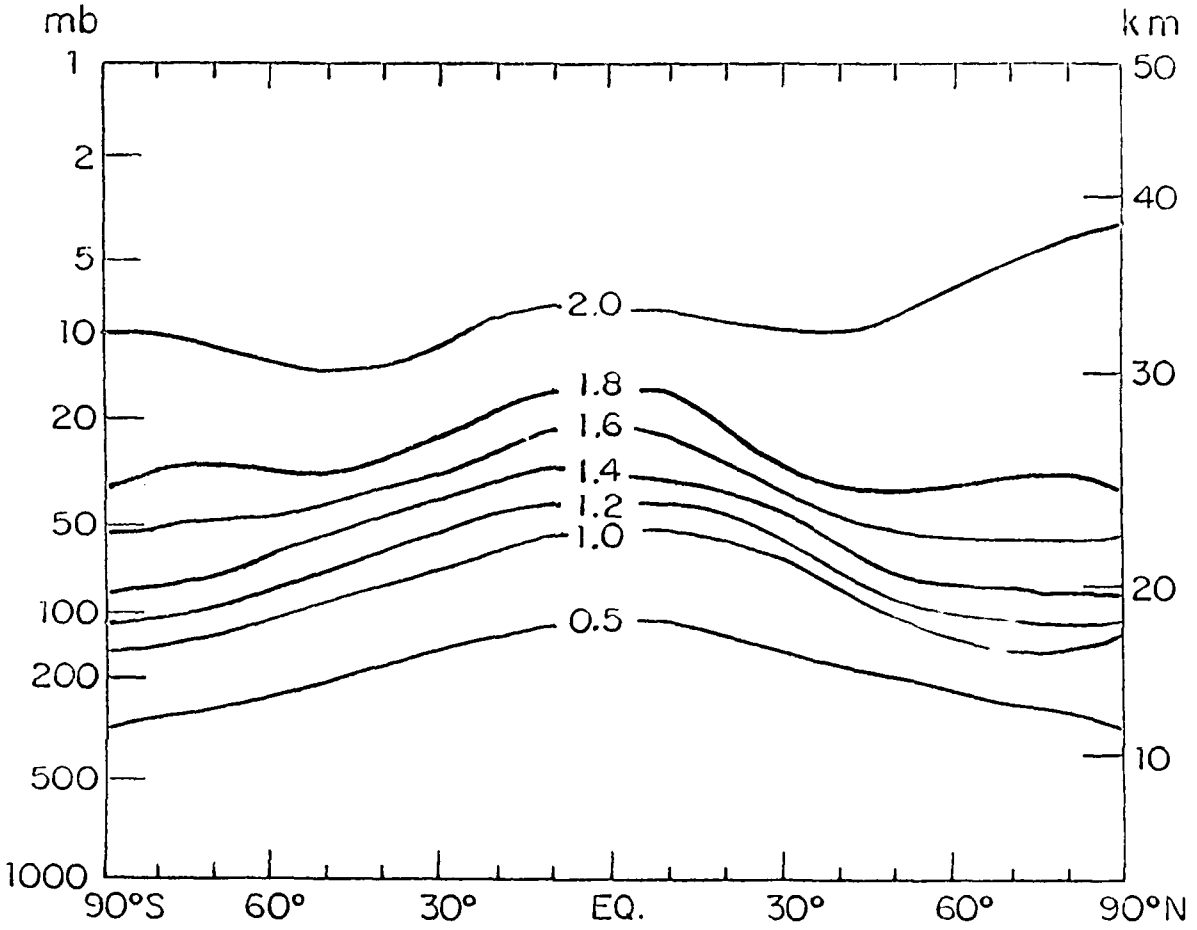

Figure 7.4

Calculated present-day Cl_x mixing ratio as a function of altitude and latitude for the month of April.

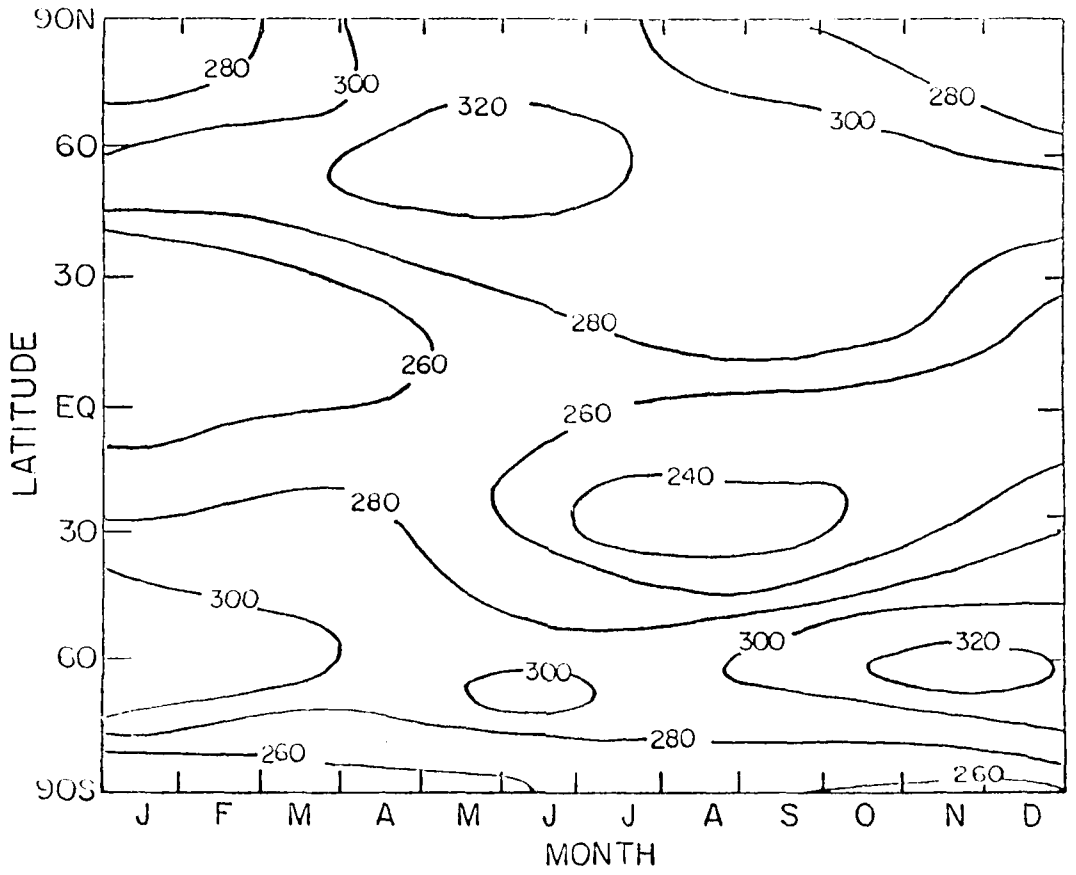

Figure 7.5

Calculated present-day ozone column density as a function of latitude and season.

AD-A092 704 ATMOSPHERIC AND ENVIRONMENTAL RESEARCH INC CAMBRIDGE MA F/G 4/1
MODELING OF CHEMICAL PROCESSES IN THE TROPOSPHERE AND STRATOSPH--ETC(U)
AUG 80 N D SZE, M K KO, R SPECHT, M LIVSHITS F19628-78-C-0215
UNCLASSIFIED AFGL-TR-80-0251 NL

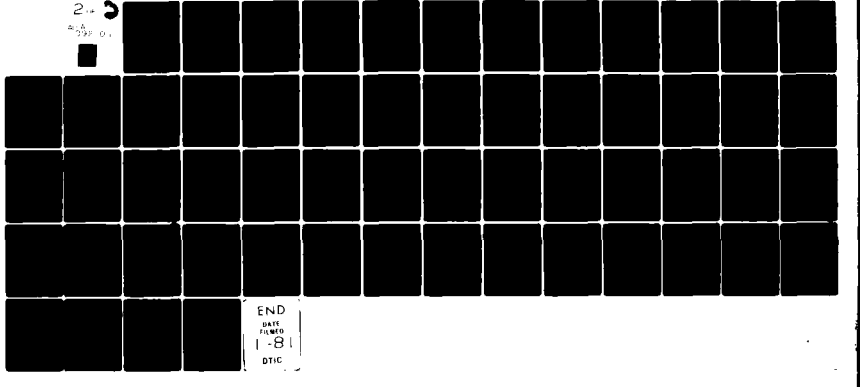

END
DATE FILMED
1-81
DTIC

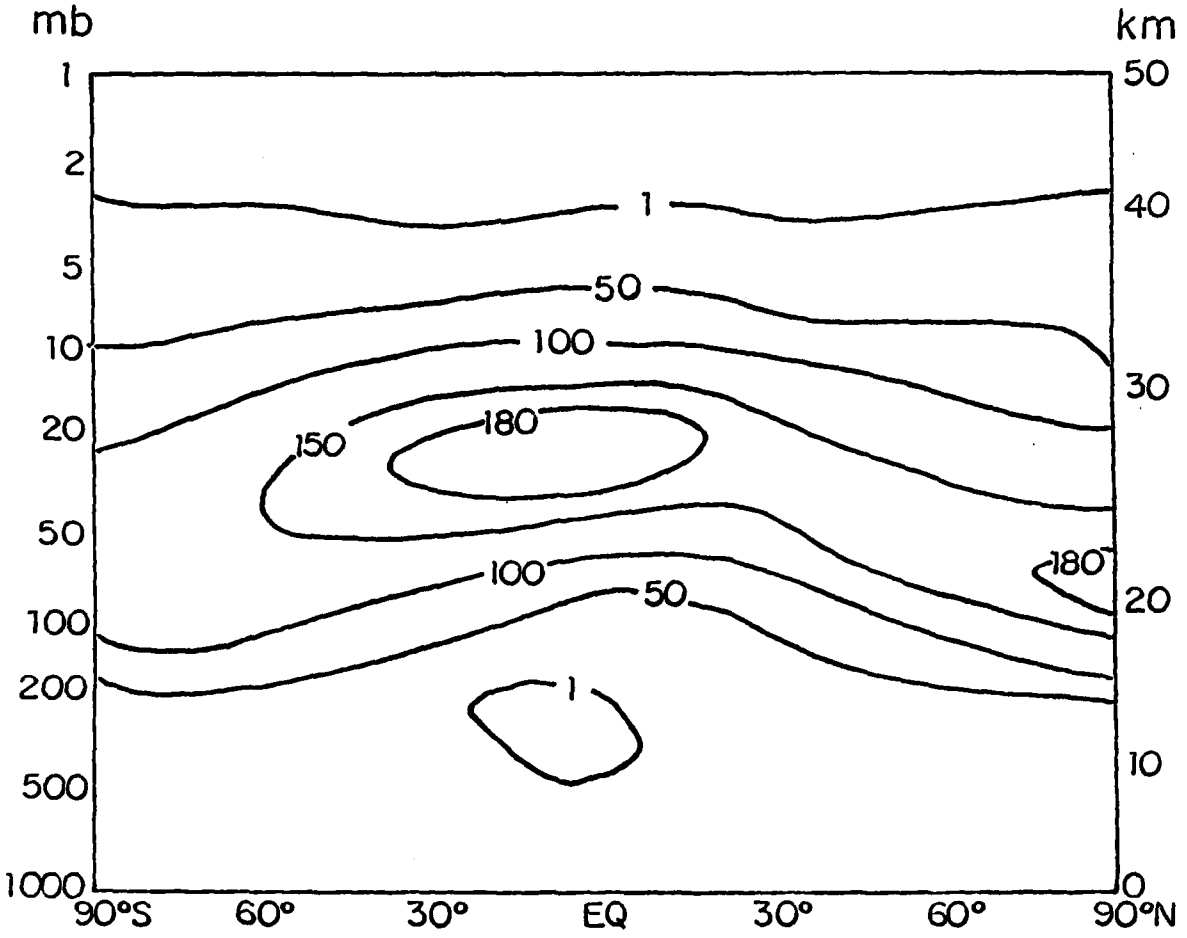

OZONE NUMBER DENSITY (nb)

April

Figure 7.6

Calculated present-day ozone number density as a function of altitude and latitude for the month of April.

low side. We will be performing analyses to try to determine if the discrepancy could be attributed to chemistry or dynamic transport.

We also performed a sensitivity study on the response of the model to changes in Cl_x concentration. More specifically, we solved the O_3 diffusion equation using twice the Cl_x concentration of the present atmosphere, in effect adding an extra 2 ppb of Cl_x to the stratosphere. The result shows that this leads to a 7% reduction of the ozone content of the atmosphere. The % column reduction as a function of season and latitude is given in Figure 7.7. Note that the largest % reduction occurs in the winter hemisphere at high latitudes while the smallest reduction occurs around the equator. The results are given in different format in Figures 7.8a and 7.8b which clearly show the seasonal variation at fixed latitude. These features are in qualitative agreement with those of Pyle (1978) and Vupputuri (1979).

Figures 7.9 through 7.11 shows the altitude and latitude cross-section of % ozone reduction for the months of January, April and July. Figures 7.9 and 7.11 again illustrate that the maximum ozone reduction occurs in the winter hemisphere. Also evident from the figures is the slight local ozone increase at the equator around 10 to 20 km. This is usually attributed to the so-called "self-healing" effect due to the increase of solar flux as a result of O_3 reduction above 20 km.

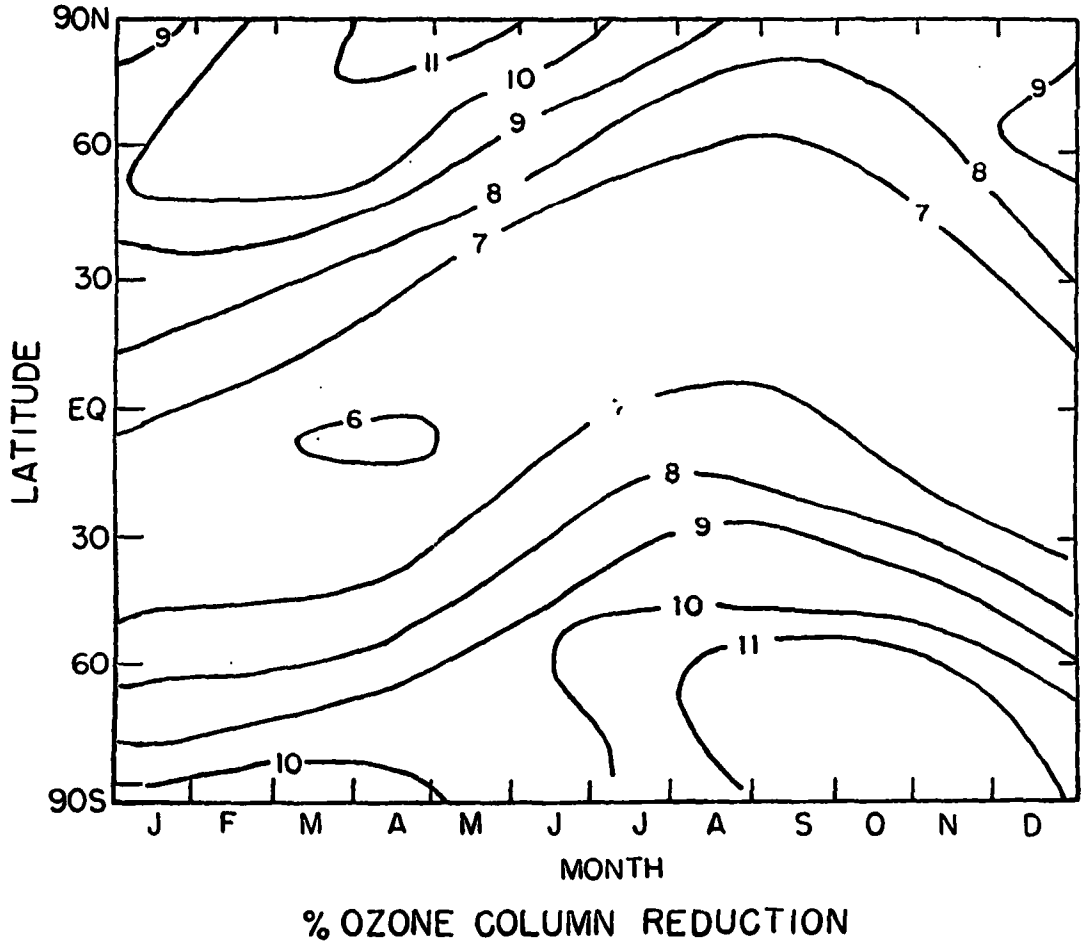

Figure 7.7

Calculated % ozone column reduction as a function of latitude and season for doubling of Cl_x concentration.

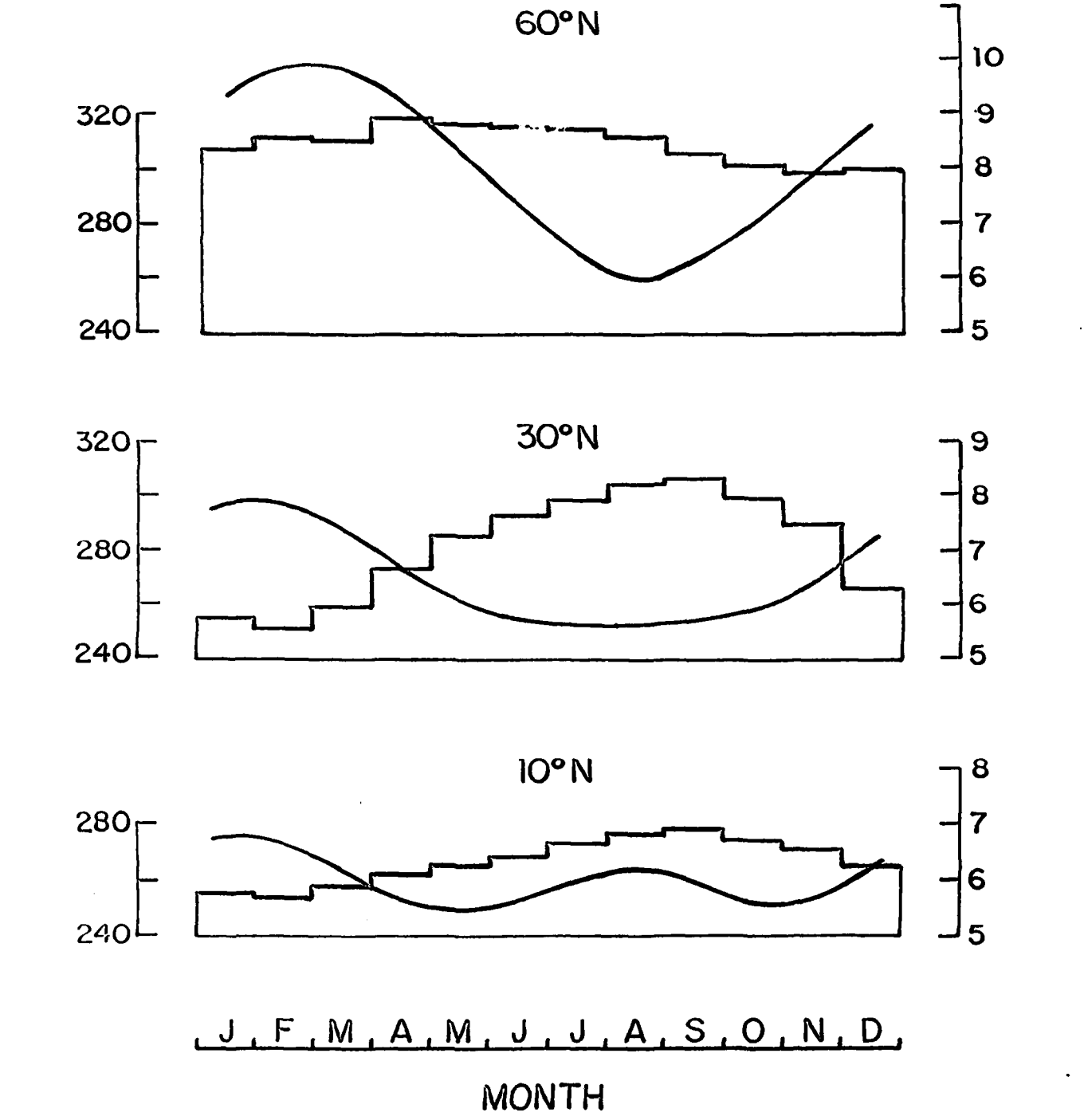

Figure 7.8a

Calculated present-day ozone column densities and % ozone reduction with Cl_x doubling as a function of season for fixed latitude in the northern hemisphere.

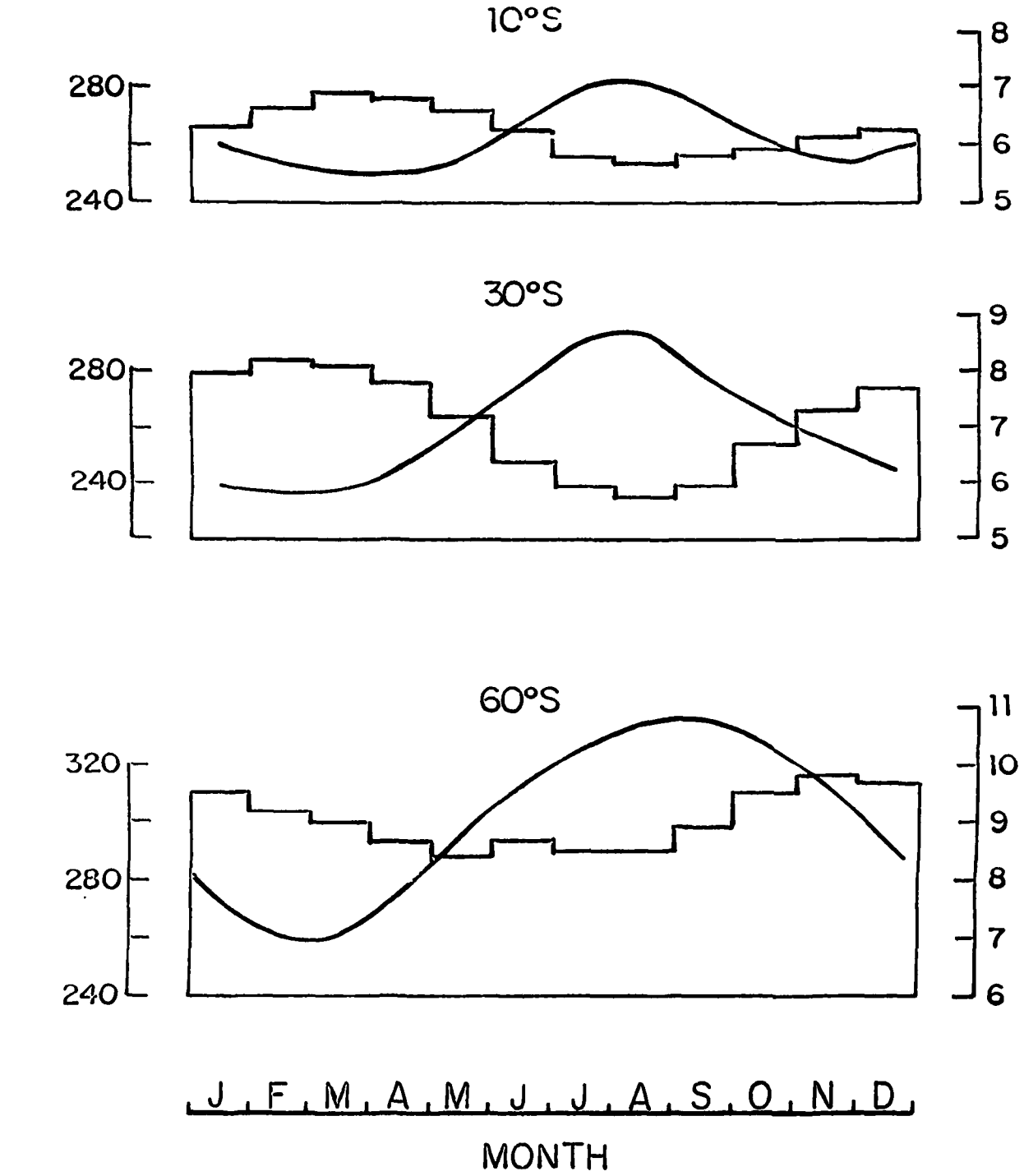

Figure 7.8b

Calculated present-day ozone column densities and % ozone reduction with Cl_x doubling as a function of season for fixed latitude in the southern hemisphere.

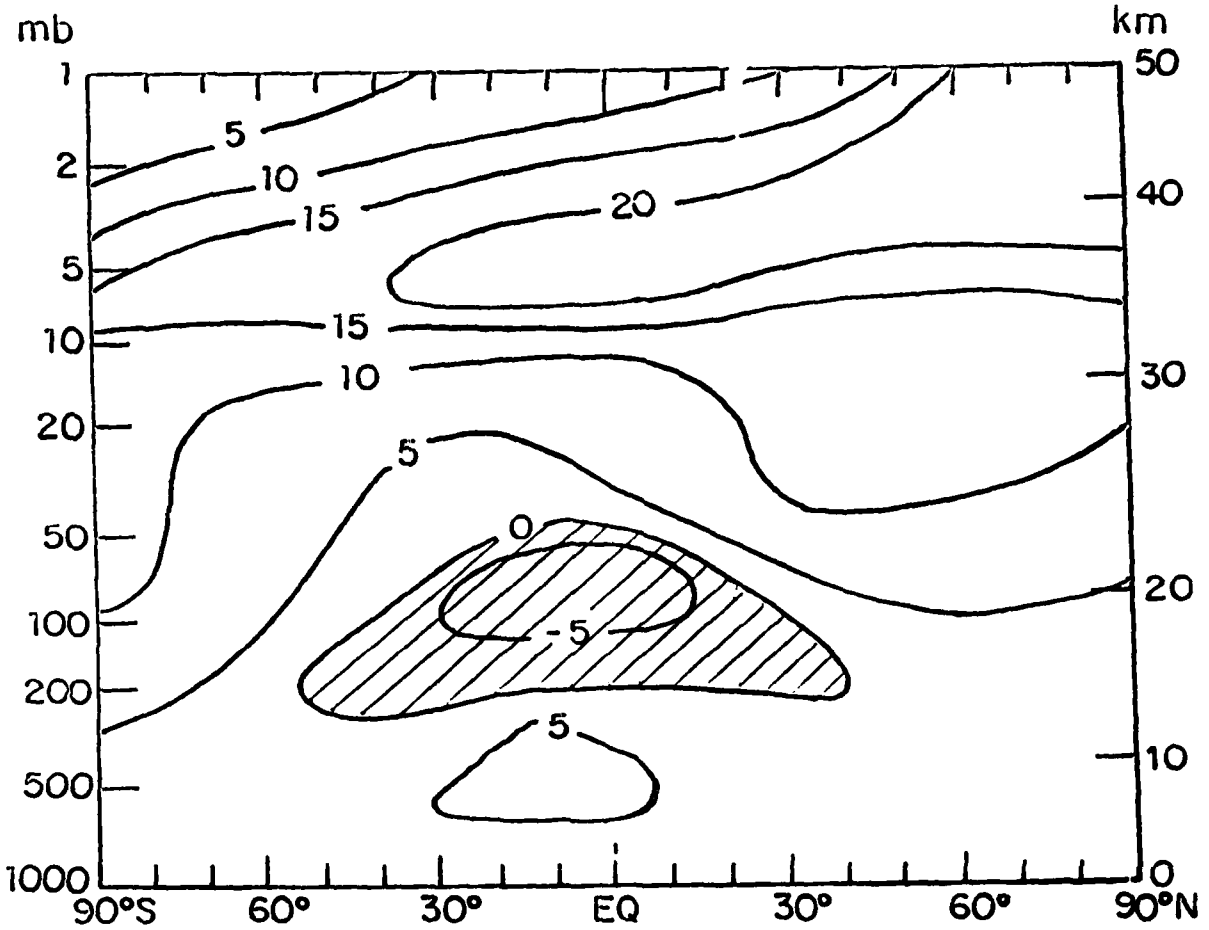

Figure 7.9

Calculated % ozone reduction for Cl_x doubling as a function of altitude and latitude for the month of January.

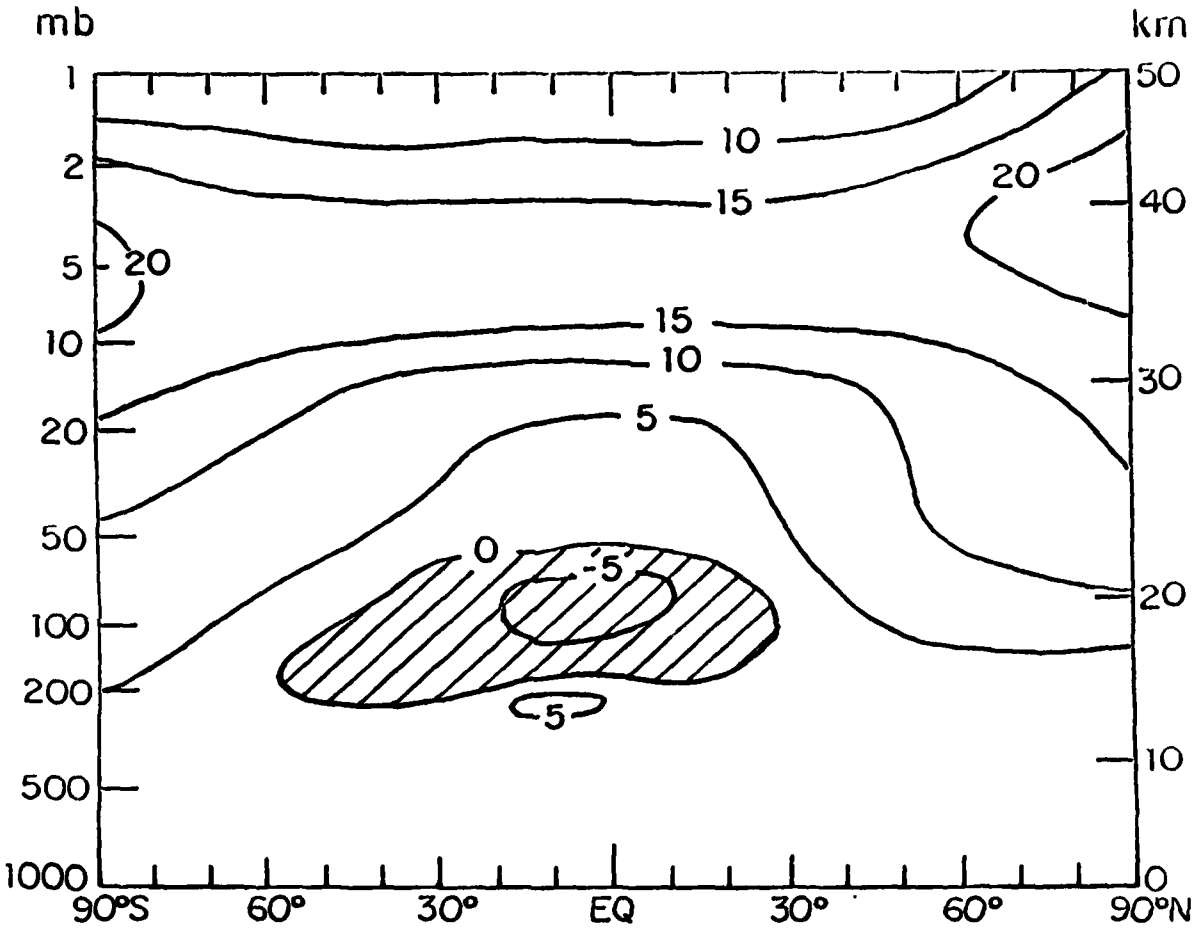

Figure 7.10

Calculated % ozone reduction for Cl_x doubling as a function of altitude and latitude for the month of April.

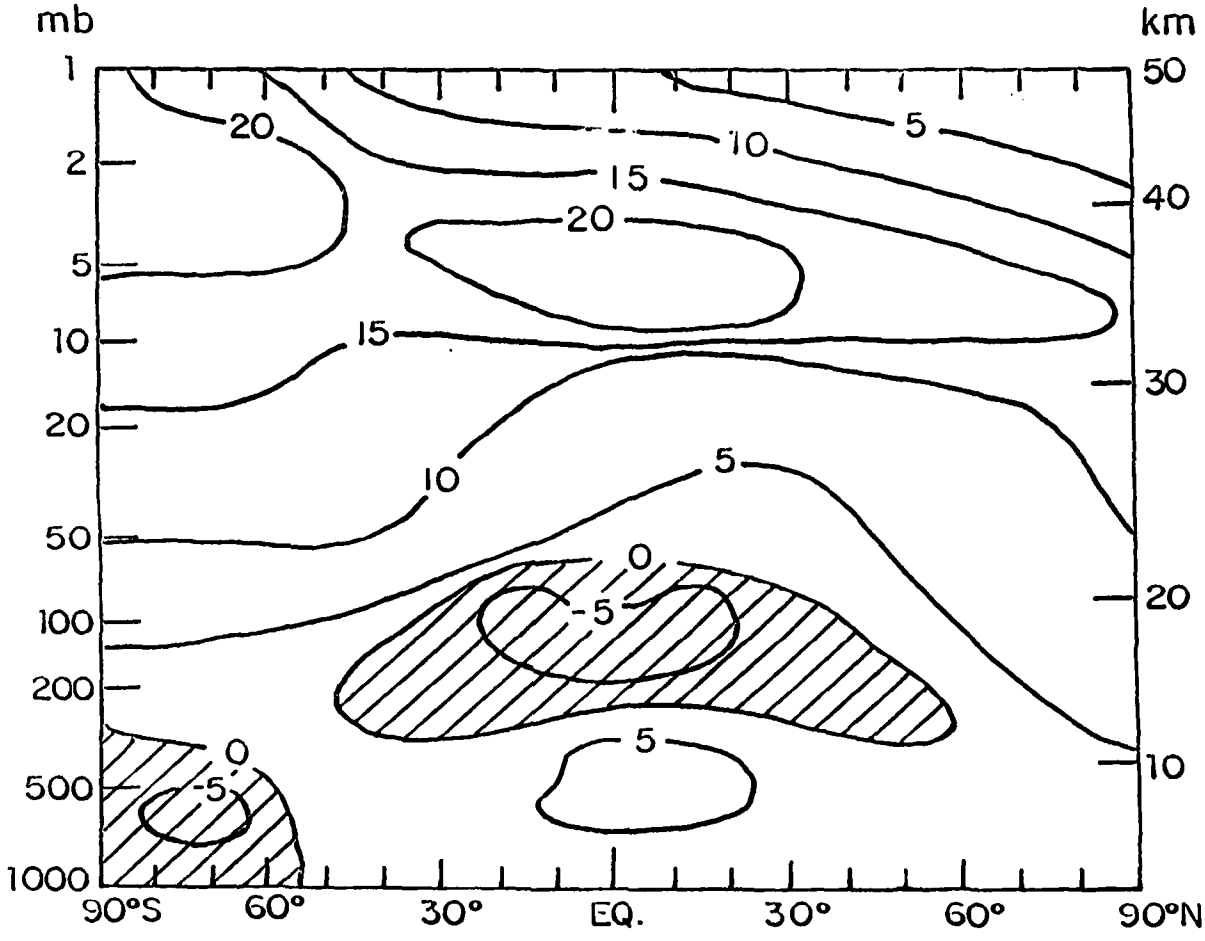

Figure 7.11

Calculated % ozone reduction for Cl_x doubling as a function of altitude and latitude for the month of July.

REFERENCES

Anderson, J.G., H.J. Grassl, R.E. Shetter and J.J. Margitan (1980) Stratospheric Free Chlorine Measured by Balloon Borne in situ Resonance Fluorescence. J. Geophys. Res., 85, 2869.

Bates, D.R. and M. Nicolet (1950) Atmospheric Hydrogen. Publ. Astron. Soc. Pacific, 62, 106.

Buijs, H.L., G. Vail and G. Tremblay (1977) Simultaneous Measurement of the Volume Mixing Ratios for HCl and HF in the Stratosphere. MCA Report, July 1977.

Burrows, J.P., D.I. Cliff, G.W. Harris, B.A. Thrush and J.P.T. Wilkinson (1978) WMO Technical Note No. 511, 25.

Cadle, R.D. (1964) Daytime Atmospheric $O(^1D)$. Disc. Fara. Soc., 37, 66.

Chang, J.S. and F. Kaufman (1978) Upper Bound and Probable Value of the Rate Constant for the Reaction $OH + HO_2 \rightarrow H_2O + O_2$. J. Phys. Chem., 82, 1683.

Chapman, S. (1930) A Theory of Upper Atmospheric Ozone. Mem. Roy. Meteor. Soc., 3, 103.

Chemical Manufacturers Association (1980) World Production and Release of Chlorofluorocarbons 11 and 12 through 1979.

Chylek, P. and T. Coakley (1974) Aerosol and Climate. Science, 83, 75.

Climatic Impact Assessment Program, Report of Findings (1974) Effects of Stratospheric Pollution by Aircraft. DOT-TST-75-50, U.S. Dept. Transportation, December 1974.

Crutzen, P.J. (1970) The Influence of Nitrogen Oxides on the Atmospheric Ozone Content. Quart. J. Roy. Meteor. Soc., 96, 320.

Crutzen, P.J. (1971) Ozone Production Rates in an Oxygen-Hydrogen-Nitrogen Oxide Atmosphere. J. Geophys. Res., 76, 7311.

Crutzen, P.J. (1976) The Possible Importance of COS for the Sulfate Layer of the Stratosphere. Geophys. Res. Lett., 3, 73.

Demore, W.B. (1979) Reaction of HO_2 with O_3 and the Effect of Water Vapor on HO_2 Kinetics. J. Phys. Chem., 83, 113.

Dütsch, H.U. (1971) Photochemistry of Atmospheric Ozone. Advan. Geophys., 15, 219.

Dütsch, H.U. (1978) Vertical Ozone Distribution on a Global Scale. Pure and Appl. Geophys., 116, 514.

Ehhalt, D.H. (1980) The Observation of Long-Lived Trace Gases in the Stratosphere. Review paper presented at the Quadrennial International Ozone Symposium, Boulder, CO., August 1980.

Evans, W.F.J., J.B. Kerr, D.I. Wardle, J.C. McConnell, B.A. Ridley and H.I. Schiff (1976) Intercompariosn of NO, NO_2, and HNO_3 Measurements with Photochemical Theory. Atmosphere, 14, 189.

Farmer, C.B. and O.F. Raper (1977) The HF:HCl Ratio in the 14-38 km Region of the Stratosphere. Geophys. Res. Lett., 4, 527.

Fontanella, J.C., A. Girand, L. Gramont and N. Louisnard (1975) Vertical Distribution of NO, NO_2 and HNO_3 as Derived from Stratospheric Absorption Infrared Spectra. Appl. Opt., 14, 825.

Green, J.S.A. (1970) Transfer Properties of Large Scale Eddies and the General Circulation of the Atmosphere. Quart. J. Roy. Meteor. Soc., 96, 157.

Hampson, J. (1964) Photochemical Behavior of the Ozone Layer. Tech. Note 1627, Can. Arm. Res. and Dev. Establ. Quebec, Canada.

Harries, J.E., D.G. Moss, N.R. Swann, G.F. Neill and P. Gildwang (1976) Simultaneous Measurements of H_2O, NO_2 and HNO_3 in the Daytime Stratosphere from 15 to 30 km. Nature, 259, 300.

Harries, J.E. (1978) Ratio of HNO_3 to NO_2 Concentration in Daytime Stratosphere. Nature, 274, 235.

Hartmann, D.L. and R.R. Garcia (1979) A Mechanistic Model of Ozone Transport by Planetary Waves in the Stratosphere. J Atmos. Sci., 36, 350.

Harwood, R.S. and J.A. Pyle (1975) A Two-Dimensional Mean Circulation Model for the Atmosphere below 80 km. Quart. J. Roy. Meteor. Soc., 101, 723.

Harwood, R.S. and J.A. Pyle (1977) Studies of the Ozone Budget Using a Zonal Mean Circulation Model and Linearized Photochemistry. Quart. J. Roy. Meteor. Soc., 103, 319.

Hering, W.S. and T.R. Borden (1967) Ozonesonde Observations over North America. Environ. Res. Papers, Vols. 2 & 4. Air Force Cambridge Research Labs.

Hochanadel, C.J., J.A. Ghormley and P.J. Ogren (1972) Absorption Spectrum and Reaction Kinetics of the HO_2 Radical in the Gas Phase. J. Chem. Phys., 56, 4426.

Holton, J.R. (1977) The Dynamics Meteorology of the Stratosphere and Mesosphere. Meteor. Monog., 15, No. 37.

Howard, C.J. and K.M. Evenson (1976) Rate Constants for the Reactions of OH with Ethane and Some Halogen Substituted Ethanes at 295 K. J. Chem. Phys., 64, 4303.

Hunten, D.M. (1975) Vertical Transports in Atmospheres. in Atmospheres of Earth and the Planets. B.M. McCormac (ed.) Dordrecht, Holland, pp. 59-72.

Johnston, H.S. (1971) Reduction of Stratospheric Ozone by Nitrogen Oxide Catalysts from Super Sonic Transport Exhaust. Science, 173, 517.

Johnston, H.S. and J. Pokolske (1978) Interpretations of Stratospheric Photochemistry. Rev. Geophys. and Space Phys., 16, 491.

Junge, C.E., C.W. Chagnon and J.E. Manson (1961) Stratospheric Aerosols. Meteor., 18, 81.

Junge, C.E. (1970) Sulphur Budget of the Stratospheric Aerosol Layer. Review paper presented at the International Conference on Structure, Composition and General Circulation of the Upper and Lower Atmospheres and Possible Anthropogenic Perturbations. Melbourne, Australia, January 1970.

Kaufman, F. (1980) Laboratory Measurements of Stratospheric Reactions: Recent Results and their Interpretation. Paper presented at the 14th Informal Conference on Photochemistry, Newport Beach, CA.

Keyser, L.F. (1980) Kinetics of Reaction $OH + H_2O_2 \rightarrow HO_2 + H_2O$ from 245 to 435° K. Paper presented at the 14th Informal Conference on Photochemistry, Newport Beach, CA.

Ko, M.K.W. and N.D. Sze (1980) The CS_2 and COS Budget. in Environmental and Climatic Impact of Coal Utilization. J.J. Singh and A. Deepak (eds.) Academic Press, NY.

Krueger, A.J. and R.A. Minzner (1976) A Midlatitude Ozone Model for the 1976 U.S. Standard Atmosphere. J. Geophys. Res., 81, 4477.

Lii, R.R., R.A. Gorse, Jr., M.C. Sauer, Jr. and S. Gordon (1980) Rate Constant for the Reaction of OH with HO_2. J. Phys. Chem., 84, 819.

Loewenstein, M. and H.F. Savage (1975) Latitudinal Measurements of NO and O_3 in the Lower Stratosphere from 5° to 82° North. Geophys. Res. Lett., 2, 448.

Logan, J.A., M.J. Prather, S.C. Wofsy and M.B. McElroy (1978) Atmospheric Chemistry: Response to Human Influence. Phil. Trans. Roy. Soc., 290, 187.

Lorentz, Z.N. (1967) The Nature and Theory of the General Circulation of the Atmosphere. WMO Tech. Note No. 218.

Luther, F.M. (1973) Monthly Mean Values of Eddy Diffusion Coefficients in the Lower Stratosphere. AIAA Paper 73-495, AIAA/AMS Conference, Denver, CO.

Mahlman, J.D. (1975) Some Fundamental Limitations of Simplified Transport Models. Proceedings of the Fourth CIAP Conference Report, pp. 132, U.S. Dept. Transportation.

Matsuno, T. (1979) Lagrangian Motion of Air Parcels in the Stratosphere in the Presence of Planetary Waves. Pure and Appl. Geophys., 118, 189.

Matsuno, T. and K. Nakamura (1979) The Eulerian and Lagrangian Mean Meridonal Circulations in the Stratosphere at Time of Sudden Warming. J. Atmos. Sci., 36, 640.

McConnell, J.C. and W.F.J. Evans (1978) Implications of Low Stratospheric Hydroxyl Concentrations for CFM and SST Scenario Calculations of Ozone Depletion. EOS Trans. AGU, 59.

McDonald, J. (1971) Presentation before the Department of Commerce Technical Advisory Board on Environmental Aspects of the Supersonic Transport, Boulder, CO., March 1971.

McElroy, M.B. and J.C. McConnell (1971) Nitrous Oxide: A Natural Source of Stratospheric NO. J. Atmos. Sci., 28, 1095.

McElroy, M.B., S.C. Wofsy, J.E. Penner and J.C. McConnell (1974) Atmospheric Ozone: Possible Impact of Stratospheric Aviation. J. Atmos. Sci., 31, 287.

McElroy, M.B., S.C. Wofsy and N.D. Sze (1980) Photochemical Sources for Atmospheric H_2S. Atmos. Environ., 14, 159.

Menzies, R.T. (1979) Remote Measurement of ClO in the Stratosphere. Geophys. Res. Lett., 6, 151.

Mihelcic, D., D.H. Ehhalt, G.F. Kulessa, J. Klomfass, M. Trainer, U. Schmidt and H. Rohrs (1978) Measurement of Free Radicals in the Atmosphere by Matrix Isolation and Electron Paramagnetic Resonance. Pure and Appl. Geophys., 116, 530.

Mitchell, J.M. (1971) The Effect of Atmospheric Aerosols on Climate with Special Reference to Temperature near the Earth's Surface. J. Appl. Meteor., 11, 651.

Murcray, D.G., A. Goldman, F.H. Murcray, F.J. Murcray and W.J. Williams (1979) Stratospheric Distribution of $ClNO_3$. Geophys. Res. Lett., 6, 257.

NAS (1976) Halocarbons: Effect on Stratospheric Ozone. National Academy of Sciences, Washington, DC.

NAS (1980) Stratospheric Ozone Depletion by Halocarbons: Chemistry and Transport. National Academy of Sciences, Washington, DC.

NASA (1977) Chlorofluoromethanes and the Stratosphere. NASA Ref. Publ. 1010, Washington, DC.

NASA (1979) The Stratosphere: Present and Future. R.D. Hudson (ed.) NASA Ref. Publ. 1049, NASA Goddard Space Flight Center.

Newell, R.A., J.M. Wallace and J.R. Mahaney (1966) The General Circulation of the Atmosphere and its Effect on the Movement of Trace Substances II. Tellus, 18, 363.

Nicolet, M. (1975) Stratospheric Ozone: An Introduction to its Study. Rev. Geophys. and Space Phys., 13, 593.

Nicolet, M. and E. Vergison (1971) L'Oxyde Azotuex dans la Straospere. Aeron. Acta., A-91.

Oort, A.H. and E. M Rasmussen (1971) Atmospheric Circulation Statistics. NOAA Prof. Paper 5. National Oceanic and Atmospheric Administration.

Plumb, R.A. (1979) Eddy Fluxes of Conserved Quantities by Small Amplitude Waves. J. Atmos. Sci., 36, 1699.

Pollack, J.B., O.B. Toon, A. Summers, B. Baldwin, C. Sagan and W. van Camp (1976) Stratospheric Aerosols and Climatic Changes. Nature, 263, 551.

Pyle, J.A. (1978) A Simple Calculation of Ozone Depletion by Chlorofluoromethanes using a Two-Dimensional Model. Nature, 271, 42.

Reed, R.J. and K.Z. German (1971) A Contribution to the Problem of Stratospheric Diffusion by Large Scale Mixing. Mon. Weath. Rev., 93, 313.

Riegler, G.R., S.K. Atreya, T.M. Donahue, S.C. Liu, B. Wasser and J.F. Drake (1977) UV Stellar Occultation Measurements of Nighttime Equatorial Ozone. Geophys. Res. Lett., 4, 145.

Rowland, F.S. and M.J. Molina (1975) Chlorofluoromethanes in the Environment. Rev. Geophys. and Space Phys., 13, 1.

Sze, N.D. (1978) Stratospheric Fluorine: A Comparison Between Theory and Measurements. Geophys. Res. Lett., 5, 781.

Sze, N.D. (1979) Odd Hydrogen Processes. in Man and Stratospheric Ozone. F.A. Bower and R.B. Ward (eds.) CRC Publ.

Sze, N.D. and M.K.W. Ko (1979a) Is CS_2 a Precursor for Atmospheric COS? Nature, 278, 731.

Sze, N.D. and M.K.W. Ko (1979b) CS_2 and COS in Stratospheric Sulfur Budget. Nature, 280, 308.

Sze, N.D. and M.K.W. Ko (1980a) CS_2 and COS in Atmospheric Sulfur Budget. in Environmental and Climatic Impact of Coal Utilization. J.J. Singh and A. Deepak (eds.) Academic Press, NY.

Sze, N.D. and M.K.W. Ko (1980b) Photochemistry of COS, CS_2, CH_3SCH_3 and H_2S: Implication for the Atmospheric Sulfur Cycle. Atmos. Environ. (in press).

Sze, N.D. and M.K.W. Ko (1980c) Could the Reaction of HO_2NO_2 with OH be a Sink for Stratospheric Odd Hydrogen? submitted to Atmos. Environ.

Thrush, B.A. (1978) Recent Developments in Atmospheric Chemistry. Nature, 276, 345.

Trevor, P.L., J.S. Chang and J.R. Barker (1980) Kinetics of Some Bimolecular Reactions of Pernitric Acid (HO_2NO_2). Paper presented at the 14th Informal Conference on Photochemistry, Newport Beach, CA.

U.S. Standard Atmosphere Supplement (1966) U.S. Government Printing Office, Washington, DC.

Wiin-Neilsen, A. and J. Sela (1971) On the Transport of Quasi-Geostrophic Potential Vorticity. Mon. Weath. Rev., 99, 447.

Wine, P.H., A.R. Ravishankara, N.M. Kreutter, R.C. Shah, J.M. Nicovich and R.L. Thompson (1980) Rate of Reaction of OH with HNO_3. submitted to J. Geophys. Res.

Wofsy, S.C. (1976) Interactions of CH_4 and CO in the Earth's Atmosphere. Ann. Rev. Earth and Planet. Sci., 4, 441.

Wofsy, S.C. and M.B. McElroy)1973) On Vertical Mixing in the Stratosphere and Lower Mesosphere. J. Geophys. Res., 78, 2619.

Yung. Y.L., J.P. Pinto, R.T. Watson and S.P. Sanders (1980) Atmospheric Bromine and Ozone Perturbations in the Lower Stratosphere. J. Atmos. Sci., 37, 339.

APPENDIX A

DOCUMENTATION OF THE AER 1-D PHOTOCHEMICAL DIFFUSION MODEL

I. GENERAL STRUCTURE

The AER one-dimensional photochemical diffusive model calculates the number densities of chemical species in the earth's atmosphere with a variety of user-selected options.

The basic design of the program has been discussed in Section 3. In Figure A-1, a more detailed flow chart of the model is presented. In what follows, each component of the model will be briefly discussed.

In this section, some of the variables used in the program will be defined. All variables that are essential to input, output are included in the following discussion.

The atmosphere is divided into 81 levels each 1 km thick. The bottom layer is at ground level. All altitude-dependent variables are given in terms of 81 element arrays; these include:

TIALT(81): Altitude array, gives the corresponding geometrical altitude of each level in cm.

TITK(81): Gives the temperature of each level (°K)

EDC(81): Gives the values of the eddy diffusion coefficient at each level (cm^2/sec)

DM(81): The air density at each level ($\frac{molecules}{cm^3}$,

SS(3240): Array for species number densities ($\frac{molecules}{cm^3}$). Number densities are stored in 40 records, each 81 elements long. The density of the I^{th} species at the J^{th} level is given by SS((I-1) x 81 + J)

SM(1458): Array for storing the calculated diurnal-averaged member densities ($n(\overline{t,z})$) for photochemical species. Number densities are stored in 18 records each 81 elements long. The mean density for the I^{th} specie at the J^{th} level is given by SM((I-1) x 81 + J)

SPAIR(9,71): Array for storing the calculated diurnal-averaged product of number densities ($\overline{n_i(t,z) \times n_j(t,z)}$). These terms are necessary for computing the production and loss rates of the diffusion species in the diurnal mode

SJ(2835): Array for storing calculated photolysis rates as functions of altitude. There are 35 records each 81 elements long. The photolysis rate for the I^{th} photolytic reaction at each level J is given by SJ((I-1) x 81 + J)

SR(4050): Array for storing the calculated altitude-dependent reaction rates. There are 50 records each 81 elements long. The I^{th} altitude-dependent reaction rate at the J^{th} level is given by SR((I-1) x 81 + J)

Since the photochemical species are solved one altitude at a time, it is convenient to define working arrays for variables at one altitude; these include:

SBUF(378): Working array for storing the time-dependent number densities at the altitude. There are 18 records each 21 elements long. The number densities for the I^{th} specie at the K^{th} time step is given by SBUF((I-1) x 21 + K) [use in diurnal option only]

J(50): Working array for storing photolysis rates at the altitude

DSJ(580): Working array for storing the time-dependent photolysis rate at the altitude. There are 27 records each 21 elements long. The I^{th} photolytic rate at K^{th} time step is given by DSJ((I-1) x 21 + K)

R(75): Working array for storing all reaction rates at the altitude

The following arrays are used in photolysis calculation. The array index corresponds to the wavelength dependence:

WL(72): Gives the wavelength of the index in $\mathring{A}$

FLX(72): Gives the unattenuated solar flux integrated over the corresponding wavelength window $(\frac{1}{cm^2 \text{ sec}})$

QA(2520): Gives the absorption cross-section (cm^2) for the photolytic processes. There are 35 records each 72 elements long. The cross-section of the I^{th} process at the J^{th} wavelength is given by QS((I-1) x 72 + J)

In addition there are:

SID(50): Alphanumeric symbols for chemical species

QID(25): Alphanumeric symbols for photolytic process

RR(4,75): Parameters for computing reaction rate constants. Each reaction is parameterized by 4 variables.

BCB(50): Bottom boundary values for the species. Two formats accepted. IF 0 < BCB(I) < 1, BCB(I) is assumed to be the bottom volume mixing ratio. Otherwise, BCB(I) is assumed to be the boundary flux in $\frac{\text{molecules}}{\text{cm}^2 \text{ sec}}$

BCT(50): Top boundary condition. The comments on formats in BCB apply here also

DELT(21): Gives the time intervals between time steps in seconds

FSF(50)
ICF(919): Array necessary for closure families

II. CHEMICAL SCHEME

The species included are:

Photochemical species

Oxygen family: $O(^1D)$, O

Hydrogen family: H, OH, HO_2, H_2O_2, CH_2O

Chlorine family: Cl, ClO, HCl, HOCl, $ClNO_3$

Nitrogen family: NO, NO_2, HNO_3, NO_3, N_2O_5, HO_2NO_2

Diffusion species

N_2O, CH_4, H_2, CH_3Cl, CCl_4, $CFCl_3$, CF_2Cl_2, CF_2O, CO, NOX, ClX, FX, O_3

Fixed species

H_2O, O_2, M

The species NOX, ClX and FX correspond to

NOX (odd nitrogen species) = NO + NO_2 + HNO_3 + NO_3 + $2 \times N_2O_5$ + HO_2NO_2 + $ClNO_3$

ClX (odd chlorine species) = Cl + ClO + HCl + HOCl + $ClNO_3$

FX (odd fluorine speices).

The chemical species react with each other via photolysis, two-body and three-body reactions. The reactions included in the model are listed in Table A-1 while the photolytic processes are given in Table A-2. The meaning of the reaction rate parameters is discussed in IV. The reaction rates quoted here follow the NASA (1979) recommendations.

In addition to chemical losses, some species are removed by heterogeneous removal processes of rainout and washout. Heterogeneous processes are included in the loss terms of HNO_3, HCl and H_2O_2. The process is modeled by a pseudo-first order rate in the troposphere with an effective lifetime of approximately 7 days (cf. Wofsy, 1976).

Finally, boundary values are prescribed for the diffusive species to simulate exchange with the ground. These are given in Table A-3.

TABLE A-1

REACTION RATE PARAMETERS

	TYPE	PAR1	PAR2	PAR3	
1	2.	1.66E-12	1.07E+03	0.	OH+CH3CL=XX+H2O,2
2	1.	2.35E-10	0.	0.	H2O+O1D=2*OH,1
3	1.	1.40E-10	0.	0.	CH4+O1D=CH2O+OH,1
4	1.	1.00E-10	0.	0.	H2+O1D=OH+H,1
5	2.	1.80E-32	-3.40E+02	0.	H+O2+M=HO2+M,2
6	2.	1.40E-10	4.70E+02	0.	H+O3=OH+O2,2
7	2.	1.60E-12	9.40E+02	0.	OH+O3=HO2+O2,2
8	2.	1.0(-11)	7.5627	0.	OH+H2O2=H2O+HO2,2
9	2.	1.40E-14	5.80E+02	0.	HO2+O3=OH+2*O2,2
10	2.	1.00E-10	2.50E+02	0.	HO2+O=OH+O2,2
11	1.	8.00E-12	0.	0.	HO2+NO=OH+NO2,1
12	1.	4.00E-12	0.	0.	HO2+CLO=HOCL+O2,1
13	1.	2.50E-12	0.	0.	HO2+HO2=H2O2+O2,1
14	1.	4.00E-11	0.	0.	HO2+OH=H2O+O2,1
15	1.	4.50E-11	0.	0.	HO2+CL=HCL+O2,1
16	1.	1.00E-11	0.	0.	H+HO2=H2+O2,1
17	2.	4.20E-10	9.50E+02	0.	H+HO2=2*OH,2
18	2.	2.10E-13	1.15E+02	0.	OH+CO=H+XX,2
19	2.	1.00E-10	2.50E+02	0.	OH+O=H+O2,2
20	2.	2.00E-12	3.13E+02	0.	OH+HCL=H2O+CL,2
21	2.	2.36E-12	1.71E+03	0.	OH+CH4=CH2O+XX,2
22	0.	2.90E+00	2.40E-11	1.30E+00	OH+NO2=HNO3+M,4
23	1.	8.50E-14	0.	0.	OH+HNO3=H2O+NO3,1
24	1.	1.70E-12	0.	0.	OH+OH=H2O+O,1
25	2.	6.70E-12	2.01E+03	0.	OH+H2=H2O+H,2
26	2.	5.70E-11	2.40E+03	0.	CL+H2=HCL+H,2
27	1.	6.00E-13	0.	0.	CL+H2O2=HCL+HO2,1
28	0.	3.40E+00	1.50E-11	1.90E+00	CLO+NO2=CLNO3+M,4
29	2.	2.80E-11	2.57E+02	0.	CL+O3=CLO+O2,2
30	2.	9.90E-12	1.36E+03	0.	CL+CH4=HCL+CH2O,2
31	2.	7.70E-11	1.30E+02	0.	CLO+O=CL+O2,2
32	1.	2.00E-11	0.	0.	CLO+NO=CL+NO2,1
33	1.	0.	0.	0.	O+HCL=OH+CL,1
34	2.	1.05E-34	-5.20E+02	0.	O+O2+M=O3+M,2
35	2.	1.30E-11	2.14E+03	0.	O+O3=2*O2,2
36	1.	1.00E-12	0.	0.	NO2+NO3=N2O5,1
37	2.	2.30E-12	1.45E+03	0.	NO+O3=NO2+O2,2
38	2.	1.20E-13	2.45E+03	0.	NO2+O3=NO3+O2,2
39	1.	9.12E-12	0.	0.	NO2+O=NO+O2,1
40	1.	5.00E-11	0.	0.	N2O+O1D=XX+O2,1
41	1.	5.00E-11	0.	0.	N2O+O1D=2*NO,1
42	1.	3.00E-10	0.	0.	O1D+CFCL3=XX+CLO,1
43	1.	3.00E-10	0.	0.	O1D+CF2CL2=XX+CLO,1

TABLE A-1 (cont.)

	TYPE	PAR1	PAR2	PAR3	
44	1.	0.	0.	0.	O1D+CH3CL=OH+XX,1
45	1.	0.	0.	0.	O1D+CCL4=XX+CLO,1
46	2.	2.10E-11	-1.07E+02	0.	O1D+M=O+M,2
47	0.	5.00E+00	6.50E-12	5.00E+00	HO2+NO2=HO2NO2+M,4
48	1.	3.00E-13	0.	0.	OH+HOCL=H2O+CLO,1
49	1.	1.00E-10	0.	0.	O1D+CF2O=XX,1
50	1.	1.00E-14	0.	0.	O+HOCL=OH+CLO,1
51	1.	1.00E-14	0.	0.	CL+HOCL=HCL+CLO,1
52	1.	9.10E-12	0.	0.	CLO+OH=HO2+CL,1
53	2.	3.50E-12	1.56E+03	0.	CH3CCL3+OH=XX+H2O,2
54	1.	4.00E-15	0.	0.	O21+O3=2*O2+O,1
55	2.	0.	0.	0.	CLO+HO2=HCL+O3,2
56	2.	0.	0.	0.	CLO+OH=HCL+O2,2
57	1.	1.00E-11	0.	0.	CH2O+OH=H2O+CO+H,1
58	2.	9.20E-11	6.90E+01	0.	CL+CH2O=HCL+CO+H,2
59	2.	5.00E-12	2.00E+02	0.	HO2NO2+OH=H2O+NO2,2
60	1.	1.00E-12	0.	0.	HO2NO2+CL=HCL+NO2,1
61	2.	5.20E-06	1.01E+04	0.	HO2NO2+M=HO2+NO2,2
62	2.	1.00E-15	0.	0.	HO2NO2+CLO=HOCL+NO2,2
63	2.	3.00E-12	8.08E+02	0.	HO2NO2+O=OH+NO2,2
64	2.	3.00E-12	8.08E+02	0.	CLNO3+O=CLO+NO3,2

TABLE A-2

PHOTOLYTIC PROCESSES

$O_2 + h\nu \rightarrow O + O$

$O_3 + h\nu \rightarrow O_2 + O$

$O_3 + h\nu \rightarrow O_2 + O(^1D)$

$NO_2 + h\nu \rightarrow NO + O$

$HNO_3 + h\nu \rightarrow OH + NO_2$

$NO_3 + h\nu \rightarrow NO + O_2$

$N_2O_5 + h\nu \rightarrow NO_2 + NO_3$

$N_2O + h\nu \rightarrow N_2 + O$

$ClNO_3 + h\nu \rightarrow ClO + NO_2$

$HCl + h\nu \rightarrow H + Cl$

$HOCl + h\nu \rightarrow OH + Cl$

$H_2O_2 + h\nu \rightarrow OH + OH$

$CH_2O + h\nu \rightarrow 2H + CO$

$CH_2O + h\nu \rightarrow H_2 + CO$

$H_2O + h\nu \rightarrow H + OH$

$HO_2NO_2 + h\nu \rightarrow HO_2 + NO_2$

$CFCl_3 + h\nu \rightarrow$ product

$CF_2Cl_2 + h\nu \rightarrow$ product

$CCl_4 + h\nu \rightarrow$ product

$CH_3Cl + h\nu \rightarrow$ products

$CF_2O + h\nu \rightarrow$ products

$CH_3Cl_3 + h\nu \rightarrow$ products

It is assumed that $CFCl_3$, CF_2Cl_2, CCl_4, CH_3Cl and CH_3Cl_3 release all their chlorine atoms following initial reactions.

TABLE A-3

BOUNDARY CONDITIONS

Fixed Mixing Ratio Boundary Conditions

N_2O	300	ppbv
CH_4	1.5	ppmv
H_2	500	ppbv
CH_3Cl	1.2	ppbv
CCl_4	130	pptv
CO	200	ppbv
NOX	100	pptv
ClX	1	ppbv
O_3	18	ppbv

Flux Boundary Conditions

$CFCl_3$	9.3×10^5	$\frac{\text{molecules}}{\text{cm}^2 \text{ sec}}$
CF_2Cl_2	1.3×10^6	$\frac{\text{molecules}}{\text{cm}^2 \text{ sec}}$
CH_3CCl_3	1.0×10^7	$\frac{\text{molecules}}{\text{cm}^2 \text{ sec}}$
CF_2O	1.0×10^3	$\frac{\text{molecules}}{\text{cm}^2 \text{ sec}}$
FX	1.0×10^3	$\frac{\text{molecules}}{\text{cm}^2 \text{ sec}}$

III. INPUT

The BLOCK DATA contains the information necessary to initialize the variables in the program.. Any changes can be made directly in the routine. The block data values are overridden by the use of Namelist INPUT, or tape input.

BLOCK DATA:

The BLOCK DATA is separated into 4 routines BD1, BD2, BD3 and BD4.

BD1: Contains a set of values for all chemical species concentrations. These correspond to the values used for the fixed species throughout the program and serve as first guess values for the calculated species. BD1 also contains an identity array for all the chemical species giving the chemical symbol of the specie in alphanumeric format. This facilitates an easy search procedure. The BLOCK DATA values can be overridden if one decides to read in previously calculated number densities attached as an input file (tape 7 input).

BD2: Contains the necessary information for setting up the chemical reaction scheme. It consists of an array, RR(4,75), specifying 4 parameters for calculating the reaction rate constant for each of the reactions. It also contains the absorption cross-sections for photolytic processes. Both

RR and QS can be entered via namelist to override BLOCK DATA values.

BD3: Contains the standard atmospheric temperature as a function of altitude; the array giving the integrated unattenuated solar flux as a function of wavelength intervals.

BD4: Contains parameters necessary for computing the eddy diffusion coefficients.

Namelist Input:

Input can also be provided by a namelist called LIST. For each case to be run, the program makes one read of the namelist LIST from a local file tape 5.

The following is a description of all the parameters in namelist LIST:

Parameter for Initialization

ZB = altitude of bottom boundary (cm)

ZT = altitude of top boundary (cm)

H(cm) = the thickness of each interval; program set up for H = 1.E5 cm or 2.E5 cm

MODE = 0; use BLOCK DATA values for species densities

= 1; read species density profiels from a local file tape 7, which contains previously calculated number densities default value is 0.

Parameters for Chemical Scheme:

RR = array containing parameters for calculating reaction rates (default to BLOCK DATA values)

QS = array containing absorption cross-sections (default to BLOCK DATA values)

PJ03 = parameter for photolysis rate of $O_3 + h\nu \rightarrow O_2 + O$ for $\lambda > 4025$ Å

W0 = sedimentation velocity (set = 0 for molecules)

FSF, ICF = indices for closure family

G22, G28, G47 = factor for adjusting the reaction rate in diurnal-average mode

GAMMA = factor parameterizing the production of O_3 due to methane oxidation

LNOX = altitude index for NOX injection

ADDNOX = amount of NOX injected ($\frac{\text{molecules}}{\text{cm}^3 \text{ sec}}$)

TA = latitude to be used for photolysis calculation (default = 30°)

DA = declination to be used for photolysis calculation (default = 0°)

Parameter for Diurnal vs Diurnal-Average Options

SST = (T,F) (diurnal-average mode, diurnal mode)

NDIV = number of divisions into which the daylight hours are divided [Note, some array sizes will have to be changed if

NDIV > 6; use only in diurnal model

Boundary Conditions:

BCB = bottom boundary values

BCT = top boundary values

Convergence Tolerance Limit:

EP1 = convergence criteria for photochemical species (used in NEWTON)

EP2 = convergence criteria for diffusive species

ITC = iteration limits; program aborts if convergence criteria not satisfied after ITC iterations

PRINT OUT OPTION

LEVP = level of print out; 6 is normal

DZ = print out densities at intervals of DZ (cm); default = 2×10^5 cm

ZBP = print out density profiles from height ZBP (cm); default = 0

ZTP = print out density profiles to height ZTP (cm); default = 48E5

IV. CALCULATION OF PRODUCTION AND LOSS TERM

The coding for calculating the production and loss rates is set up in JACOB. For example, for species I_1, it gives

$$PR(I_1) = R(k_1)SP(I_2)SP(I_3) + J(j_1)SP(J_4) + \ldots$$

$$LO(I_1) = R(k_2)SP(I_5) + J(j_2) + \ldots$$

where $R(k_1)$ is the reaction rate for reaction k_1,

$J(j_1)$ is the photolysis rate for photolytic reaction j_1,

$SP(I_2)$ is the number density for the I_2 species,

With all values corresponding to the same altitude. The R array is set up in subroutine COMR, the J array in subroutine COMJ. JACOB also give the Jacobian $\frac{\partial f_i}{\partial n_i}$ necessary for solving the photochemical species.

For diffusive species, the production and loss rates are stored in SSPC(81) and SSLC(81) as functions of altitude for use in subroutine DIFUSE.

Calculation of Reaction Rates [COMR]

Parameters necessary to calculate the reaction rate $R_K(z)$ are stored in array RR(I,K), where

I = reaction parameter index

K = reaction index (see BLOCK DATA BD2 for list of reactions)

RR(1,K) contains the parameter defining the type of reaction:

a) RR(1,K) = 1.0

$R_K(z) = RR(2,K)$

b) RR(1,K) = 2.0

$R_K(z) = RR(2,K)e^{-\frac{RR(3,K)}{T(z)}}$, T(z) = temperature at altitude z

c) RR(1,K) = 3.0

$R_K(z) = \frac{RR(2,K)e^{-\frac{RR(3,K)}{T(z)}}}{RR(4,K) + N}$, N = number density of air

d) RR(1,K) = <1

$$R_K(z) = \frac{k_o(T(z)M(z)}{1 + \frac{k_o(T(z)M(z)}{k_\infty(T(z))}} \; 0.6^{\{[\log_{10}\frac{k_o(T(z)M(z)}{k_\infty(T(z)}]^2\}^{-1}}$$

where $k_o(T(z) = RR(1,K) * (\frac{T(z)}{300})^{-RR(2,k)}$

$k_\infty((T(z)) = RR(3,k) * (\frac{T(z)}{300})^{-RR(4,k)}$

The parameter RR(I,K) can be changed from namelists.

Calculation of Photolysis Rate [COMJ]

The photolysis rate J is defined by

$$J(L) = \Sigma \; QS(I) \times FLX(1) \times TAU(L,I)$$

over 72 wavelengths

where QS(I) is the absorption cross-section at the I^{th} wavelength

FLX(I) is the unattenuated integrated solar flux at the I^{th} wavelength interval

TAU(L,I) is the transmission function at the L^{th} altitude and I^{th} wavelength.

The transmission function is calculated in the subroutine TAU where

$$TAU = e^{-\frac{\tau}{\cos\theta(t)}}$$

with τ the optical thickness which is a function of O_3 and O_2 distribution; $\theta(t)$ is the zenith angle, which is a function of latitude, declination and local time. For the diurnal-average option, the transmission corresponds to the averaged transmission over a 24 hr day

$$TAU = \frac{1}{24\ hr} \int_{\substack{over \\ daylight \\ hour}} e^{-\tau/\cos\theta(t)} dt \quad .$$

V. TREATMENT OF PHOTOCHEMICAL SPECIES

In calculating the new species number densities, the user has the option of either solving one large system, generated by considering all of the photochemical species, simultaneously, or letting the program group the photochemical species into families which are then processed sequentially, as sub-systems. The justification for this approach comes from the fact that the coupling among the species within each family is much stronger than the coupling to species outside the family. Presently, there are four photochemical families: oxygen ($O(^1D)$, O), hydrogen (H, OH, HO_2, H_2O_2, CH_2O), chlorine (Cl, ClO, HCl, HOCl, $ClNO_3$) and nitrogen (NO, NO_2, HNO_3, NO_3, N_2O_5, HO_2NO_2).

The Diurnal-Averaged Option

In the diurnal-averaged option, one has the set of equations

$$\{P_i(\vec{n}) - L_i(\vec{n}) \times n_i = 0\}_{i = 1,m\ (species)}, \qquad (A\text{-}1)$$

where $\vec{n} = (n_1, n_2, \ldots n_m)$ are the species densities.

Depending on whether or not all of the photochemical species are being solved together as a group or are being processed by families, the number densities n represent, either the entire group of photochemical species or just one particular photochemical family.

The system of equation (A-1) is solved by Newton's method as follows:

Defining the set of functions

$$\{f_i(\vec{n}) \equiv P_i(\vec{n}) - L_i(\vec{n}) \times n_i\}_{i=1,m} \tag{A-2}$$

and expanding the f_i in Taylor series to first order in Δn_j about $\vec{n}_o$ where $\vec{n}_o$ is either a guess solution or a solution from the previous interation, we have

$$\{f_i(\vec{n}) = f_i(\vec{n}_o) + \sum_{j=1}^{m} \frac{\partial f_i(\vec{n}_o) n_j}{\partial n_j} + O(\Delta n_j)^2\}_{i=1,m} \tag{A-3}$$

where $\Delta n_j = n_j - n_j^o$.

Since $f_i(\vec{n}) = 0$, for i=1, m, the following system of simultaneous linear equations for Δn_j , the first order correction to $\vec{n}_o$, is obtained

$$\{\sum_{j=1}^{M} \frac{\partial f_i(\vec{n}_o)}{\partial n_j} \Delta n_j \cong f_i(\vec{n}_o)\}_{i=1,m} \quad . \tag{A-4}$$

The equations are generated by the program as follows. Using an inital guess for the solution $\vec{n}_o$ (supplied by either BLOCK DATA values or restart values, previously calculated and stored on disk), subroutine NEWTON calculates the $f_i(\vec{n}_o)$ and

subroutine JACOB calculates the Jacobian terms $\frac{\partial f_i(\vec{n}_o)}{\partial n_j}$.

For the chlorine and nitrogen family, the system of equations (A-4) cannot be solved as is because they turn out to be ill-conditioned. One can define the species concentrations

$$ClX = Cl + ClO + HCl + HOCl + ClNO_3$$

$$NOX = NO + NO_2 + HNO_3 + NO_3 + N_2O_5 + N_2O_5 + HO_2NO_2 + ClNO_3 \quad .$$

If treated as species on their own, the production and loss terms for ClX (NOX) are just the sum of the production and loss terms of each of the species on the right hand side. It turns out that this net production and loss term is small compared to the individual contributions. Thus, the terms on the right hand side sum approximately to zero and the system of equation is ill-conditioned in that it is degenerate. To remedy this, in processing the chlorine and nitrogen family, the species have the maximum number density is found. The corresponding equation in the system is replaced by another equation formulated from number density closure considerations. In the case of chlorine, we require

$$\Delta n_{Cl} + \Delta n_{ClO} + \Delta n_{HCl} + \Delta n_{HOCl} + \Delta n_{ClNO_3} = Cl_x - (Cl + ClO + HCl + HOCl + ClNO_3) \quad .$$

In the case of nitrogen,

$$\Delta n_{NO} + \Delta n_{NO_2} + \Delta n_{HNO_3} + \Delta n_{NO_3} + 2 \times \Delta n_{N_2O_5} + \Delta n_{HO_2NO_2} + \Delta n_{ClNO_3} = NO_x - (NO + NO_2 + HNO_3 + NO_3 + 2 \times N_2O_5 + HO_2NO_2 + ClNO_3)$$

is the replacement equation. The two equations demand that the sum of the odd chlorine and nitrogen species is conserved and also provide some feedback from diffusion processes.

The system of linear equations is solved in FUNCTION LINEQN, using Gaussian elimination and the changes in density Δn_i are returned. The new densities $n = n_o + \Delta n$ are used to recalculate the production and loss terms, P_i and $L_i n_i$. The value of $f_i = P_i - L_i n_i$ is then found and the ratios f_i/P_i are tested for convergence at that altitude. If $\left|\frac{f_i}{P_i}\right| <$ EP1, convergence has been achieved, the program goes on to the next altitude. Otherwise, it goes back and recalculates all of the families again.

Diurnal Option

In calculating the photochemical species under the diurnal option, one seeks a solution to

$$\left\{\frac{\partial n_i(t)}{\partial t} = P_i(\vec{n}(t)) - L_i(\vec{n}(t)) x n_i(t)\right\}_{\substack{i=1,m \\ \text{(species)}}} \qquad \text{(A-5)}$$

with a periodic boundary condition requiring that $n_i(t,z) = n_i(t + 24 \text{ hours}, z)$ for all times t.

Equation (A-5) is a system of coupled non-linear differential equations in time. One seeks the solution in two steps. First, a finite difference method has to be derived to propagate $\vec{n}(t)$ in time. The scheme is then used to propagate $\vec{n}(t)$ in time until the periodic condition is satisfied by all the species. A periodic solution for $\vec{n}(t)$ exists since the driving term $P_i - L_i n_i(t)$ has the 24 hr periodicity.

The finite difference scheme is first discussed. Using the notation that $\vec{n}^k$ represents the number densities at the k^{th} time step, we can rewrite (A-5) in finite difference form

$$\left\{\frac{n_i^{k+1} - n^k}{(\Delta t)_{k+1}} = P_i(\vec{n}^{k+1}) - L_i(\vec{n}^{k+1}) \times n_i^{k+1}\right\}_{i=1,m}$$

or

$$\left\{n_i^{k+1} - \Delta t_{k+1}[P_i(n^{k+1}) - L_i(n^{k+1}) \times n_i^{k+1}] - n_i^k = 0\right\}_{i=1,m} \tag{A-6}$$

where $(\Delta t)_{k+1} = t^{k+1} - t^k$. In the above equation, $\vec{n}^{k+1}$ is the unknown and it is assumed that $\vec{n}^k$ has been computed in the previous time step. We define

$$\{g_i(\vec{n}^{k+1}) \equiv n_i^{k+1} - \Delta t_{k+1}[P_i(\vec{n}^{k+1}) - L_i(\vec{n}^{k+1}) \times n_i^{k+1}] - n_i^k\}_{i=1,m} \quad . \tag{A-7}$$

The required solution $\vec{n}^{k+1}$ is then given by

$$\{g_i(\vec{n}^{k+1})\}_{i=1,m} = 0 \quad . \tag{A-8}$$

If $\vec{n}_o^{k+1}$ is the guess solution or the solution from the previous iteration, one can expand g_i in Taylor series to first order in Δn_i^{k+1} around $\vec{n}^{k+1}$ to obtain

$$\left\{g_i(\vec{n}^{k+1}) \simeq g_i(\vec{n}_o^{k+1}) + \sum_{j=1}^{M} \frac{\partial g_i(\vec{n}_o^{k+1})}{\partial n_j^{k+1}} \Delta n_j^{k+1}\right\}_{i=1,m} \tag{A-9}$$

from (A-8), (A-9) gives a set of linear equations for Δn_j^{k+1}, namely, the first order correction term to $\vec{n}_o^{k+1}$,

$$\left\{ \sum_{j=1}^{M} \frac{\partial g_i(\vec{n}^{k+1})}{\partial n_j} \Delta n_j^{k+1} \cong -g_i(\vec{n}_o^{k+1}) \right\}_{i=1,m} . \qquad \text{(A-10)}$$

Note that

$$\frac{\partial g_i(\vec{n}^{k+1})}{\partial n_j^{k+1}} = \begin{cases} -\Delta t \dfrac{\partial f_i(n^{k+1})}{\partial n_j^{k+1}} & \text{if } i \neq j \\ 1-\Delta t \dfrac{\partial f_i(n^{k+1})}{\partial n_j^{k+1}} & \text{if } i = j \end{cases} ,$$

Thus, subroutine JACOB can be used to generate $\frac{\partial g_i(\vec{n}^{k+1})}{\partial n_j^{k+1}}$ with minor modification. The system of linear equations (A-10) is solved using subroutine LINEQN to return the density changes Δn_j^{k+1}. The new densities $\vec{n}^{k+1} = \vec{n}_o^{k+1} + \vec{\Delta n}^{k+1}$ are used to recalculate the production and loss terms P_i and $L_i n_i$. The g_i are then found and, after being normalized, are tested for convergence against EP1. If convergence has been achieved, the program goes on to the next time step. If not, it goes back and recalculates all of the fast families again.

The equations are then propagated forward in time until the 24 hour periodic boundary conditions are satisfied. Subroutine SETUP is then used to calculate diurnally-averaged fast species densities and photolysis rates, as well as certain terms which contribute to the production and loss of selected slow species. These values are saved in preparation for entering the slow chemistry phase of the calculation.

VI. DIFFUSIVE SPECIES

The diffusive species are comprised of N_2O, CH_4, H_2, CH_3Cl, CCl_4, $CFCl_3$, CF_2Cl_2, CH_3CCl_3, CF_2O, CO, XX, NO_x, Cl_x and O_3. The slow species concentrations are obtained by solving the diffusion equation one species at a time. The diffusion equation can be written in the form

$$\frac{d}{dz}\left(KN\frac{dt}{dz}\right) = P(z) - \mathcal{L}(z)f(z) \qquad \text{(A-11)}$$

where z is geometrical altitude, K is eddy diffusion coefficient, N is air density, P is the product rate and $\mathcal{L}(z)$ is the loss frequency given by L x N.

The differential operator is converted to a finite difference operator using central differencing.

Using the notation that f_j stands for $f(z_j)$, we have

$$\frac{d}{dz}\left(KN\frac{df}{dz}\right) = \frac{(KN)_{j+\frac{1}{2}}\dfrac{f_{j+1}-f_j}{\Delta z} - (KN)_{j-\frac{1}{2}}\dfrac{f_j-f_{j-1}}{\Delta z}}{\Delta z}$$

or

$$\frac{d}{dz}\left(KN\frac{df}{dz}\right) = \qquad \text{(A-12)}$$

$$\frac{(KN)_{j-\frac{1}{2}}f_{j-1} + \{-(KN)_{j-\frac{1}{2}} - (KN)_{j+\frac{1}{2}}\}f_j + (KN)_{j+\frac{1}{2}}f_{j+1}}{(\Delta z)^2}$$

Thus, (A-11) reduces to

$$A_j f_{j-1} + B_j f_j + C_j f_{j+1} = F_j \quad , \tag{A-13}$$

where $A_j \equiv \frac{(KN)_{j-\frac{1}{2}}}{(\Delta z)^2} = \frac{(KN)_j + (KN)_{j-1}}{2(\Delta z)^2} = \frac{K_j N_j + K_{j-1} N_{j-1}}{2(\Delta z)^2}$

$$C_j \equiv \frac{(KN)_{j+\frac{1}{2}}}{(\Delta z)^2} = \frac{(KN)_{j+1} + (KN)_j}{2(\Delta z)^2} = \frac{K_{j+1} N_{j+1} + K_j N_j}{2(\Delta z)^2}$$

$$B_j = -A_j - C_j - \mathcal{L}_j \quad ,$$

and $F_j = -P_j$. Note that (A-13) holds only for j=2 through n-1 where n is the top altitude.

To find the production and loss terms P_i and $\mathcal{L}_i$, the program calls FUNCTION FUNPL. Calculation of the eddy diffusion coefficients K_j is done in subrouting FUNK and the A_j, B_j, C_j, F_j are calculated in subroutine ABCF.

The above set of equations will generate a system of n-2 linear equations in the n unknonws f_j. In order to produce two additonal equations, bottom and top boundary conditions are used. Either mixing ratio or flux boundary conditions may be used. When mixing ratio boundary conditions are chosen,

f_i = given mixing ratio of the species at altitude z, and/or

f_n = given mixing ratio of the species at altitude z_n are the equations provided. If flux boundary conditions are used, we have

$$\left[\frac{-2(KN)_1}{(\Delta z)^2}\right] f_1 + \left[\frac{2(KN)_1}{(\Delta z)^2}\right] f_2 =$$

$$-4\phi_1 \left[1.5 - 0.5 \frac{(KN)_1}{(KN)_2}\right] / (2\Delta z) \qquad \text{(A-15)}$$

$$\frac{\left[\frac{(KN)_{n-1} + (KN)_n}{2}\right]}{\Delta z} f_{n-1} + \frac{-\left[\frac{(KN)_{n-1} + (KN)_n}{2}\right]}{\Delta z} f_n \qquad \text{(A-16)}$$

$$= \phi_n$$

where ϕ_1 and ϕ_n are the specified flux at the bottom and top respectively.

Hence, including the two equations provided by the bottom and top boundary conditions, we have a system of n linear equations in the n unknowns f_j. Furthermore, the system is tridiagonal and is solved in FUNCTION TRIDIA, which returns the new mixing ratios at altitudes $z_{i=1,n}$.

As each slow chemistry species is calculated, the new mixing ratios f_j are converted back to number densities and compared with those from last iteration. If the relative changes are all less than a pre-specified value, at all altitudes, then that species is determined to have an acceptable density profile. If, on a particular interation, all slow species have acceptable new density profiles, then the entire set of species, both fast and slow, is considered to have converged. Otherwise, the program recalculates the O_3 column densities and then the photolysis rates in beginning the next iteration and recalculation of the fast chemistry.

VII OUTPUT

In the diurnal-averaged option, the level of output is conrolled by the parameter LEVP

LEVP = 1 PRINT altitude array for densities and mixing ratio for diffusive species

LEVP = 2 PRINT altitude array for photochemical species

LEVP = 3 PRINT altitude array for fixed species (M, H_2O, O_2), temperature, eddy diffusion coefficients and O_2 column density

LEVP = 4 PRINT reaction rate tables and boundary conditions

LEVP = 5 PRINT altitude array for photolysis rates and O_3 column density

LEVP = 6 PRINT selected reaction rates and calculated fluxes

LEVP = 7 PRINT wavelength, solar flux and absorption cross-section.

The program is set up so that all options lower than the specified number are included in the print out. In addition, the altitude arrays are controlled by the parameters

ZBP(cm): bottom level to be printed out

ZTP(cm): top level to be printed out

DZ(cm): increments between print out levels.

A listing of a sample output is included in this Appendix.

VIII. RUNNING INSTRUCTIONS

The program is currently being run on the AFGL CDC 6600. A typical deck setup together with a typical namelist input is given in Table A-4.

The typical running time of the diurnal average version is about 60-80 seconds on the CDC 6600. For the diurnal version, the time required is approximately 2,000 sec. for a complete run. If one only executes the part to solve the photochemical species only, the time required is reduced to about 600 seconds.

Table A-4

```
PROGA, CM120000, T100.                    1234      PROGRAMMER
FTN, I = INPUT, OPT = 2, SL, R = 3.
COPYCF, INPUT, TAPE5.
REWIND, TAPE5.
COPYCF, TAPE5, OUTPUT.
REWIND, TAPE5.
LDSET (PRESET = ZERO).
LGO.
7/8/9
```

FORTRAN DECK (Fortran IV)

```
7/8/9

 $LIST
 FSF(1?)=?.,
 ICF(3,1)=1,ICF(3,2)=>1,
 ICF(4,1)=2,ICF(4,2)=30,ICF(4,?)=12,
 RR(1,22)=2.6E-30,
 RR(1,28)=1.6E-31,
 RR(1,47)=2.1E-31,
 PJ03=2.4E-4,
 KC=0.0,
 K=1.E5,
 NDIV=6,
 MODE=3,ITC=50,
 EP1=2.05-4,EP2=2.0E-3,
 ZE=0.1,ZT=70.0E5,
 ZBP=3.3,ZTP=70.0E5,DZ=1.E5,
 LEVP=6,TRAN=.TRUE.,
 EI1=1.E-3,EI2=.1,
 BCB(18)=3.E-7,
 BCB(20)=1.5E-6,
 BCB(21)=5.E-7,
 BCB(22)=1.2E-9,
 BCB(23)=1.3E-10,
 BCB(24)=9.3E+5,
 BCB(25)=1.3E+6,
 BCB(26)=1.27,
 BCB(27)=1.E+3,
 BCB(28)=3.E-7,
 BCB(29)=1.E+3,
 BCB(30)=1.E-12,
 BCB(31)=1.E-3,
 BCB(32)=1.8E-9,BCT(32)=0.,
 SST=.TRUE.,
 $END
```

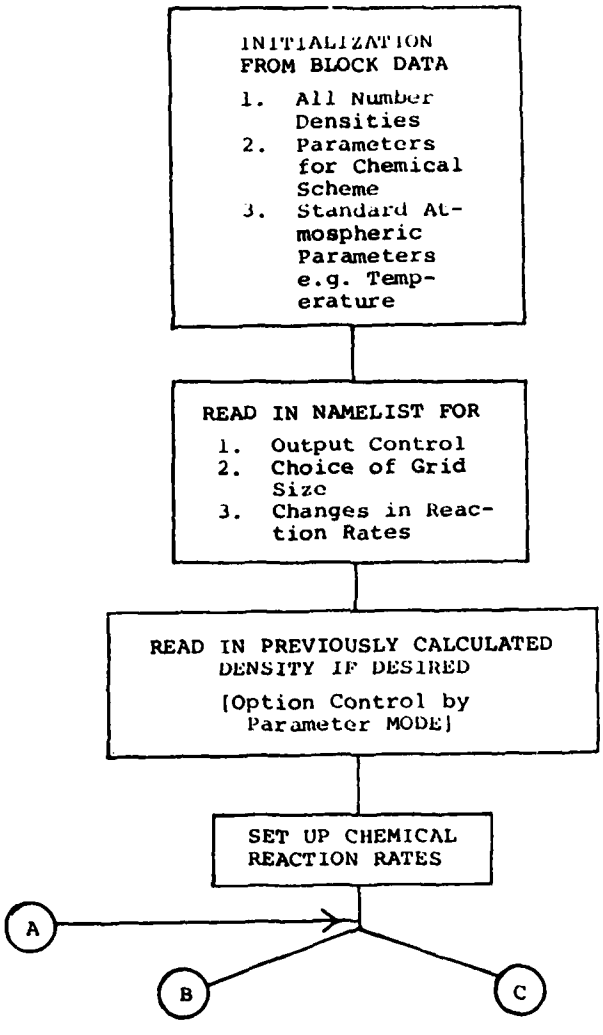

Figure A-1

Schematic Flow Chart for 1-D Model

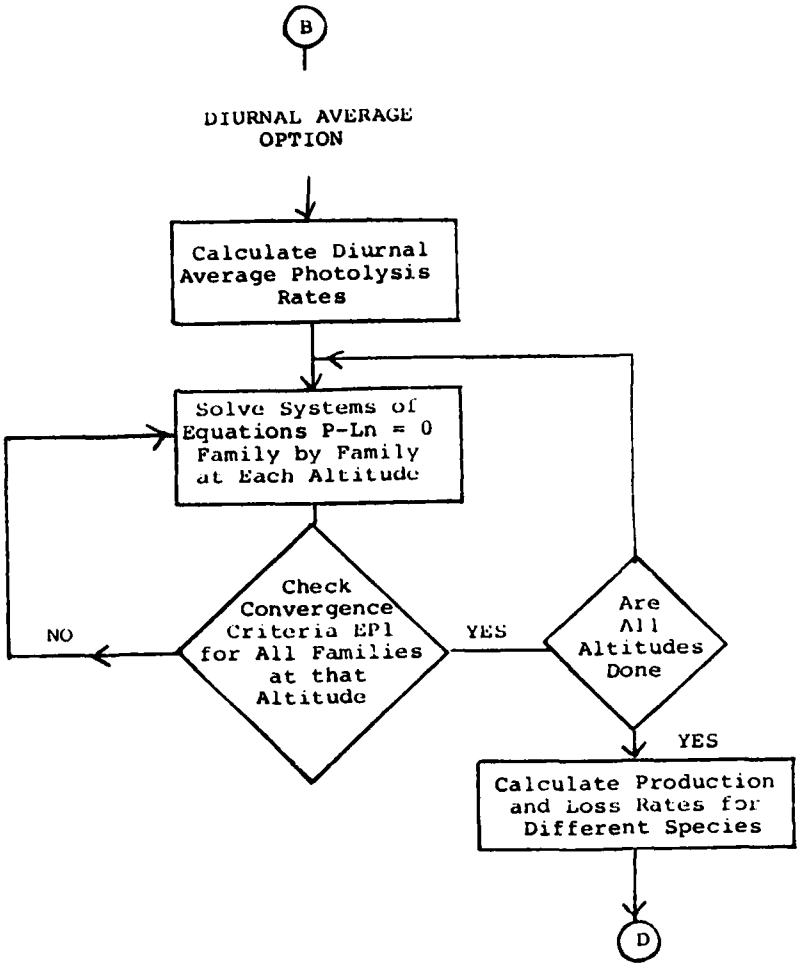

Figure A-1 (cont.)

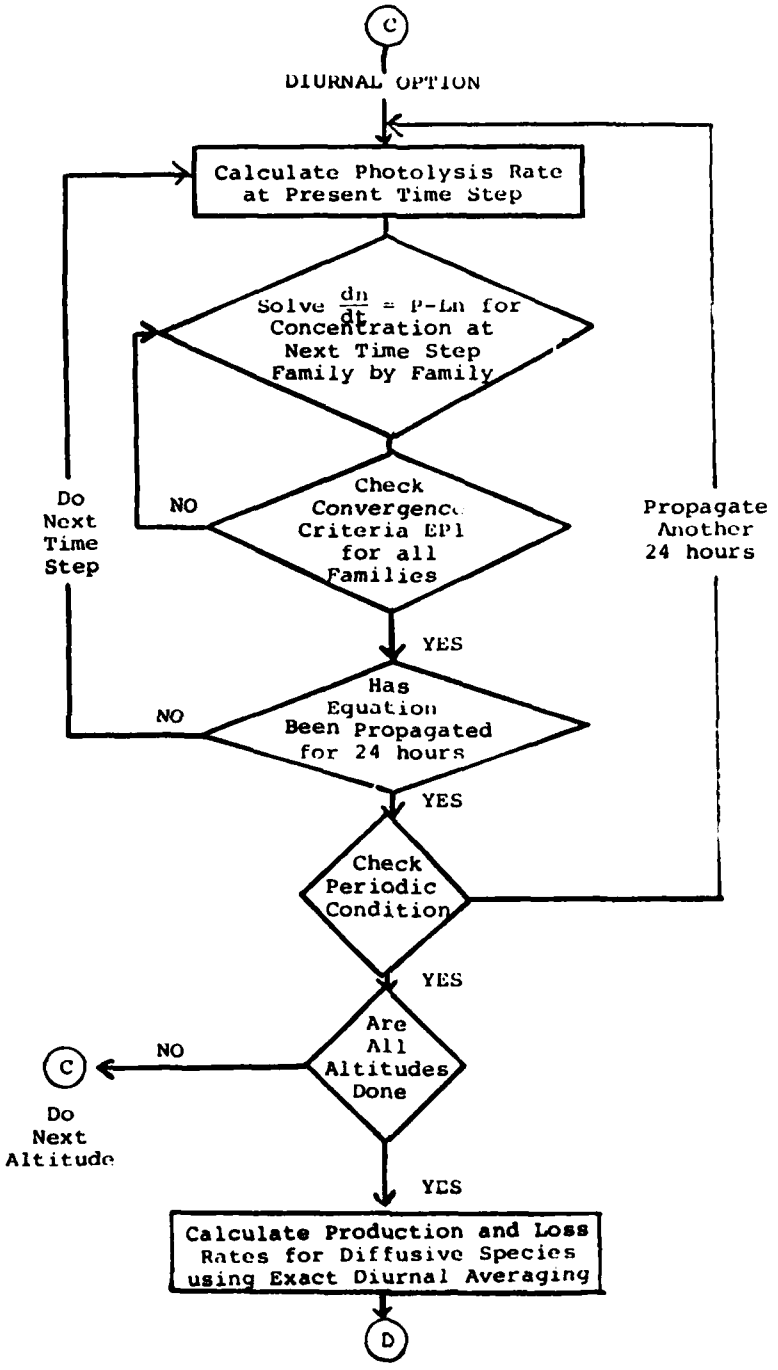

Figure A-1 (cont.)

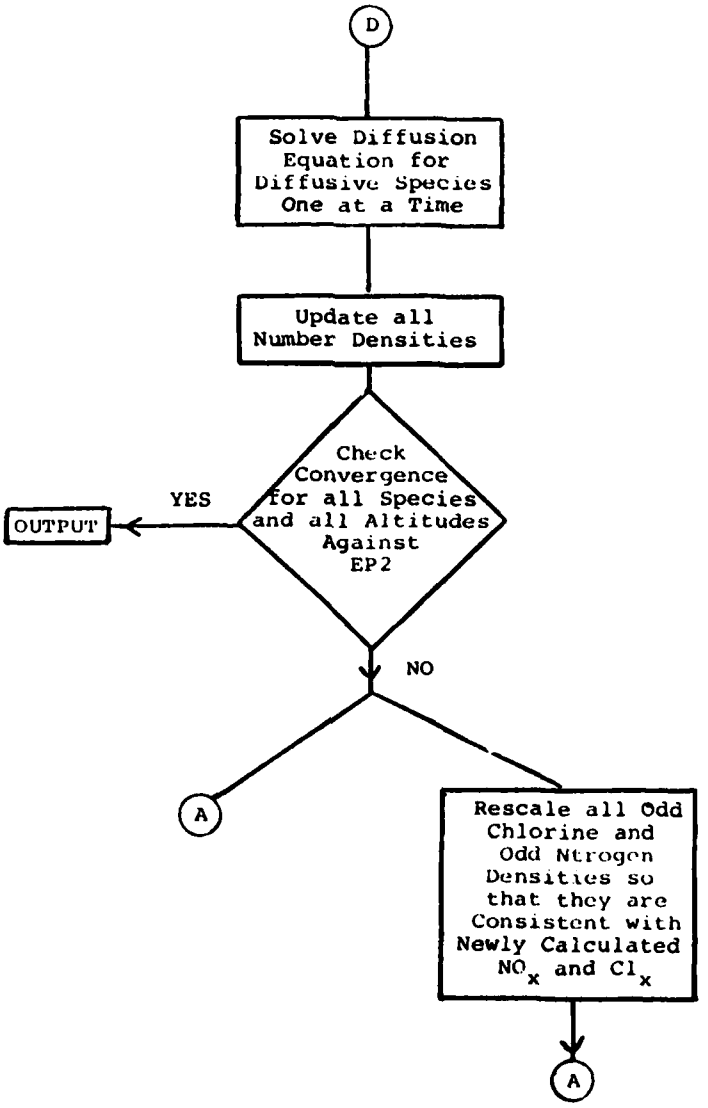

Figure A-1 (cont.)

APPENDIX B

DESCRIPTION OF 2-D MODEL

I. General Background

II. Chemical Scheme

III. Treatment of Photochemical Species

IV. Treatment of Diffusive Species

1. GENERAL BACKGROUND

The atmosphere is divided into grids. The coordinates used are the latitude ϕ and log-pressure coordinates

$$\xi = \ln \frac{p_o}{p}$$

where p_o is the surface pressure. In this coordinate, the vertical velocity $\omega = \frac{d\xi}{dt}$ is related to $w = \frac{dp}{dt}$ via

$$\omega = -\frac{1}{p} w$$

and

$$p\frac{\partial}{\partial p} = -\frac{\partial}{\partial \xi} \quad .$$

Using the coordination transformation, we can rewrite (7.2-10) and (7.2-14) as follows

$$\frac{\partial f}{\partial t} + \frac{1}{a\cos\phi}\frac{\partial}{\partial \lambda}(fu) + \frac{1}{a\cos\phi}\frac{\partial}{\partial \phi}(f v \cos\phi) +$$

$$e^{\xi}\frac{\partial}{\partial \xi}(f e^{-\xi} w) = Q/\rho \qquad \text{(B-1)}$$

$$\frac{1}{a\cos\phi}\frac{\partial u}{\partial \lambda} + \frac{1}{a\cos\phi}\frac{\partial}{\partial \phi}(v\cos\phi) + e^{\xi}\frac{\partial}{\partial \xi}(e^{-\xi} w) \qquad \text{(B-2)}$$

$$= 0 \quad .$$

Introducing the variables

$$V = v e^{-\xi} \cos\phi$$
$$W = \omega e^{-\xi} \cos\phi \qquad \text{(B-3)}$$

one can recast (B-1) and (B-2) in the form

$$\frac{\partial f}{\partial t} + \frac{1}{a\cos\phi}\frac{\partial}{\partial\lambda}(fu) + \frac{e^{\xi}}{a\cos\phi}\frac{\partial}{\partial\phi}(fV) + \frac{e^{\xi}}{a\cos\phi}\frac{\partial}{\partial\xi}(fW) = \frac{Q}{\rho} \qquad \text{(B-4)}$$

$$\frac{1}{a\cos\phi}\frac{\partial u}{\partial\lambda} + \frac{e^{+\xi}}{a\cos\phi}\frac{\partial}{\partial\phi}V + \frac{e^{\xi}}{\cos\phi}\frac{\partial}{\partial\xi}W = 0 \quad . \qquad \text{(B-5)}$$

Upon zonal averaging, one obtains

$$\frac{\partial\bar{f}}{\partial t} = \frac{e^{\xi}}{\cos\phi}\left[-\frac{1}{a}\frac{\partial}{\partial\phi}(\bar{V}\bar{f}) - \frac{\partial}{\partial\xi}(\bar{W}\bar{f}) - F_f + \frac{\bar{Q}}{\rho}e^{-\xi}\cos\phi\right] \qquad \text{(B-6)}$$

$$\frac{1}{a}\frac{\partial\bar{V}}{\partial\phi} + \frac{\partial\bar{W}}{\partial\xi} = 0 \quad . \qquad \text{(B-7)}$$

Equation (A-7) implies the existence of a stream function Ψ, where

$$\bar{V} = -\frac{\partial\Psi}{\partial\xi}$$
$$\bar{W} = +\frac{1}{a}\frac{\partial\Psi}{\partial\phi} \quad . \qquad \text{(B-8)}$$

Finally, the eddy fluxes are parameterized by eddy diffusion tensor, giving

$$F_f = -\frac{1}{a}\frac{\partial}{\partial\phi}\left[e^{-\xi}\cos\psi\left(K_{\phi\phi}\frac{\partial\bar{f}}{\partial\phi} + K_{\phi\xi}\frac{\partial\bar{f}}{\partial\xi}\right)\right] - \frac{\partial}{\partial\xi}\left[e^{-\xi}\cos\psi\left(K_{\xi\phi}\frac{\partial\bar{f}}{\partial\phi} + K_{\xi\xi}\frac{\partial\bar{f}}{\partial\xi}\right)\right] \quad \text{(B-9)}$$

The globe is covered by 19 latitude belts each $\sim$9.5° wide (or $\sim$1,000 km across). The vertical direction is divided into layers with equal spacing in ξ with $\Delta\xi = 0.5$ (or $\sim$3 km high). The model is set up to accommodate a maximum of 29 layers.

Fig. B-1 shows a schematic diagram of the grid together with typical points within a grid for which variables are defined. Variables are defined at points A (at center of boxes) with indices J, K with the corresponding coordinates given by

$$\phi = (J-1)\times\frac{\pi}{19} + \frac{\pi}{38} - \frac{\pi}{2} \qquad J = 1,19$$

$$\xi = \frac{K-1}{2} + 0.25 \qquad K = 1,29$$

SP(I,J,K): diffusive species mixing ratio, I is species index

T(J,K): temperature

M(J,K): air number density

DADT(J,K): local time rate of change of mixing ratio $\frac{\partial\bar{f}}{\partial t}$.

Variables are defined at points C and G with

$$\phi = (J-1)\times\frac{\pi}{19} + \frac{\pi}{38} - \frac{\pi}{2} \qquad J = 1,19$$

$$\xi = \frac{K-1}{2} \qquad K = 1,30$$

$K_{\xi\xi}(J,K)$: $\xi\xi$ component of eddy diffusion tensor

$W(J,K)$: zonal mean vertical wind speed $\bar{W}$

$VF(J,K)$: vertical eddy fluxes $(K_{\xi\phi}\frac{\partial\bar{f}}{\partial\phi} + K_{\xi\xi}\frac{\partial\bar{f}}{\partial\xi})$

Variables are defined at points B, D, F, H with

$$\phi = (J-1)\frac{\pi}{19} - \frac{\pi}{2} \qquad J = 1,20$$

$$\xi = \frac{K-1}{2} \qquad K = 1,30$$

$\Psi(J,K)$: stream functions that general $\bar{V}$, $\bar{W}$

$K_{\phi\xi}(J,K)$: diagonal element of eddy diffusion tensor.

Variables are defined at points E, I with

$$\phi = (J-1) \times \frac{\pi}{19} - \frac{\pi}{2} \qquad J = 1,20$$

$$\xi = \frac{K-1}{2} + 0.25 \qquad K = 1,29 \ .$$

$K_{\phi\phi}(J,K)$: triagonal component of eddy diffusion coefficient

$V(J,K)$: zonal mean horizontal velocity V

$HF(J,K)$: horizontal eddy fluxes $(K_{\phi\phi}\frac{\partial\bar{f}}{\partial\phi} + K_{\phi\xi}\frac{\partial\bar{f}}{\partial\xi})$.

The variables are defined in this way so that upon applying the finite difference scheme to obtain the appropriate spatial derivatives, all quantities that enter into (B-6) are defined at the centers of the boxes.

The overall proceeding for solving the atmospheric species is outlined in Fig. B-2. At present, all the dynamic variables are read from a local file. The temperature, stream function and the photochemical species concentrations are updated every 10 days, while the eddy diffusion tensor is updated once every 30 days. Some of the components outlined in Fig. B-2 will be

discussed in the following sections.

II. CHEMICAL SCHEME

The chemical scheme in the 2-D model is similar to that set up in the one-dimensional model. The species are divided into the photochemical species, diffusive species and the fixed species.

The photochemical species include:

Oxygen family: $O(^1D)$, $O(^3P)$

Hydrogen family: H, OH, HO_2, H_2O_2

Chlorine family: Cl, ClO, HCl, HOCl, $ClNO_3$

Nitrogen family: NO, NO_2, HNO_3

The diffusive species are:

CH_3Cl, CH_3CCl_3. CCl_4, F-11, F-12, ClX, N_2O, NOX and O_3

The fixed species are:

CH_4, CO, H_2O.

The chemical reactions and photolytic processes adopted correspond to the appropriate subset of the 1-D model chemistry as listed in Appendix A. The boundary conditions are also similar except for F-11 and F-12. A time-dependent flux boundary condition is used for both species. The release of F-11 and F-12 is restricted to between 25° N and 60° N. The release rate follows the data compiled by the CMA Fluorocarbon Panel (1980). The values are given in Table B-1 for reference.

TABLE B-1

FLUOROCARBON RELEASE RATES

FLUOROCARBON PRODUCTION AND RELEASE
MILLION KILOGRAMS

REPORTING COMPANIES ONLY

FC-11

YEAR	ANNUAL PROD	ANNUAL REL	TOTAL PROD	TOTAL REL	TOTAL UNREL
1950	6.6	5.4	18.6	14.4	4.1
1951	9.1	7.5	27.6	21.9	5.7
1952	13.6	10.8	41.2	32.7	8.5
1953	17.3	14.7	58.5	47.4	11.1
1954	20.9	18.3	79.4	65.7	13.7
1955	26.3	22.6	105.6	88.3	17.4
1956	32.5	28.2	138.1	116.5	21.6
1957	35.9	31.6	172.0	148.1	23.9
1958	29.5	29.7	201.6	177.8	23.8
1959	35.6	30.3	237.1	208.1	29.0
1960	49.7	39.7	286.9	247.9	39.0
1961	60.5	51.2	347.3	299.0	48.3
1962	78.1	69.1	425.4	368.1	62.3
1963	93.3	78.5	518.7	441.7	77.0
1964	111.1	93.2	629.8	534.9	94.9
1965	122.8	106.3	752.6	641.2	111.4
1966	141.0	119.0	893.7	760.2	133.4
1967	159.8	135.1	1053.4	895.3	158.1
1968	183.1	153.9	1236.5	1049.2	187.4
1969	217.3	178.4	1453.8	1227.6	226.2
1970	238.1	202.8	1691.9	1430.4	261.6
1971	263.2	222.7	1955.1	1653.1	302.0
1972	306.9	250.8	2262.0	1903.9	358.0
1973	349.1	286.8	2611.1	2190.7	420.3
1974	369.7	315.4	2980.8	2506.1	474.7
1975	314.1	305.5	3294.8	2811.6	483.2
1976	339.8	295.8	3634.7	3107.4	527.3
1977	320.5	297.2	3955.1	3404.6	550.6
1978	308.9	281.0	4264.0	3685.6	578.4
1979	289.5	261.9	4553.5	3947.5	606.0

FC-12

YEAR	ANNUAL PROD	ANNUAL REL	TOTAL PROD	TOTAL REL	TOTAL UNREL
1950	34.6	27.1	198.3	129.5	68.8
1951	36.2	30.2	234.5	159.6	74.9
1952	37.2	31.5	271.7	191.1	80.6
1953	46.5	35.5	318.2	226.6	91.6
1954	49.1	40.3	367.4	266.9	100.4
1955	57.6	45.2	425.0	312.1	112.9
1956	68.7	52.6	493.6	364.7	129.0
1957	74.2	59.8	567.8	424.5	143.3
1958	73.4	62.6	641.2	487.1	154.2
1959	87.6	69.6	728.8	556.7	172.1
1960	99.4	68.2	828.3	624.9	203.3
1961	108.5	93.2	936.8	733.2	203.6
1962	128.1	107.1	1064.9	840.3	224.6
1963	146.4	125.8	1211.3	966.1	245.1
1964	170.1	146.6	1381.4	1112.7	268.7
1965	190.1	165.6	1571.4	1278.4	293.1
1966	216.2	184.3	1787.6	1462.7	324.9
1967	242.8	208.3	2030.4	1670.9	359.4
1968	267.5	233.6	2297.9	1904.6	393.3
1969	297.3	260.1	2595.1	2164.6	430.5
1970	321.1	284.2	2916.2	2448.9	467.4
1971	341.6	304.8	3257.8	2753.7	504.1
1972	379.9	331.2	3637.7	3084.9	552.8
1973	423.3	366.5	4061.0	3451.4	609.6
1974	442.8	396.5	4503.8	3847.9	655.9
1975	381.0	382.8	4884.8	4230.8	654.0
1976	410.7	363.9	5295.5	4594.6	700.9
1977	362.8	344.9	5658.3	4939.6	718.8
1978	372.1	316.2	6030.4	5255.8	774.6
1979	357.2	305.8	6407.6	5561.6	845.0

III. TREATMENT OF PHOTOCHEMICAL SPECIES

The treatment of photochemical species is exactly analogous to the diurnal-averaged version of the 1-D model. Since there is no spatial coupling among the equations, the photochemical species can be solved locally and there is no difference between the 1-D and 2-D models. A detailed description of the method can be found in the corresponding section in Appendix A.

IV. TREATMENT OF DIFFUSIVE SPECIES

An explicit time difference scheme is used to propagate the specie volume mixing ratio forward in time. Given the current values of f, $\bar{v}$, $\bar{w}$, K and T at time tk, the program calculates each individual term on the right hand side of (F-6) to obtain $(\frac{\partial f}{\partial t})_{tk}$. The value of f at time tk+1 is obtained by the Adam-Bashford Scheme,

$$f_{tk+1} = 1.5(\frac{\partial f}{\partial t})_{tk} \Delta t - 0.5(\frac{\partial f}{\partial t})_{tk-1} \Delta t \qquad \text{(B-10)}$$

Because an explicit time scheme is used, the time step must be sufficiently small to ensure stability. With the present choice of grid sizes, a time step of 4 hours is required.

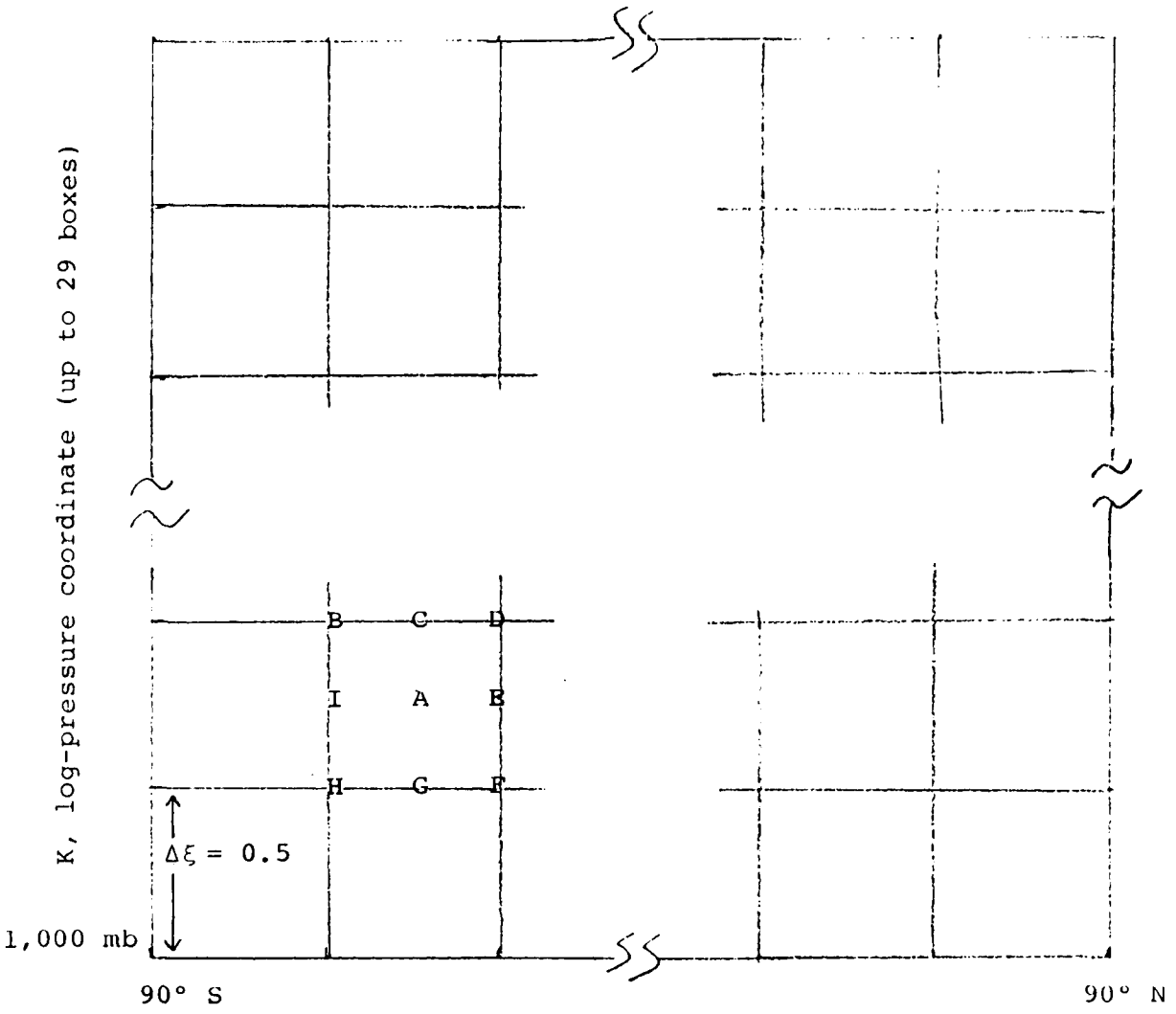

Figure B-1

Diagram Showing the Grid System Employed

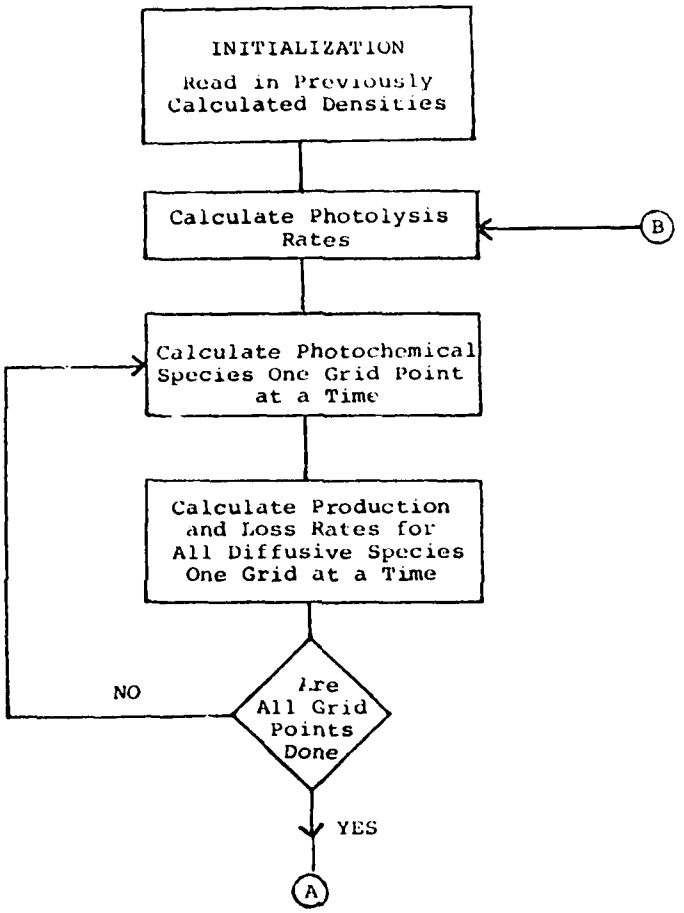

Figure B-2

Schematic Flow Chart for 2-D Model

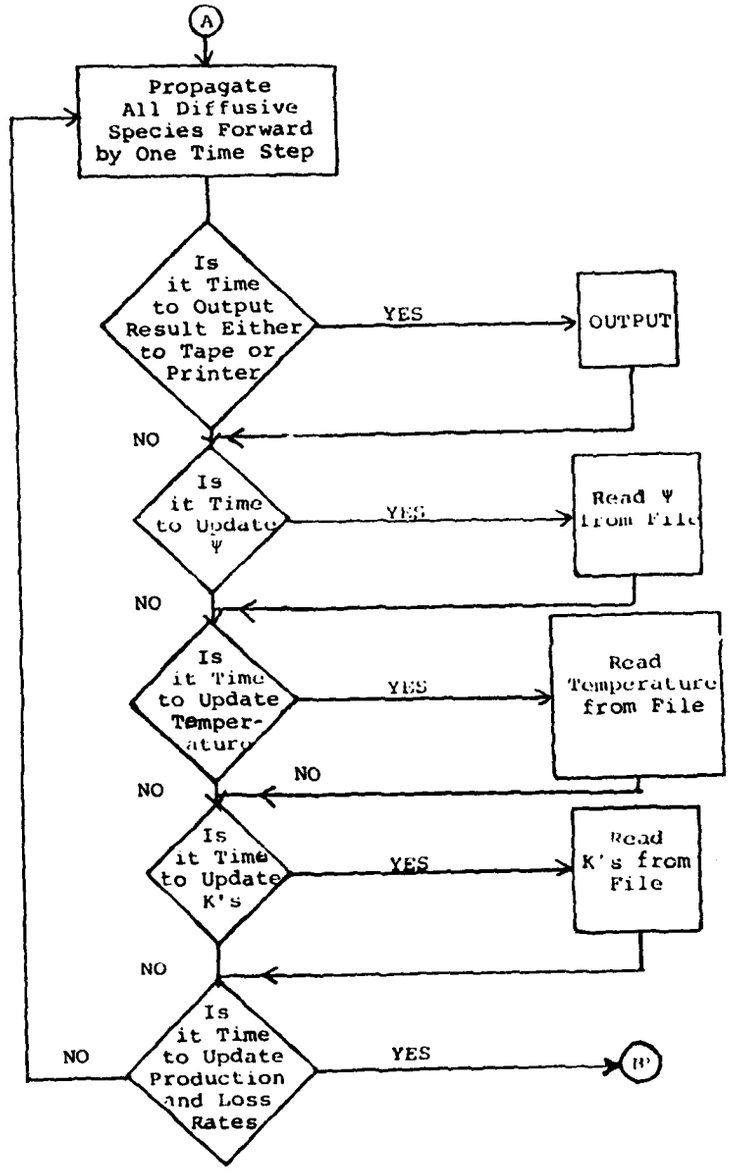

Figure B-2 (cont.)